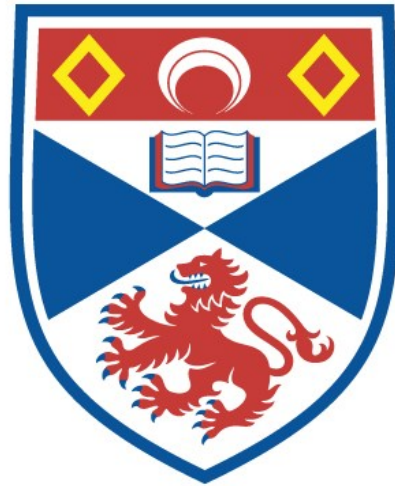


# University of St Andrews



Full metadata for this thesis is available in  
St Andrews Research Repository  
at:

<http://research-repository.st-andrews.ac.uk/>

This thesis is protected by original copyright

AN EXPERIMENTAL INVESTIGATION OF THE  
THERMAL EXPANSION OF ALKALI HALIDES AT  
LOW TEMPERATURES.

by

BRIAN W. JAMES B.Sc., Grad. Inst. P.

A thesis presented to the University of St. Andrews for the degree of  
Master of Science in Physics, June 1964.



Declarations.

I hereby declare that this special study has been carried out and the thesis composed by myself and that this thesis has not been accepted in fulfilment of the requirements of any other degree or professional qualification.

We hereby certify that Brian William James has spent four terms in research work on the thermal expansion of alkali halides at low temperatures, that he has fulfilled the conditions of Ordinance 51 (St. Andrews) and that he is qualified to submit the accompanying thesis in application for the Degree of Master of Science.

Curriculum vitae.

In 1956 I entered St. Andrews University and attended the course in Natural Philosophy. I graduated in October 1959 with an ordinary B.Sc. degree in Natural Philosophy and Mathematics, and in June 1960 I obtained a Third Class Honours Degree in Natural Philosophy. I then joined Pilkington Brothers Ltd. in October 1960, where I worked for a year as a Development Physicist on the Float Glass Process. In the following year, October 1961, I joined the Physics Department of Bradford Institute of Technology as a full-time research assistant, and registered as an external research student for the M.Sc. Degree of the University of St. Andrews.



## Index.

	Page
Introduction.	1
Chapter 1. The Theory of Heat Capacity of Solids.	4
Dulong and Petit's Law.	5
Einstein's Theory of Specific Heats.	6
The Specific Heat for a System of Oscillators with a Spectrum of Frequencies.	7
The Choice of the Spectrum of Frequencies.	8
The Debye Theory of Specific Heats.	9
Equation of State of Solids.	10
Moments of the Frequency Distribution.	12
Debye-Waller Factor.	14
Chapter 2. Methods of Measuring the Linear Thermal Expansion Coefficient.	16
The Optical Lever.	16
Optical Photometer.	18
Optical Interference.	19
Electrical Capacitor Methods.	21
X-ray Methods.	23
Requirements for the Present System.	24
Chapter 3. The Fizeau Interferometer.	26
The Optical System.	27
The Index Mark.	30

<u>Index continued.</u>		Page
	Flatness of the Optical Flats.	31
	The Variation of Path Difference with Gas Density,	33
	Experimental Difficulties Experienced with the Optical System.	34
Chapter 4.	Temperature Measurement.	39
	Choice of Resistance Thermometer Material.	40
	The Gas Thermometer.	41
	The Gas Thermometer Calculations.	44
	The Results of the Calibration.	48
	Gas Thermometer Failure *	50
Chapter 5.	The Vacuum System.	51
	Temperature Variation.	52
	Procedure for Measuring Thermal Expansion.	53
	Photography.	56
	The Use of the Microphotometer for Fractional Fringe Shifts.	57
Chapter 6.	The Results, and the Specimen Purities.	58
	1) Copper.	58
	2) Caesium Iodide.	59
	3) Rubidium Bromide.	59
	4) Sodium Fluoride.	60

<u>Index continued.</u>	Page
Analysis of the Results.	60
The Grüneisen Parameter and the Debye Characteristic Temperature.	61
Moments of the Frequency Distribution.	65
Debye-Waller Factor.	67
Errors in Thermal Expansion Measurements.	68
Estimated Errors in Associated Data.	70
Errors in the Results of the Analysis.	70
 Chapter 7.    Conclusions.	 82
 References.	 84
 Acknowledgements.	 88
 Plates	
1. The Indium Thermometer Mount	After page 40
2. The Gas Thermometer - General View.	42
3. The Gas Thermometer - the Telescope and the Manometer.	42
4. The Specimen Chamber.	53
5. General View of the Apparatus.	54

## Introduction.

An important aim in solid state physics is the understanding of lattice dynamics, which may be revealed by measurements of such lattice properties as specific heat, elastic constants and thermal expansion. Alkali halide crystals have a simple structure and to a first approximation relatively simple interatomic forces. As a consequence their measurable properties are particularly suitable for direct comparison with the predictions of lattice theory. Grüneisen<sup>(1,2)</sup> (1912, 1926) introduced the quantity  $\gamma = \frac{\beta V}{C_v \chi_T}$  where  $\beta$  is the volume coefficient of expansion,  $V$  is the molar volume,  $C_v$  the molar heat, and  $\chi_T$  the isothermal compressibility.  $\gamma$  can be expressed as the variation with volume of the single characteristic lattice frequency used by Einstein in his theory of the specific heat of solids. In Debye's<sup>(3,4)</sup> (1912, 1913) work, where a spectrum of lattice vibrations with frequencies  $\nu_i$  is assumed, the corresponding Grüneisen parameters  $\gamma_i = \frac{-d(\ln \nu_i)}{d(\ln V)}$  are all taken to be equal to  $\gamma = \frac{d(\ln \theta_D)}{d(\ln V)}$ , where  $\theta_D = \frac{h \nu_D}{K}$ ,  $\nu_D$  is the maximum frequency of the Debye distribution,  $h$  is Planck's constant, and  $K$ , Boltzmann's constant. Experiments have shown that  $\gamma$  is temperature independent only over restricted temperature ranges.

Although there is no reason to believe that in a real crystal the  $\gamma_i$  are even approximately equal to one another, Born<sup>(5)</sup> (1923) has shown that in general there are high and low temperature limiting values,  $\gamma_\infty$  and  $\gamma_0$  respectively, of  $\gamma$  and rigorous treatments have been given recently by a number of authors, Dayal<sup>(6)</sup> (1944), Barron<sup>(7)</sup>

(1955), and Blackman<sup>(8)</sup> (1957). An outline of the theoretical background is given in Chapter 1.

In order to obtain data for some alkali halide crystals, which could be considered in the light of some of these ideas, an investigation was initiated in 1959 which led to the determination of the expansion coefficients of LiF, NaCl, KCl, KBr, and KI in the temperature range 20°K to 270°K by Yates and Panter<sup>(9)</sup> (1962). One conclusion from this work was that more accurate determinations of expansion coefficients were desirable, particularly at the lower temperatures, in order that more reliable comparisons between experimental observations and theoretical predictions could be made. To achieve this end attention has been directed towards an improvement of the accuracy with which the two observables might be measured, i.e., temperature and small changes of length. The experimental method used is described in Chapters 3 to 5. Other experimental methods are reviewed in Chapter 2 and the relative merits of each are discussed.

The expansion coefficients for Cu, NaF, RbBr, and CsI have been measured from 20°K to 270°K; these results are given in Chapter 6. A search of the literature for associated thermodynamic data required for calculations of the Grüneisen parameter revealed specific heat measurements at low temperatures only for RbBr, and elasticity data at low temperatures only for CsI. Thus it has been possible to test the predictions of theory only for RbBr, using estimated elasticity data. Moments of the frequency distribution for RbBr have been calculated following the procedure outlined by Barron, Berg, and Morrison<sup>(22)</sup> (1957).

Recently Barron, Leadbetter, Morrison, and Salter<sup>(10)</sup> (1963) have pointed out that the calculation of Debye-Waller factors from thermodynamic data gives more accurate values for the Debye-Waller characteristic temperature  $\Theta^M$  than may be obtained by direct measurements from X-ray, electron, or neutron diffraction.  $\Theta^M$  has been calculated for RbBr.

Chapter 1.

The Theory of Heat Capacity of Solids.

The heat capacity of a solid is measured experimentally as  $C_p = \left( \frac{\Delta Q}{\Delta T} \right)_p$  where  $C_p$  is the heat capacity at constant pressure,  $\Delta Q$  is the heat input, and  $\Delta T$  is the temperature change. The heat capacity which is required for comparison with most theoretical calculations is  $C_v$ , the heat capacity at constant volume. This arises from the thermodynamic relation  $C_v = \left( \frac{\partial U}{\partial T} \right)_v$  where  $U$  is the internal energy. Using this relation, theoretical values for  $C_v$  may be obtained from the internal energy calculated on the basis of statistical mechanics.

The thermodynamic equation

$$C_p - C_v = C_p \left( 1 + \frac{\chi_s C_p}{V \beta^2 T} \right) \dots\dots\dots(1)$$

where  $\beta$  is the volume expansion coefficient and  $\chi_s$  the adiabatic compressibility, can be used to obtain values of  $C_v$  from experimental results of  $C_p$ . In equation (1) it is seen that a knowledge of the expansion coefficient is necessary for any proper comparison between theory and experiment, but later it is shown how the expansion coefficient is more intimately involved in the theory of the solid state.

As Zemansky<sup>(13)</sup> (1957) has pointed out, in general the calculation of  $U$  is extremely complicated since the total internal energy of a crystalline solid may be due to:

- 1) Translational motions of the free electrons.
- 2) Vibrations of the molecules about their equilibrium positions, called briefly lattice vibrations.
- 3) Vibrations of the atoms within each molecule.



- 4) Partial rotations of the molecules.
- 5) Excitations of the upper energy levels of the molecules.
- 6) Possible anomalous effects.

Fortunately all these effects do not take place in all solids, and some effects are only significant in particular temperature ranges.

Dulong and Petit's Law.

The simplest assumptions that can be made are that solids are isotropic, that the internal energy depends only on the lattice vibrations, and that these vibrations are simple harmonic vibrations. Now using these assumptions and the laws of classical physics it is found that the internal energy,

$$U = 3\mathcal{N}KT \dots\dots\dots(2)$$

where K is Boltzmann's constant,  $\mathcal{N}$  is the number of atoms per mole, and T is the absolute temperature; hence

$$C_v = \left(\frac{\partial U}{\partial T}\right)_v = 3\mathcal{N}K \dots\dots\dots(3)$$

In the nineteenth century Dulong and Petit stated the principle that the product of the specific heat and atomic weight of each solid element is a constant. The Dulong and Petit constant is found to be approximately numerically equal to  $3\mathcal{N}K$ , thus suggesting that the value of the specific heat of a solid depends on the lattice vibrations.

Whilst Dulong and Petit's law was found to hold for all solids at sufficiently high temperatures, Nernst<sup>(11)</sup> (1906) in his measurements found that at low temperatures many substances had values of  $C_v \ll 3\mathcal{N}K$ .



Einstein Theory of Specific Heats.

Einstein<sup>(12)</sup> (1907), applying quantum theory to the problem, made the simple assumptions that the atoms in a solid are all independent, and that each atom acts as a simple harmonic oscillator with a common frequency  $\nu$ . Thus the energy of each oscillator is given by  $\epsilon = nh\nu$  where  $\nu$  is the natural frequency,  $h$  is Planck's constant, and  $n$  can take integral values. This gives a system of non-degenerate energy levels. The probability that an oscillator will have an energy

$$\epsilon_i = n_i h \nu \dots\dots\dots(4)$$

is given by

$$P_i = \frac{e^{-\epsilon_i/(KT)}}{\sum_i e^{-\epsilon_i/(KT)}} \dots\dots\dots(5)$$

in accordance with the Boltzmann distribution law, where the summation is to be carried out over all the levels. This gives

$$P_i = e^{-n_i h \nu / (KT)} (1 - e^{-h \nu / (KT)}) \dots\dots\dots(6)$$

The mean energy of an oscillator is given by

$$\bar{\epsilon} = \sum_i P_i \epsilon_i \dots\dots\dots(7)$$

which leads to

$$\bar{\epsilon} = \frac{h \nu}{(e^{h \nu / (KT)} - 1)} \dots\dots\dots(8)$$

It follows that the molar heat is given by

$$C_v = \frac{\partial}{\partial T} (3N\bar{\epsilon}) = 3NK \frac{(h \nu / KT)^2 e^{h \nu / (KT)}}{(e^{h \nu / (KT)} - 1)^2} \dots\dots\dots(9)$$

At high temperatures this equation for  $C_v$  approaches the Dulong and Petit value of  $3NK$ . It is convenient to discuss this theory in terms of the Einstein characteristic temperature  $\theta_E$ , defined by

$$\theta_E = h \nu / K \dots\dots\dots(10)$$

Plotting  $C_v$  against  $KT/(h\nu) = T/\theta_E$  as in figure 1, shows how  $C_v$  varies with  $T/\theta_E$ . At low temperatures experimental results show  $C_v \propto T^3$  whereas Einstein's theory gives

$$C_v \propto 3NK (h\nu/KT)^2 e^{-h\nu/(KT)}.$$

Nernst and Lindemann modified Einstein's theory to include oscillations of  $\nu/2$  as well as  $\nu$ . The function they obtained for  $C_v$  gave a better fit with experimental observations but still failed at the lowest temperatures. The failure of his theory at low temperatures, which he thought to be a result of the use of a single frequency for the oscillations, led Einstein to suggest that a whole band of frequencies be employed in the theory.

The Specific Heat for a System of Oscillators with a Spectrum of Frequencies.

The evaluation of  $\bar{E}$ , the mean energy of  $N$  oscillators of different frequencies  $\nu_i$  was performed almost simultaneously by Born and von Kármán<sup>(14)</sup> (1912, 1913) and Debye<sup>(3)</sup> (1912).

In all, there will be three modes of oscillation per atom and this can be used to fix the range of the frequency distribution. If there is such a distribution of frequencies, then the mean energy of the system of  $N$  oscillators is given by

$$\bar{E} = \sum_{i=1}^{3N} \frac{h\nu_i}{(e^{h\nu_i/(KT)} - 1)} \dots\dots\dots(11)$$

where the summation is to be carried out over all the  $3N$  possible frequencies. When the distribution of wave numbers or of frequencies can be represented by an integrable function, this sum can be replaced by an integral.

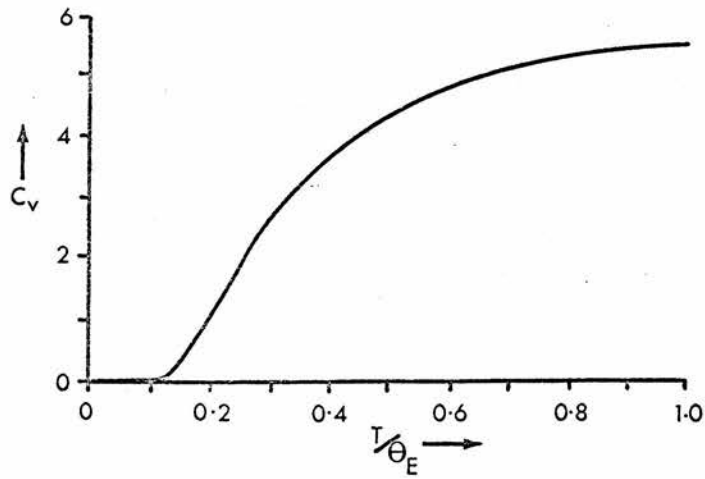


Figure 1. Plot of  $C_v$  against  $T/\theta_E$  for Einstein's Theory.

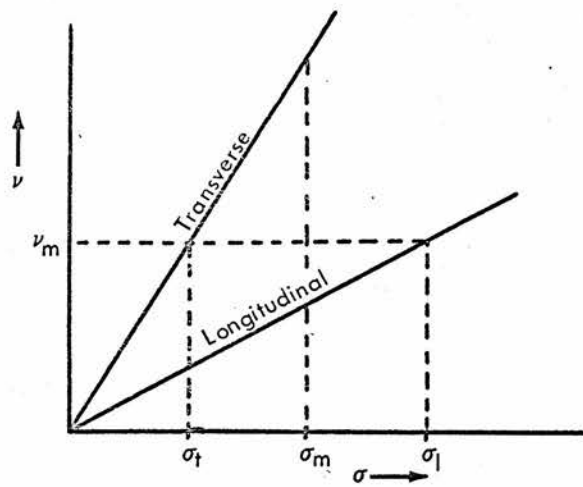


Figure 2. Plot of  $\nu$  against  $\sigma$ .

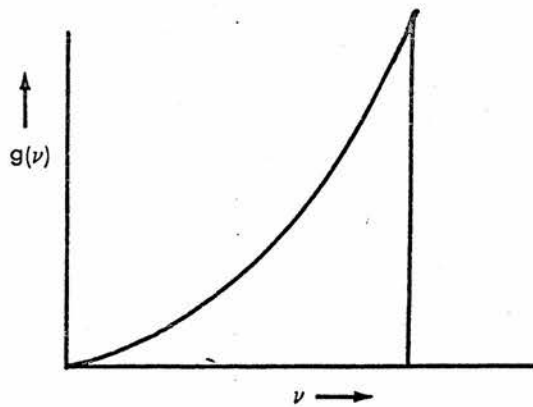


Figure 3. Plot of  $g(\nu)$  against  $\nu$ .

Thus

$$\bar{E} = \int_0^{\gamma_m} \frac{h\nu}{e^{h\nu/(KT)} - 1} g(\nu) d\nu \dots\dots\dots(12)$$

where  $g(\nu)d\nu$  is the number of modes with frequencies which lie between  $\nu$  and  $\nu + d\nu$ . The corresponding expression for the specific heat is

$$C_v = \int_0^{\gamma_m} g(\nu) \left[ \frac{(h\nu/KT)^2 e^{h\nu/(KT)}}{(e^{h\nu/(KT)} - 1)^2} \right] d\nu \dots\dots\dots(13)$$

where  $\gamma_m = \sigma_m c$ ,  $\gamma_m$  is the maximum frequency,  $\sigma_m$  the maximum wave number, and  $c$  the wave velocity.

The Choice of the Spectrum of Frequencies.

In his theory Debye<sup>(3)</sup> (1912) assumed a solid to be a dispersionless continuous medium and suggested that the total number of modes of vibration should be used to specify a cut-off (or maximum) frequency  $\gamma_0$ . Born and von Kármán<sup>(14)</sup> (1912, 1913) suggested that the total number of modes of vibration should be used to specify a cut-off wave number. This concept follows necessarily from their idea that the distribution function should be determined by a detailed examination of the dynamics of the crystal lattice atoms. These two approaches to the determination of  $g(\nu)d\nu$  are not in general identical. Consider the graph of  $\nu$  against  $\sigma$  in figure 2; the full lines represent the two kinds of wave, transverse and longitudinal, that occur in solids. Debye selected  $3N$  possible modes of vibration by choosing all the waves which have a frequency less than  $\gamma_0$ . Thus transverse modes with wave numbers  $\sigma_t$  to  $\sigma_\lambda$  are excluded, whereas corresponding longitudinal modes are included. This constitutes a serious objection to the Debye theory. The Born and von Kármán theory is more firmly based on the rigorous principles of lattice dynamics and is to be greatly preferred to the Debye treatment.

However the Born and von Kármán theory leads to expressions which are complicated, and make the evaluation of  $C_v$  very difficult. Because of these difficulties the Debye theory has been used more frequently as a criterion in interpreting specific heat data.

The Debye Theory of Specific Heats.

In Debye's theory the distribution function  $g(\nu)$  is obtained by considering the number of independent vibrations of a continuous medium. The equation obtained is

$$g(\nu)d\nu = 4\pi V \left( \frac{2}{c_t^3} + \frac{1}{c_l^3} \right) \nu^2 d\nu \dots\dots\dots(14)$$

where  $V$  is the molar volume,  $c_t$  the velocity of transverse waves, and  $c_l$  the velocity of longitudinal waves. Now the condition for the cut-off frequency  $\nu_0$  is

$$\int_0^{\nu_0} g(\nu)d\nu = 3N \dots\dots\dots(15)$$

From equations (14) and (15) it can be shown that

$$g(\nu)d\nu = \frac{9N}{\nu_0^3} \nu^2 d\nu \dots\dots\dots(16)$$

i.e.  $g(\nu) \propto \nu^2$  upto a cut-off frequency  $\nu_0$ . Figure 3 shows a graph of  $g(\nu)$  against  $\nu$ . If equation (16) for  $g(\nu)d\nu$  is substituted in equation (13) for  $C_v$  then

$$C_v = \frac{9N}{\nu_0^3} \int_0^{\nu_0} \nu^2 \left[ \frac{(h\nu/KT)^2 e^{h\nu/(KT)}}{(e^{h\nu/(KT)} - 1)^2} \right] d\nu \dots\dots\dots(17)$$

It is convenient to express  $\nu_0$  in terms of the Debye characteristic temperature  $\Theta_D$  defined by  $K\Theta_D = h\nu_D$ . The values of  $C_v$  calculated on the basis of this equation have been found to give fair agreement with experimental results. However the parameter  $\Theta_D$  has not been found to have a constant value for a given substance, but is found

to be a function of temperature. Using the Born and von Kármán theory Blackman<sup>(23)</sup> (1937) has had some success in explaining the variation of  $\theta_D$  for a simple cubic lattice using the interactions of the nearest and the next nearest neighbours, the latter being assumed to be one twentieth of the former.

Equation of State of Solids.

It is now necessary to see how a more general theory of solids is evolved, since so far only the specific heat at constant volume has been considered. Starting with the well known thermodynamic relation

$$U = F - T \left( \frac{\partial F}{\partial T} \right)_V = \left( \frac{\partial (F/T)}{\partial (1/T)} \right)_V \dots\dots\dots(18)$$

where U is the internal energy and F the Helmholtz free energy, the pressure is given by

$$P = - \left( \frac{\partial F}{\partial V} \right)_T \dots\dots\dots(19)$$

Now  $F = U_0(V) + F_D(T,V) \dots\dots\dots(20)$

where  $U_0(V)$  is the internal energy at 0°K, and  $F_D(T,V)$  is the contribution of the lattice vibrations to the free energy, calculated on the Debye theory. If it is assumed that the dependence of  $F_D$  on the volume at temperature T,  $V_T$ , is adequately described by specifying the dependence of the Debye temperature  $\theta_D$  on  $V_T$ , then from (19) and (20)

$$P = - \left( \frac{\partial U_0}{\partial V} \right)_T - \left( \frac{\partial F_D}{\partial \theta_D} \right)_T \left( \frac{\partial \theta_D}{\partial V} \right)_T \dots\dots\dots(21)$$

In the Debye theory the internal energy,  $U_D$ , due to lattice vibrations involves T times a function of  $\theta_D/T$ .

$$F_D = T f(\theta_D/T) \dots\dots\dots(22)$$

so that

$$\frac{\partial F_D}{\partial \theta_D} = f' = \frac{1}{\theta_D} \left[ \frac{\partial}{\partial (1/T)} \left( \frac{F_D}{T} \right) \right] = \frac{U_D}{\theta_D} \dots\dots\dots(23)$$

Thus from equation (21) we have the Debye equation of state

$$P = - \left( \frac{\partial U}{\partial V} \right) + \gamma_T \left( \frac{U_D}{V_T} \right) \dots\dots\dots(24)$$

where  $\gamma_T = - \frac{d(\log \theta_D)}{d(\log V_T)} = - \frac{V_T}{\theta_D} \frac{d\theta_D}{dV} \dots\dots\dots(25)$

$\gamma_T$  is known as the Grüneisen parameter at temperature T. Note that

$\gamma_\nu = \frac{d(\log \nu_\nu)}{d(\log V_T)}$  where  $\nu_\nu$  is a frequency. On differentiating equation (24),  $\left( \frac{\partial P}{\partial T} \right)_V = \gamma_T \frac{C_V}{V_T}$ . Now the linear expansion

coefficient at temperature T,  $\alpha_T$  is  $\frac{1}{3}\beta_T$ , the volume expansion coefficient at temperature T, so that for an isotropic solid

$$\alpha_T = \frac{1}{3V_T} \left( \frac{\partial V}{\partial T} \right)_P = \frac{(1/3V) (\partial P / \partial T)_V}{(\partial P / \partial V)_T} = \frac{\chi_T (\partial P / \partial T)_V}{3V_T} = \frac{\chi_T \gamma_T C_V}{3V_T} \dots\dots\dots(26)$$

where  $\chi_T$  is the isothermal compressibility. Hence

$$\gamma_T = \frac{3\alpha_T V_T}{\chi_T C_V} \dots\dots\dots(27)$$

which may be evaluated from experimental data. For an ideal substance with a Debye spectrum  $\gamma_T$  would have a constant value, assuming that  $\alpha_T \propto C_V$ , and that  $\chi_T$  is independent of temperature. On the basis of the point charge ion model, Blackman<sup>(8)</sup> (1957) predicted that the high temperature value of  $\gamma_T$ , i.e.  $\gamma_\infty$ , would lie between  $\gamma_\infty = 1.50$  and  $\gamma_\infty = 1.76$ , and that at low temperatures  $\gamma_T = \gamma_0$  would lie between  $\gamma_0 = 1.15$  and  $\gamma_0 = 1.46$ . Sheard<sup>(24)</sup> (1958), using the anisotropic continuum model and third order elastic constants, has found values



for  $\gamma_0$  and  $\gamma_\infty$ . In particular  $\gamma_0 = 0.525$  and  $\gamma_\infty = 1.57$  for KCl, and  $\gamma_0 = 1.23$  and  $\gamma_\infty = 1.60$  for NaCl.

Moments of the Frequency Distributions.

Although the Debye theory has been found very useful in describing the specific heat of solids in terms of the frequency distribution  $g(\nu)$ , it is known that this distribution is only approximately true. It is therefore important to obtain more information about real frequency spectra so that a more accurate theory of the equation of state may be evolved. It is, however, convenient to use the Debye theory as the starting point.

Let  $\overline{\nu^n}$  be the nth moment of the real frequency spectrum; then if  $\nu_D(n)$  is the maximum frequency of a Debye spectrum with the same nth moment  $\overline{\nu^n}$  then

$$\nu_D(n) = \left\{ \frac{1}{3}(n+3) \overline{\nu^n} \right\}^{1/n}, \text{ for } n > -3 \text{ and } n \neq 0 \dots\dots(28)$$

Now if the real spectrum were a Debye spectrum the values of  $\nu_D(n)$  would all be the same; thus variations of  $\nu_D(n)$  with n give some idea of the real frequency spectrum compared with the Debye spectrum.

Thirring<sup>(17)</sup> (1913) derived an expression for  $C_v$  at high temperatures in terms of  $\overline{\nu^n}$ , namely

$$C_v = 3NK \left( 1 - \frac{B_2}{2!} \frac{\overline{\nu^2}^*}{T^2} + \frac{3B_4}{4!} \frac{\overline{\nu^4}^*}{T^4} - \frac{5B_6}{6!} \frac{\overline{\nu^6}^*}{T^6} + \dots \right) \dots\dots(29)$$

where  $\overline{\nu^n}^* = (h/K)^n \overline{\nu^n}$  and  $B_2, B_4, B_6$  are Bernoulli numbers,

$$B_2 = 1/6, \quad B_4 = 1/30, \quad B_6 = 1/42. \quad \text{Barron, Berg and Morrison}^{(16)} \text{ (1957)}$$

have used the expression



$$e_D^2 = e_\infty^2 \left[ 1 - A(e_\infty/T)^2 + B(e_\infty/T)^4 - \dots \right] \dots\dots\dots(30)$$

obtained by Domb and Salter<sup>(18)</sup> (1952) from the Thirring expansion for  $C_v$ , to find the positive even moments  $\overline{v^2}$ ,  $\overline{v^4}$ , and  $\overline{v^6}$  which are given by

$$e_\infty = \frac{h}{K} \left[ \frac{5}{3} \overline{v^2} \right]^{\frac{1}{2}}$$

$$A = \frac{3}{100} \left[ \frac{\overline{v^4}}{(\overline{v^2})^2} - \frac{25}{21} \right]$$

$$B = \frac{1}{1400} \left[ \left\{ \frac{\overline{v^6}}{(\overline{v^2})^3} - \frac{125}{81} \right\} - 100A \right]$$

where  $e_\infty$  is the theoretical limiting value of  $e$  as  $T \rightarrow \infty$ . Equation (30) has been used to obtain the positive even moments in preference to equation (29) since its convergence is much more rapid.

Hwang<sup>(19)</sup> (1954) has pointed out that the moments  $\overline{v^{-1}}$  and  $\overline{v^{-2}}$  can be obtained from

$$\int_0^\infty \frac{C_v}{T^n} dT = 3NK \Gamma(n+1) \cdot \zeta(n) \overline{v^{1-n}}^*, \quad 1 < n < 4 \dots\dots\dots(31)$$

where  $\Gamma(n+1)$  is the gamma function, and  $\zeta(n)$  is the Riemann Zeta function. Barron, Berg, and Morrison<sup>(16)</sup> (1957) have pointed out that  $\overline{v_D(0)}$  may be obtained from the geometric mean frequency  $\overline{v_g}$ ,

$$\overline{v_D(0)} = e^{\frac{1}{3}} \overline{v_g} \dots\dots\dots(32)$$

where  $\overline{v_g}$  is obtained from the equation

$$S = 3NK \left( 1 - \ln \frac{h \overline{v_g}}{KT} + \frac{B_2 \overline{v^2}^*}{2 \cdot 2! T^2} - \frac{3B_4 \overline{v^4}^*}{4 \cdot 4! T^4} + \frac{5B_6 \overline{v^6}^*}{6 \cdot 6! T^6} - \dots \right) \dots\dots\dots(33)$$

obtained by Salter<sup>(20)</sup> (1955). A plot of  $\exp(S - 3NK)/3NK$  against  $T$  has a limiting slope at high temperatures of  $h \overline{v_g}/K$ . Thus the values of  $\overline{v_g}$  can be found and hence  $\overline{v_D(0)}$ .

Finally  $\nu_D(-3) = K e_0 / h \dots\dots\dots(34)$

The positive odd values of  $\nu_D(n)$  for  $n = 1, 3, 5$ , may be found by interpolation. The value  $\nu_D(1)$  gives us a value for the zero point energy,  $E_z$ , since

$$E_z = \frac{3}{2} \sqrt{h \nu^1} \dots\dots\dots(35)$$

The calculation of the moments, the maximum frequencies of the equivalent Debye spectrum, and the zero point energy are dealt with in more detail in Chapter 6.

Barron and Morrison<sup>(21)</sup> (1960) have used the moments of the real frequency spectra for some alkali halides to determine frequency spectra with the same moments and the same specific heats. The spectra obtained will not be identical to the real spectra but are better approximations than the Debye spectrum. It is problematical whether it is worth proceeding to this analysis for the present results since their data were more extensive.

Debye-Waller Factor.

Recently Barron, Leadbetter, Morrison, and Salter<sup>(10)</sup> (1963) have pointed out that  $\theta^M(T)$ , the characteristic temperature for the Debye-Waller effect, may be calculated from thermodynamic data. They have shown that at low temperatures, i.e.  $T/\theta < \text{about } 0.04$

$$\theta^M(T) = \theta_0^M \left[ 1 + 6.580 \left\{ 1 - \left( \frac{\theta_0^M}{\theta^C} \right)^3 \right\} \left( \frac{T}{\theta_0^M} \right)^2 \dots \right] \dots\dots (36)$$

where  $\theta_0^C = \theta_0$  from specific heat data, and  $\theta_0^M = \frac{h \nu_D(-1)}{K}$ ,  $\dots\dots(37)$

and that, at high temperatures,

$$\theta^M(T) = \theta_\infty^M \left[ 1 + \frac{1}{7200} \left\{ \left( \frac{\theta_\infty^C}{\theta_\infty^M} \right)^2 - 1 \right\} \left( \frac{\theta_\infty^M}{T} \right)^4 + \frac{1}{423360} \left\{ \left( \frac{\nu_D(4)}{\nu_D(-1)} \right)^4 - 1 \right\} \left( \frac{\theta_\infty^M}{T} \right)^6 + \dots \right] \dots\dots (38)$$

where  $\Theta_{\infty}^M = \frac{h \nu_D (-2)}{K} \dots \dots \dots (39)$

The results at high temperatures are corrected for thermal expansion by the equation

$$\frac{\Theta^M(T, V_T)}{\Theta^M(T, V_0)} = \left( \frac{V_0}{V_T} \right)^{\gamma} \dots \dots \dots (40)$$

where  $\gamma = \gamma(-2)$  which was obtained from

$$\gamma(n) = \frac{\int_0^{\infty} C_V T^{n-1} dT}{\int_0^{\infty} C_V T^{n-1} dT} \quad (-3 < n < 0) \dots \dots \dots (41)$$

as is shown by Barron, Leadbetter, and Morrison<sup>(22)</sup> ( to be published).

These results should be of use in the analysis of complex scattering processes.

Chapter 2.

Methods of Measuring the Linear Thermal Expansion Coefficient.

In devising a method of measuring any physical property of a substance it is necessary to keep certain minimum requirements in mind, namely sensitivity, accuracy, and working range. Several methods have been used in the past for the measurement of thermal expansion. Each method has particular limitations, such as lack of sensitivity or a limited range of temperatures over which the experiment may be carried out.

If the solid can be obtained in the form of a bar, the simplest method is to make two scratches on the bar and place it horizontally in a temperature bath. The scratches are viewed through separate microscopes, which are mounted on a rigid stand kept at constant temperature. If a change in length  $L_1-L_2$  is produced by a change in temperature  $T_1-T_2$  then  $\alpha = \frac{1}{L_1} \left( \frac{L_1-L_2}{T_1-T_2} \right)$ . The sensitivity of this method is limited to the fineness of vernier available but will not be much better than  $10^{-4}$  cm. This accuracy can be adequate if long specimens are used. Larger temperature intervals increase the percentage accuracy with which  $T_1-T_2$  and  $L_1-L_2$  may be found but if  $\alpha$  is varying rapidly with temperature this is not very satisfactory.

The Optical Lever.

In the optical lever method a beam of light falls almost perpendicularly on to a mirror and is reflected from it on to a scale. If the mirror rotates through a small angle the spot of light moves along the scale through twice the angle of rotation of the mirror. The

distance moved along the scale by the spot depends on how far the scale is from the mirror. Figure 4 illustrates a simple application of this principle to the measurement of thermal expansion. The mirror is supported on two pillars which stand on a firm base. One pillar is kept at a constant temperature ( the reference pillar ) whilst the other is heated up and expands ( the specimen ) thus causing the mirror to rotate through a small angle  $a$ . Let the specimen length be  $x$  and increase by  $dx$ ,  $L$  is the distance between mirror support points,  $S$  the shift along the scale, and  $t$  the distance from the mirror to the scale. Then

$$\begin{aligned} S/t &= \tan^{-1} 2a \\ \therefore S/t &= 2 dx / L \\ \therefore dx &= \frac{LS}{2t} \end{aligned}$$

Thus if  $t = 100\text{cm}$ ,  $L = 1\text{ cm}$ ,  $S = 0.01\text{ cm}$ , (probable limit of visual detection) then  $dx = 50 \times 10^{-6}\text{ cm}$ . which is the sensitivity of the method.

Huzan, Abbis and Jones<sup>(32)</sup> (1961), using an autocollimator with a 5 cm. long specimen, have obtained a sensitivity of  $0.3 \times 10^{-6}$  radians. Jones<sup>(33)</sup> (1960) has developed an optical lever with a sensitivity of  $10^{-10}$  radians. This very high sensitivity is obtained using the optical system shown in figure 5. A source  $S$  is focussed by the lens  $L_1$  on to the optical lever mirror  $M$ . The image of the source on the mirror is focussed by lens  $L_2$  on to the double photo-cell  $X_1 X_2$ . The lens  $L_3$  forms an image of the grid  $G_1$  on the grid  $G_2$ . The grid  $G_2$  is arranged so that one half will pass light from  $G_1$  when the other half will not pass light from  $G_1$ . This is done by having two clear strips

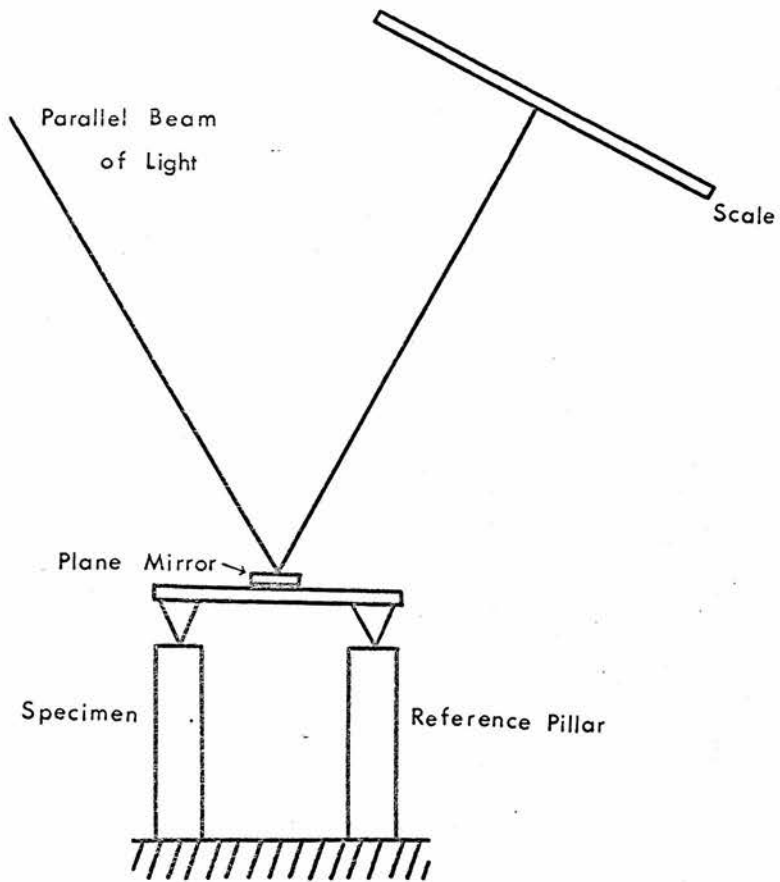


Figure 4.

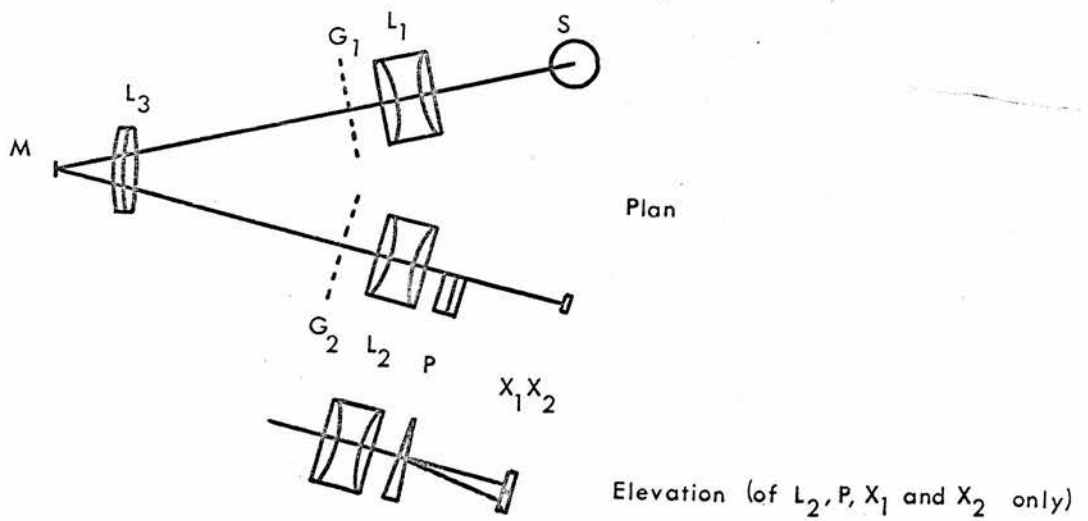


Figure 5.

in the middle of  $G_2$  and alternate dark and clear strips on either side of the middle. The narrow angled prism P deflects light from one half of  $G_2$  to fall on the lower section of the photocell. There is thus an image of S falling on each half of the photocell; as M rotates the intensity changes due to the varying degrees of overlap between the image of  $G_1$  and the two halves of  $G_2$ . This variation in intensity can be fed to a pen recorder via a suitable amplifier to indicate the change in angle of M.

One common drawback to the optical lever methods for measuring is that they require a reference pillar at constant temperature close to the specimen whose temperature is varied. If it were possible to heat the specimen uniformly without heating the reference pillar this could be used as an absolute method. However it is not often possible to heat the specimen uniformly without heating the reference pillar uniformly too, and then the method is no longer absolute. The high sensitivity has made the method attractive for some work despite these difficulties. The high sensitivity of Jones' optical lever would limit the range since only that angle between  $X_1$  fully illuminated and  $X_2$  fully illuminated can be used. For larger angles coarser grids must be used which have lower sensitivity.

#### Optical Photometer.

Andres<sup>(34)</sup> (1961) has developed a method in which length changes are transformed into changes of light intensity without using an optical lever. The working principle is the same as that involved



in Jones' optical lever. Light is passed through two closely spaced grids one of which is held fixed and the other is attached to the free end of the specimen whose expansion is to be measured. The first grid is like Jones' grid  $G_1$  and the second like Jones' grid  $G_2$ . Two photocells are placed behind the second grid, one behind each half. The output of the differentially connected photocells is a linear function of grid displacement for low intensities of illumination. The signal from the photocells is fed to a pen recorder. In the actual apparatus, which is used at helium temperatures, perspex light pipes are used to take the light down to the grids and bring it out from each half of the grids to the photocells. Length changes of about  $10^{-9}$  cm. can be detected with this apparatus. Difficulty is experienced, however, in heating only the specimen and not the framework relative to which it is to expand. It is also difficult to heat the specimen uniformly. In Andres' method the range is limited to changes of length corresponding to one grid spacing.

#### Optical Interference.

Fizeau was the first to apply the phenomenon of interference to the measurement of small changes in length; he did this about 100 years ago. The Fizeau interferometer is shown in figure 6. Parallel monochromatic light illuminates the interferometer flats  $I_1$  and  $I_2$ . The lower surface of  $I_2$  is rough ground. The upper surface of  $I_2$  is polished and the specimens stand on this surface. The two surfaces of  $I_1$  are polished, the upper one being at an angle of about  $20^\circ$  to the lower



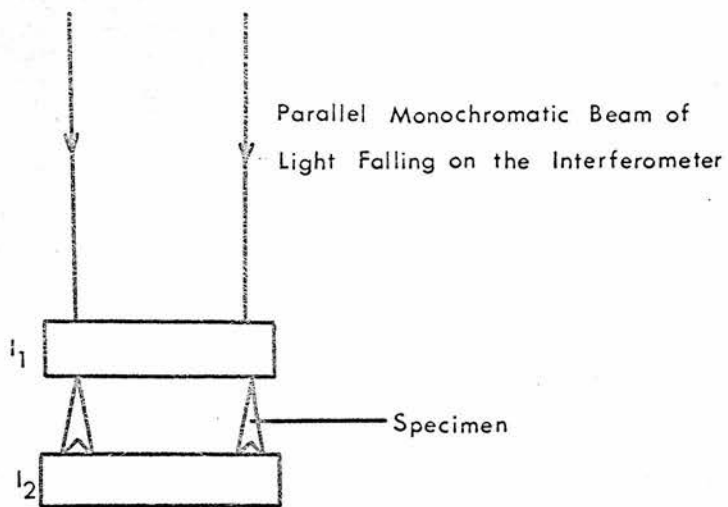


Figure 6.

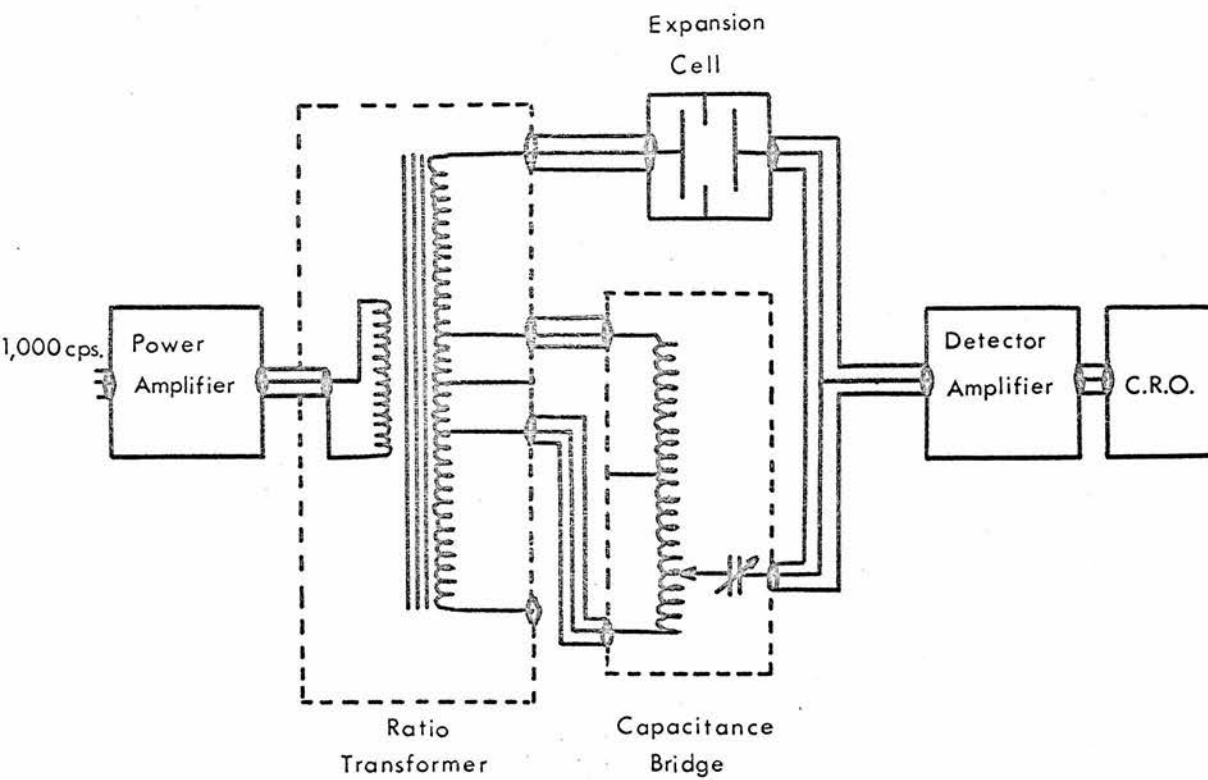


Figure 7.

surface. The upper flat rests on the specimens. The specimens are in the form of small pyramids with three feet, and are about 1 cm. high. The length of the specimens is adjusted until interference is obtained between the beam reflected from the lower surface of the upper flat and the beam reflected from the upper surface of the lower flat. Since the upper surface of the upper flat is at an angle of 20', the beam reflected from this surface does not spoil the interference pattern.

If the separation of the optical flats of the interferometer increases because of thermal expansion and if wedge fringes are being formed then the fringe pattern will move across the field of view. For each increase of separation of  $\lambda/2$ , where  $\lambda$  is the wavelength of the light being used, the pattern will shift by one whole fringe width. It is possible, using a simple telescope and crosswire, to detect movements of  $1/10$  of a fringe width, thus giving a sensitivity of  $1.5 \times 10^{-6}$  cm.

Rubin, Altman, and Johnston<sup>(35)</sup> (1954) using circular fringes were able to measure fringe shifts to within  $1/100$  of a fringe width, thus their sensitivity was  $15 \times 10^{-8}$  cm. The fractional fringe shift was found from the relation

$$\frac{(r'_{j+1})^2 - r'_j{}^2}{(r_{j+1})^2 - r_j{}^2} = \text{fraction of } \lambda/2 \text{ increase in flat separation}$$

where  $r_j$  is the initial radius of the  $j$ th ring and  $r'_j$  is the new radius of the  $j$ th ring. Whole fringe shifts were observed visually with reference to a fiduciary mark.

The Fizeau interferometer has the advantage of being a fairly sensitive method which is also an absolute method. It is possible to obtain results of high accuracy since the specimens and optical flats can be contained in a thermostatically controlled chamber remote from the observer. The experiment can be carried out over a wide range of temperatures, from near the absolute zero up to about  $600^{\circ}\text{C}$ , if the specimens will stand this range. Above  $600^{\circ}\text{C}$  the optical flats will soften if made of glass and there will be too much black body radiation.

Meinke and Graham<sup>(36)</sup> (1962), using a tubular 5 cm. specimen as a spacer for a Fabry Perot etalon, have obtained a sensitivity of  $10 \times 10^{-8}$  cm using a photomultiplier to detect the change in central fringe intensity as the specimen expands. The signal from the photomultiplier together with that from a thermocouple are fed to an X-Y plotter. The record of fringe intensity against temperature is used to determine the thermal expansion coefficient. This method has the advantage of being an absolute method but the disadvantage that readings are recorded during temperature changes with the risk of temperature gradients in the specimen. Also the electronics associated with the photomultiplier add a further complication.

#### Electrical Capacitor Methods.

The capacity  $C$  of a parallel plate capacitor is given by  $C = \frac{kA}{4\pi d}$  where  $A$  is the area of the plates,  $k$  is a constant, and  $d$  is the separation of the plates. If the separation of the plates varies, the capacity of the capacitor varies, and thus if one plate is fixed to a

specimen which expands we can measure the amount of expansion by the change in capacity.

White<sup>(38)</sup> (1961) has made the most sensitive apparatus to use this principle. He has used a three terminal capacitor in a bridge circuit with transformer ratio arms. Figure 7 shows a block diagram of the transformer bridge and figure 8, the differential expansion cell he used, the experimental cell being mounted in a thermostatically controlled specimen chamber. He has measured the expansion of materials relative to copper. Figure 9 shows the absolute cell made of copper used by White to measure the thermal expansion coefficient of copper. In operation this cell was immersed in liquid helium or liquid oxygen with helium exchange gas around the inner cylinder. The exchange gas was pumped away when the inner cylinder had cooled and the inner cylinder was then heated to the required temperature. The expansion of the cylinder C on heating changes the capacity between it and the ring R. This change in capacity was measured with the bridge described above. Hence the thermal expansion coefficient of copper was found. The advantage of this method is the high sensitivity possible, about  $0.5 \times 10^{-8}$  cm. The disadvantages are that apart from the measurements on copper it has been a relative method and that the operating range is often restricted to about  $40^{\circ}\text{K}$  for a given specimen, although a new specimen of slightly different length enables a new range of about  $40^{\circ}\text{K}$  to be covered.

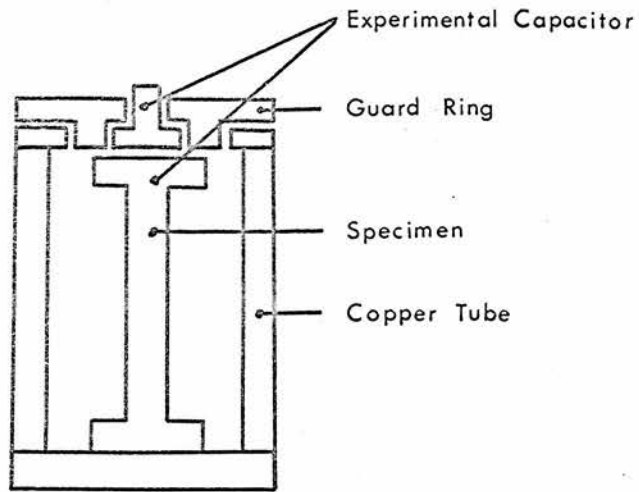


Figure 8. Differential Expansion Cell. This cell is placed in a thermostatically controlled specimen chamber.

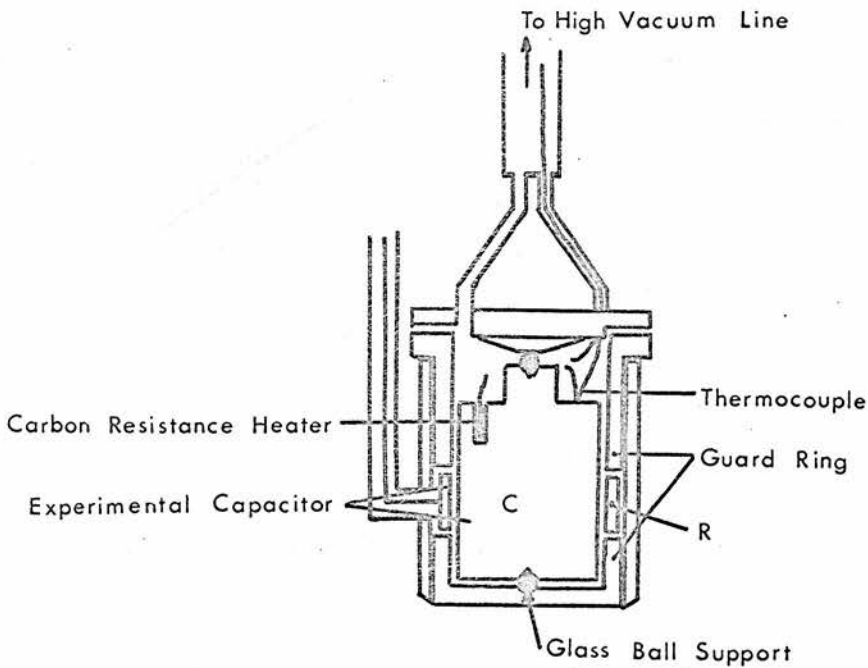


Figure 9. The Absolute Cell. This cell is immersed in the liquid refrigerant.

### X-ray Methods.

For a crystalline substance, X-ray crystallography techniques may be used to determine the lattice constants. If this is done at various temperatures, the change in the lattice constant may be determined. From this the coefficient of expansion may be found. Figgins, Jones, and Riley<sup>(37)</sup> (1956) have used Debye Scherrer photographs of a wire of aluminium at various temperatures to determine the expansion coefficient. The wire was mounted on a small copper block to which it was thermally anchored with silicone grease. A reservoir in the block could be filled with liquid hydrogen by condensation. The specimen temperature was measured with a copper-constantan thermocouple. They have been able to measure expansion coefficients down to  $5 \times 10^{-6} \text{ deg}^{-1} \text{ K}$ . Their sensitivity of about 1 in  $10^6$  is of the same order as that obtained with direct visual observations of Fizeau fringes. The X-ray method is an absolute one and it is particularly suitable if only very small specimens are available. The temperature range that can be covered is that during which the specimen has a crystalline structure.

Another advantage of the X-ray method is that the size of the unit cell is given directly and therefore the thermal expansion coefficient found is that for the unit cell. The other methods described give the thermal expansion coefficient of the bulk material. Pathak and Pandya<sup>(47)</sup> (1960) have suggested that differences between X-ray and macroscopic determinations of expansion coefficients are caused by the migration of the ions forming Schottky defects to the surface, where they form a

fresh extension to the lattice and thus increase the apparent macroscopic expansion. They further suggest that more accurate measurements would enable an estimate to be made of the extent of this migration of ions.

#### Requirements for the Present System.

The aim of the present investigation was to measure the expansion coefficients of NaF, RbBr, and CsI between 20°K and 270°K. Measurements of expansion coefficients by Yates and Panter<sup>(9)</sup> (1962) suggested that the value of  $\alpha$  (the linear expansion coefficient) would be likely to vary between approximately  $0.5 \times 10^{-6} \text{ deg}^{-1} \text{ K}$  and  $50 \times 10^{-6} \text{ deg}^{-1} \text{ K}$ . Yates and Panter had used a Fizeau interferometer with visual estimation of the fractional fringe shifts, a sensitivity of  $\frac{1}{10}$  of a fringe width being obtained. Their results indicated that if this sensitivity could be increased by a factor of 10 then it would be possible to measure linear expansion coefficients as small as  $0.5 \times 10^{-6} \text{ deg}^{-1} \text{ K}$ . If the sensitivity could be increased by a larger factor then it would mean that the Fizeau interferometer could be used for still smaller expansion coefficients, and it would be worth going down to lower temperatures. Although some of the methods outlined above have large sensitivities they could not cover the whole range required in the present work. Rubin, Altman, and Johnston<sup>(35)</sup> (1954) had claimed a sensitivity 10 times that of Yates and Panter<sup>(9)</sup> (1962) but they had used circular fringes which are difficult to obtain with soft specimens like alkali halides. It was decided to keep to wedge fringes.



If the variation of intensity across the fringes of a Fizeau interferometer is examined it is found that the intensity varies smoothly and regularly. If a photograph of a Fizeau interferometer and an index mark were taken at some steady temperature and a second photograph at some new steady temperature, then these photographs might be analysed on a microphotometer. The microphotometer traces would then show the variation in intensity across the fringes and the index mark. Thus it would be possible to find the position of the fringes relative to the index mark, and hence the fractional fringe shift between the two pictures. This is the method that has been used in the present investigation and is described in more detail in Chapters 3 and 5.



Chapter 3.

The Fizeau Interferometer.

Consider two plane reflecting surfaces, not necessarily parallel, illuminated by a point source S of quasi-monochromatic light as shown in figure 10. It can be shown (see Born and Wolf<sup>(39)</sup> (1959) for instance) that the phase difference at P between a ray reflected at A and one reflected at C is

$$\delta = \frac{4\pi}{\lambda} nd \cos\theta \dots\dots\dots(42)$$

where  $\lambda$  is the wavelength of the light, n the refractive index, d the separation of the surfaces, and  $\theta$  the angle of incidence at the lower surface.

In general, for a given point P, both d and  $\theta$  vary with the position of S, and a small extension of the source makes the range of  $\delta$  at P so large that no fringes appear. Fringes may be seen in practice by observing near normal incidence with a restricted entrance pupil to limit the area of the source used. This procedure keeps the range of d and  $\cos \theta$  small. Taking into account the phase change of  $\pi$  on reflection at one of the surfaces there are maxima of intensity for normal incidence when

$$2nd \pm \lambda/2 = m\lambda \quad m = 0, 1, 2, \dots \dots\dots(43)$$

and minima of intensity when

$$2nd \pm \lambda/2 = (m + \frac{1}{2})\lambda \quad m = 0, 1, 2, \dots\dots\dots(44)$$

Thus we see that, since  $2nd$  is the path difference for the two rays, the fringes seen are loci of points at which the two surfaces are at

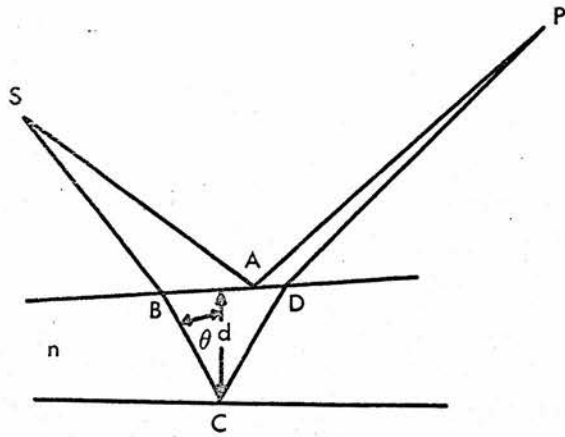


Figure 10.

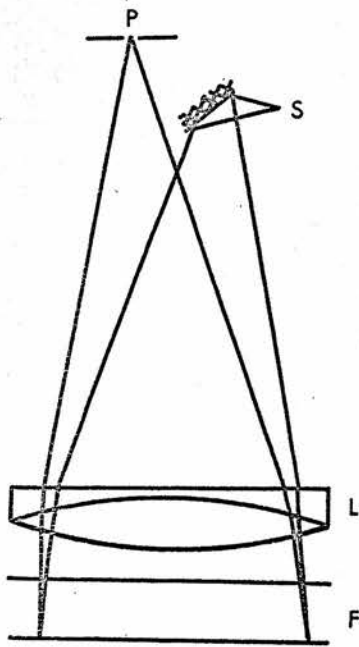


Figure 11.

constant optical path difference, and for this reason they are often called "fringes of equal thickness." The fringes seen are contours of film thickness at intervals of  $\lambda/2$ .

The conditions for distinct fringes can be satisfied simultaneously over a large area of film with the Fizeau Interferometer<sup>(40)</sup> (1862). Light from a quasi-monochromatic source S, (see figure 11), after reflection at a small mirror, is collimated by the lens L and falls on the film F at nearly normal incidence. The light reflected from the surfaces of the film returns through L and converges to an aperture P in the focal plane of L. To an eye placed immediately behind P, and accommodated for the film, fringes are visible over the whole area illuminated by L, following lines of equal optical thickness.

It can be shown mathematically and experimentally, that when fringes are viewed at normal incidence for non-parallel surfaces, the fringes are localized between the surfaces of the interferometer. Further it may be shown that the approximate tolerable angular radius of the source for distinct fringes is

$$\varepsilon \approx \frac{1}{2n'} \sqrt{\frac{\lambda n}{d}} \dots\dots\dots(45)$$

where  $n'$  is the refractive index of the surrounding media,  $n$  is the refractive index of the matter between the surfaces of the interferometer,  $d$  is the separation of the surfaces, and  $\lambda$  is the wavelength of the light being used.

The Optical System.

Figure 12 shows the optical system used during the present

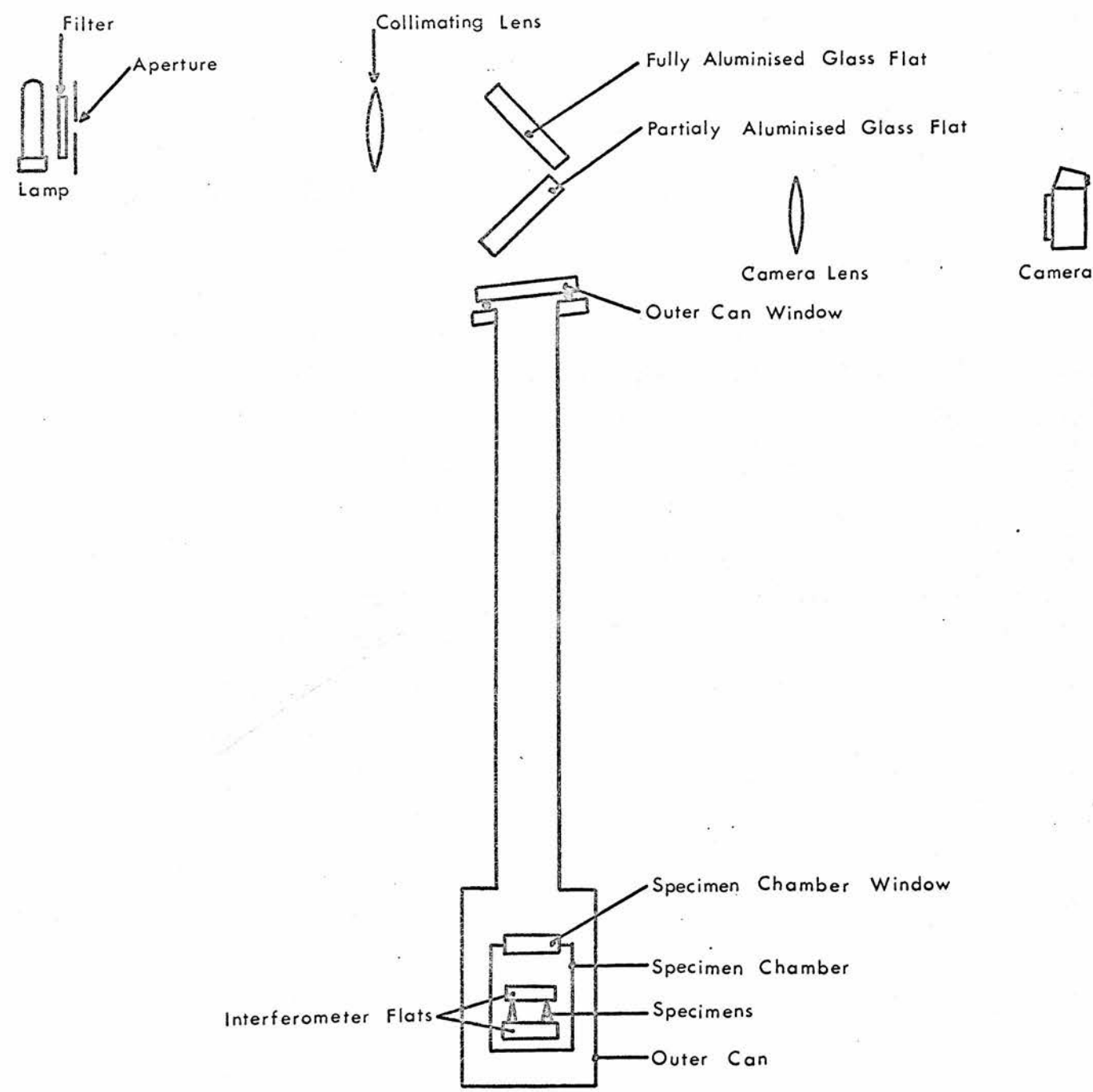


Figure 12.

investigation. Light from an Osira Cadmium Lamp passed through the filter, initially a green combination gelatin filter (Wratten No.45 and No.48 ), and later an interference filter and a No.3 Wratten filter. Both filters passed only the cadmium green line of  $5085.822\text{\AA}$ . This line was chosen as a compromise between short wavelengths for maximum sensitivity and wavelengths for which the eye has a high sensitivity. The  $5085.822\text{\AA}$  line has also the advantage of being a single line. The change to an interference filter was made because of the higher light transmission that could be obtained using it. Next the light passed through an aperture. The diameter of the aperture was chosen for a particular specimen length by using equation (45) as a guide. For a 1 cm long specimen an aperture of 1.4 mm diameter was used. The light emerging from the aperture acts as a source for the collimating lens, with the diameter of the aperture limiting the angle subtended by the source at the lens. After the collimating lens, the parallel beams of light were reflected by a fully aluminized glass optical flat down into the specimen chamber, first passing through a partially aluminized mirror at  $90^\circ$  to the first (to deflect the outcoming light to the observer). So that the outer can was an air tight container, the light next passed through the outer can window which sat on an "O" ring and then down a 1 inch diameter stainless steel pipe to the specimen chamber. The specimen chamber was also an air tight container, but since it was cooled to low temperatures the window could not be sealed by an "O" ring but instead it was araldited to a truncated copper cone,

0.008 inches thick. This design was based on that for a window for helium temperatures by Roberts<sup>(41)</sup> (1954). After the light had passed through these two windows, both of which were angled so that reflections from them were thrown off-axis, it fell on the interferometer. The upper optical flat of the interferometer was made with one surface at an angle of 40' to the other, so that there would be no unwanted reflections from the upper surface in the interference pattern. The upper flat was supported by the specimens, which stood on the upper surface of the lower optical flat. Light was reflected from both the partially aluminized lower surface of the upper flat and the fully aluminized upper surface of the lower flat. The optical flats of the interferometer were aluminized as described in order to increase the light reflected from the interferometer, meanwhile improving fringe visibility, so that the fringes could be seen more clearly, and so that the exposure time for photographs of the fringe pattern should be as short as possible. The specimen lengths were adjusted before the apparatus was sealed up so that about 6 - 8 fringes were formed across the 2.7 cm. diameter of the upper optical flat. The specimen chamber was supported in the outer can by three 2 mm. diameter german silver tubes, which had levelling screws at one end. The light coming out from the interferometer was reflected by the half aluminized mirror outside the outer can, towards the camera lens, which formed an image of the interferometer, and thus the interference pattern, in the camera. The inside of the one inch diameter stainless steel tube

was lined with matt black paper, otherwise some light would have been reflected from it into the camera and would have spoilt the image of the interference pattern. The whole system from the aperture to the outer can window, and then to the camera, was contained in a light tight box which had stops after the collimating lens and the camera lens. The inside of this box was painted matt black.

#### The Index Mark.

As mentioned in chapter 2, it is necessary to have an index mark in the system against which fringe shifts may be measured. Yates and Panter<sup>(9)</sup> (1962) used the crosswires in their telescope as the index. This suggested the idea that was tried first. An illuminated slit was placed below the level of the collimating lens so that the camera lens formed an image of the slit in the camera outside the area of the fringe pattern. The slit could be rotated so that it was parallel to the fringes. This arrangement gave photographs that could be conveniently analysed on the microphotometer. But later it was found that on changing the temperature of the specimen chamber there were small movements of the specimen chamber, and thus of the fringes relative to the index mark. This made an index mark which was remote from the specimen chamber unsatisfactory for the accurate measurements of expansion coefficients. Therefore an index mark actually in the specimen chamber was required. It was found impossible to adjust the lengths of the specimens so that the fringes would always lie in one direction, and therefore it was realised that the index mark should be available for use, regardless



of fringe orientation. This could have been arranged by having a rotatable index line in the specimen chamber, but this would have raised difficulties with vacuum seals.

It was then decided to use a circular index mark which would not need to be aligned with the fringe pattern. A 1 mm. diameter, fully aluminized spot was therefore deposited by vacuum evaporation in the centre of the lower surface of the upper optical flat, whilst the upper surface of the lower optical flat had a 3 mm. diameter piece of black insulating tape put on it, at the centre. Thus, when scanning with the microphotometer, the central aluminized spot was always entered from the same background. The absence of such a background would have given rise to difficulty in locating the centre of the index mark for some possible fringe positions. The fringes could still be analysed by the microphotometer outside the 3 mm. diameter, matt, black spot. Thus the fringe position could be measured to a fiduciary mark.

#### Flatness of the Optical Flats.

Ideally the surfaces of the optical flats of the interferometer would not deviate from plane surfaces. It is impossible to attain this ideal in practice. Any variation from a plane surface for the flats will alter the spacing of the fringes, and variations in fringe spacing lead to inaccuracies in determining the fractional fringe shifts. The manufacturers of optical flats usually specify the flatness of their optical flats in terms of the fraction of a wavelength that the surface is different from a plane. The wavelength of light



referred to is usually about 6000 Å. The interferometer flats were flat to  $\lambda/20$  and all the other windows and mirrors were flat to  $\lambda/5$ . The interferometer flats were 0.5 cm. thick.

A calculation for the bending of the interferometer flats under their own weight was made. Timoshenko and Woinowsky-Krieger<sup>(42)</sup> (1959) have shown that for a disc of radius  $a$ , supported at three points  $120^\circ$  apart the deflection at the centre is  $w = 0.0362 \frac{P a^2}{D}$

when the load is uniformly distributed, where  $P = \pi a^2 q$ ,  $q$  is the intensity of the load at any point, and  $D = \frac{E h^3}{12(1-\eta)^2}$ , where  $E$  is

Young's modulus of elasticity,  $h$  is the thickness of the flat, and  $\eta$  is Poisson's ratio. For the quartz plates of the interferometer, 2.7 cm. in diameter and 0.5 cm. thick, the deflection,  $w$ , is  $0.627 \times 10^{-10}$  cm.

The windows and mirrors used were about 1 cm. thick and 5 cm. in diameter and would deflect under their own weight by  $1.54 \times 10^{-10}$  cm. These deflections are several orders of magnitude smaller than the best flatness obtainable so the deflection of the flats from a plane under their own weight can be neglected.

The interferometer flats must be free to expand and contract on heating and cooling because any restraint would distort the surfaces temporarily. The index system described above however requires that the two flats be concentric within about 1 mm.; a restraint with this freedom does not conflict with the above requirement for space to expand. The flats were initially located relative to each other by a tubular basket in which they were free to slide up and down during the

expansion of the specimen. The basket allowed sufficient clearance round the flats for the differential contraction on cooling.

The Variation of Path Difference with Gas Density.

Equation (44) for a maximum of intensity in the fringe pattern involves on the L.H.S. the path between the two optical flats. This is equivalent to twice the separation of the flats times the refractive index of the gas between the flats, i.e.  $\Delta = 2nd$ . Now in order to measure the thermal expansion for a temperature interval  $T_1 - T_2$  the change in length  $d_1 - d_2$  is needed, since  $\alpha = \frac{d_1 - d_2}{d_{295}(T_1 - T_2)}$ ,

where  $d_{295}$  is the specimen length at room temperature. The observations of the fringe pattern as the temperature changes from  $T_1$  to  $T_2$  give the change in path difference  $\Delta_{1,2} = 2(n_1 d_1 - n_2 d_2)$ . If the refractive index was that for a vacuum, i.e. unity, the change in path difference would be exactly twice the change in length. However in the present apparatus helium exchange gas was used in the specimen chamber to ensure thermal equilibrium between the specimens and the resistance thermometer. Therefore corrections were made for the presence of this gas.

The Lorenz-Lorentz Law, (see Longhurst<sup>(43)</sup> (1957) for instance) states that  $\frac{n^2 - 1}{(n^2 + 2)\rho} = \text{a constant}$ , where  $\rho$  is the density and  $n$  the refractive index. This may be rewritten

$$\left( \frac{n-1}{\rho} \right) \left( \frac{n+1}{n^2+2} \right) = \text{a constant.}$$

Now for a gas the refractive index does not differ widely from unity, so that the second factor is almost constant. Hence for a gas

$$\frac{n-1}{\rho} = \text{a constant.}$$

This is known as the law of Gladstone and Dale. Thus if the refractive index for some particular density is known, the refractive index at some other density may be found. It is simple to find the density of gas present at any temperature by noting the temperature and pressure of the exchange gas. The resistance thermometer gave the temperature, and a butyl phthalate manometer was connected to the specimen chamber to measure the pressure. The value of  $n$ , 1.0000350 at 0°C for a standard atmosphere, used in the calculations, was obtained by using the Cauchy equation  $(n - 1) = A(1 + \frac{B}{\lambda^2})$  where  $\lambda$  is the wavelength used, and A and B are constants. The values of A and B were found in Kaye and Laby<sup>(44)</sup> (1947).

Experimental Difficulties Experienced with the Optical System.

The apparatus used was that described by Yates and Panter<sup>(9)</sup> (1962) except for modifications made to the system to incorporate the camera and the specimen chamber manometer. The first material for which the expansion coefficient was measured was copper, which was done as a check on the apparatus. The results are discussed in the next chapter. The copper specimen was made from a 1 inch diameter cylinder, the inside of which was turned away until there was a  $\frac{1}{16}$  inch walled tube. A section 1 cm. long was cut off and this was filed until there were three feet 120° apart at each end. This specimen was then vacuum annealed at 700°C for 10 minutes. The final adjustments of length were made with very fine emery paper. The fringe system obtained with this specimen stayed in the same direction and had the same fringe spacing

throughout the measurements.

After the measurements on copper, three rectangular shaped specimens of CsI about 1 cm. long and 0.4 cm. square were put into the interferometer. Each of these specimens had three feet ground from their bases which stood on the lower optical flat. The upper optical flat was supported by the slightly spherical top of each specimen. Difficulties were experienced immediately measurements began. The fringe pattern obtained did not remain in the same direction, and the number of fringes changed when the temperature changed, thus making it impossible to use the sensitive photographic technique to measure the thermal expansion. At first it was thought that these difficulties were caused by vibration. The vacuum lines were therefore re-arranged to transmit less vibration, and the electrical equipment was taken off the framework which supported the interferometer. This however did not cure the difficulties.

The following observations on the fringe system were made:

- 1) At a constant temperature the fringe pattern stayed exactly the same over a period of hours.
- 2) If the temperature was raised or lowered from one equilibrium temperature to another equilibrium temperature there was almost invariably a change in fringe spacing or a change of orientation of  $10^{\circ}$  -  $15^{\circ}$ , or both, for a  $10^{\circ}\text{K}$  change in temperature.
- 3) When the temperature was increased the change in orientation observed was usually clockwise but on some occasions, for no apparent reason, there would either be no rotation or the rotation would be anti-clockwise.

- 4) If the temperature was raised to a new equilibrium temperature and then allowed to return to the initial equilibrium condition, a rotation of the pattern or change in fringe spacing might occur during warming up but not reverse on cooling down.
- 5) A sharp knock with a small hammer on the specimen chamber support would sometimes return the fringe pattern to the form it had before the temperature was raised.

If any systematic effect had been noted in the changes of the fringe pattern it would have suggested that there was some difference in the expansion coefficients of the three specimens. This seemed unlikely since the impurities were of the order of parts per million. The variation in impurities was confirmed not to be the cause of the changes of the fringe pattern by the random nature of these changes. It was thought that these changes in fringe pattern might be caused by the upper optical flat, or by the small brass tube which was on top of the flat (for stability) rubbing or even catching on the cage (which limited the movement of the flat and tube horizontally to 1 mm.). The cage was necessary to ensure that the fully aluminized mark on the upper optical flat was over the matt black area on the lower optical flat.

It was decided to ensure the location of the optical flats another way which would eliminate any possibility of rubbing. Figure 13 shows the modified specimen chamber. The lower optical flat was placed between two rings which were connected by three thin foil strips; this

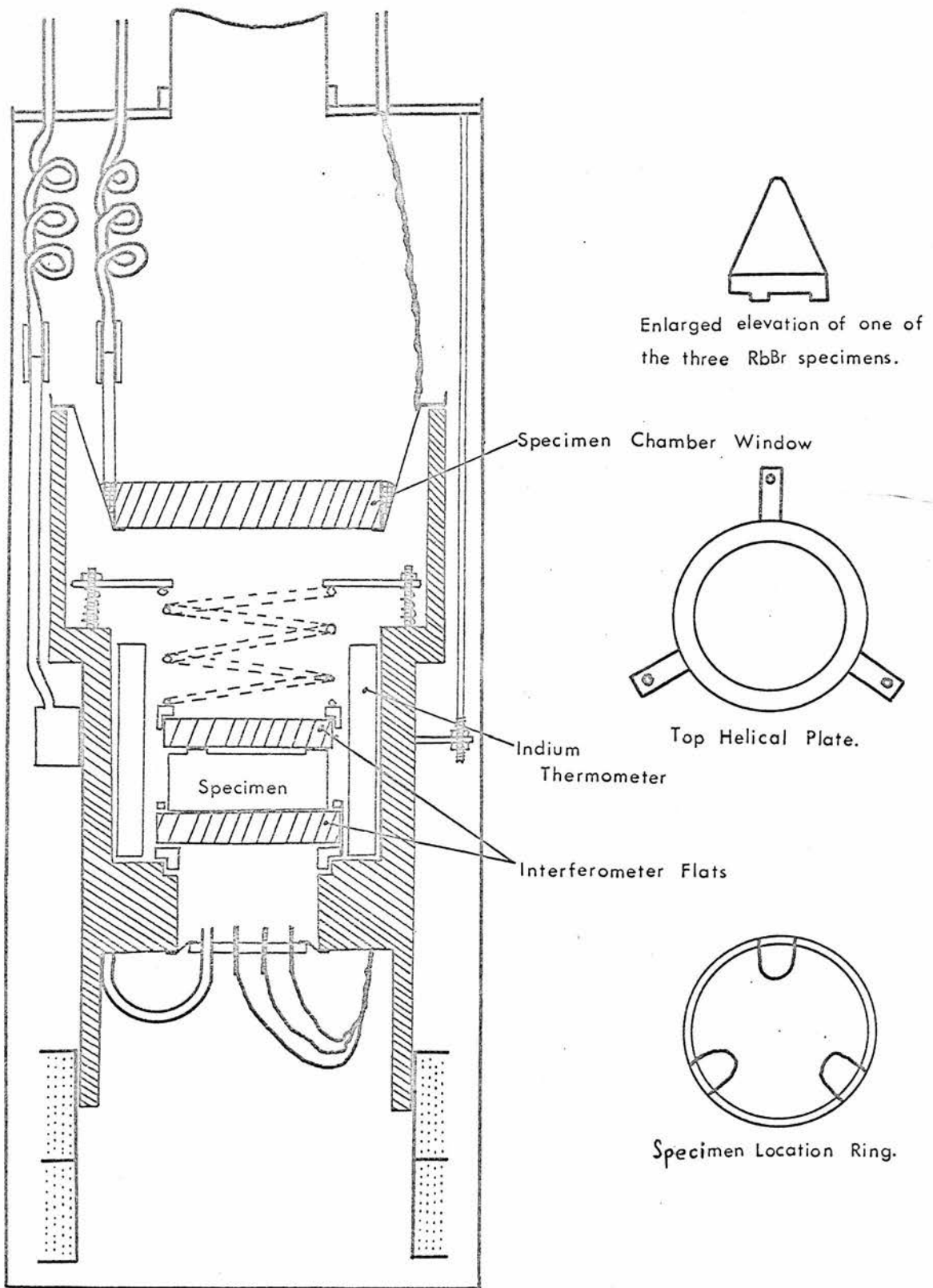


Figure 13. The Specimen Chamber and the Outer Can.



restricted the lateral movement of the flat to 1 mm. (enough to allow for differential contraction on cooling). The lower ring was then located in the specimen chamber by a circular groove. Thus the lower flat was fixed to within about 1 mm. relative to the specimen chamber. The specimens were then placed on the optical flat, in three U shaped wires which were attached horizontally to the perimeter of the upper ring. The wire U's allowed the crystals a clearance of 1 mm., but fixed them sufficiently to form a roughly equilateral triangle. The upper optical flat was then placed on the specimens and a grooved ring ( 1 mm. larger in diameter than the optical flat to allow for differential contraction on cooling) was put on top of the flat. The grooved ring or collar was connected to the lower end of a helical spring. The upper end of the helical spring was fixed to another ring which had three projections which were connected by spring loaded levelling screws to the specimen chamber. Thus the upper optical flat was also fixed, within 1 mm., relative to the specimen chamber. Since the two flats were aligned the index mark on the top flat fell over the matt black area on the lower flat.

This modified specimen chamber, shown in figure 13, was first used with three specimens of RbBr which took the form shown. The RbBr crystals had been kindly grown by Dr. R.W.H.Stevenson of Aberdeen University, after considerable difficulty, using very pure RbBr powder which was obtained from L.Light and Co. The same changes in fringe pattern described above were again experienced. These changes in fringe pattern had not been noticed with the tubular copper specimens, and so tubular

specimens of the alkali halides NaF, RbBr, and CsI were obtained. The use of tubular specimens of the alkali halides resolved all the difficulties with changes in fringe pattern, and it was at last possible to use the photographic technique to obtain more accurate results for the expansion coefficients. It was inferred that the changes in fringe pattern were due to small movements of the crystals from the vertical, caused by the lateral expansion or contraction of the optical flats. The tubular specimens of the alkali halides were about 1 cm. long and had one end polished flat and the other filed so that three feet projected about  $\frac{1}{2}$  mm., at  $120^\circ$  to each other; the final adjustments of length were made with very fine emery paper on these feet. The inside diameter of the specimens was about 1.8 cm., and the outside diameter was about 2.7 cm.

Further details of the experimental procedure, the photographing of the fringe pattern, and the analysis of the photographs are given in Chapter 5.



## Chapter 4.

### Temperature Measurement.

In investigations concerned with the temperature dependent properties of solids, the temperature measurement is of prime importance. The accuracy and sensitivity required depend on the rate of change with temperature of the property being studied. Consideration must also be given to the time taken to obtain a temperature reading, the space taken up by the thermometer, the repeatability of the readings, and the ease with which readings can be taken. In order to determine the expansion coefficient of a solid it is necessary to know its length  $d_1$  at a temperature  $T_1$  and its new length  $d_2$  at some other temperature  $T_2$ , the linear expansion coefficient being defined by  $\alpha = \frac{d_1 - d_2}{d_{295}(T_1 - T_2)}$ , where  $d_{295}$  is the specimen length at room temperature.

There are several methods by which one may measure temperatures between  $20^\circ\text{K}$  and  $270^\circ\text{K}$ . The constant volume gas thermometer is an absolute instrument that can be both sensitive and accurate, but which is rather slow in operation. Vapour pressure thermometers can be used for parts of the temperature range where suitable substances exist; however the whole range cannot be covered in this way. Thermocouples have been developed that will cover the range  $20^\circ\text{K}$  to  $270^\circ\text{K}$ , but the thermal e.m.f.s are usually rather small and the final accuracy obtained for a temperature interval of  $10^\circ\text{K}$  is rather low. Resistance thermometers, which depend on the variation of resistance of a conductor with temperature, are well suited to temperature measurement. The variation of resistance with temperature is usually found first by using a gas

thermometer against which the resistance thermometer is calibrated. Resistance thermometers are fairly rapid in use and more sensitive and reproducible than thermocouples. The reproducibility of a resistance thermometer is usually very good if care is taken to mount the wire so that it is not strained during cooling down or warming up. Another feature of resistance thermometers is that they give the average temperature over the space that they occupy.

#### Choice of Resistance Thermometer Material.

Platinum is frequently used for resistance thermometers, but it requires high temperature annealing after it has been wound. White and Woods<sup>(25)</sup> (1957) have suggested the use of indium for low temperature thermometry. At low temperatures indium has a higher value of  $\frac{1}{R_{273}} \left( \frac{dR_T}{dT} \right)$  than platinum, where  $R_{273}$  is the ice point resistance and  $R_T$  is the resistance at temperature T. Another advantage of indium is that it self anneals at room temperature. The indium thermometer of Yates and Panter<sup>(9, 26)</sup> (1962, 1961) had shown a systematic drift in ice point resistance, which was attributed to mechanical shocks. A new thermometer mount was designed by James and Yates<sup>(27)</sup> (1963) to provide a completely strain free and shockproof support for the indium wire. A copy of this paper is attached at the end of the thesis. Plate 1 shows the perspex mount made for the indium thermometer. The resistance of the thermometer was found by measuring the drop in potential across it when a current of 10 mA. was passing through it. The current was adjusted so that the potential drop across a standard ohm was 10 millivolts. The

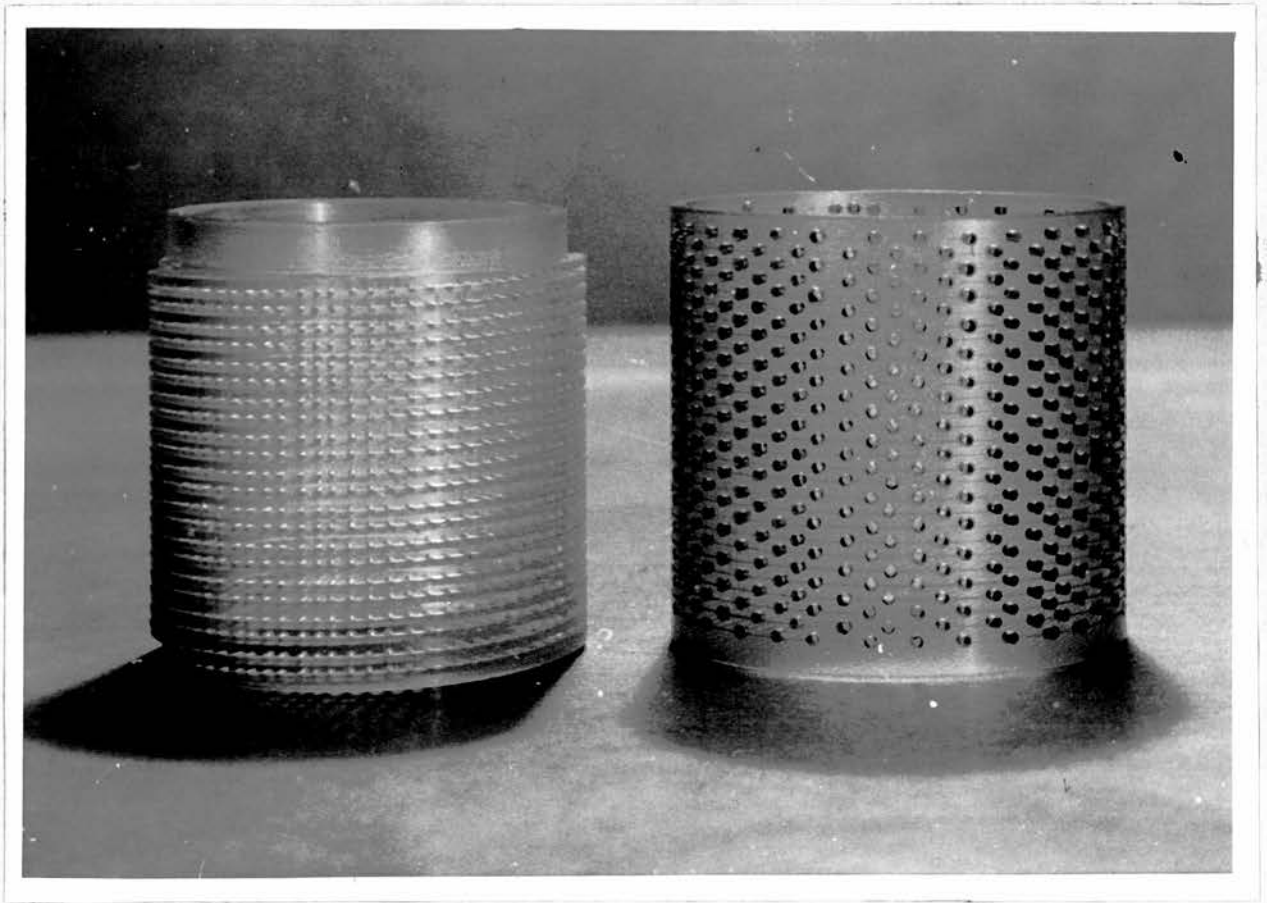


Plate 1. The Indium Thermometer Mount.

potentiometer circuit and associated resistance thermometer circuit are shown in figure 14. The results of Yates and Panter<sup>(26)</sup> (1961) showed that for different specimens individual calibration was desirable. It was decided therefore to calibrate the indium resistance thermometer against a constant volume helium gas thermometer.

#### The Gas Thermometer.

A constant volume helium gas thermometer was chosen because it provided the most convenient means of calibrating the indium resistance thermometer. Also there were sufficient data of the virial coefficients of helium available, and it was realised that there would be no difficulties with the helium liquefying in the thermometer bulb as there would be with hydrogen. The thermometer bulb, volume approximately 11 cc., was made from sterling silver, so that there should be no difficulties with adsorption of the thermometer gas. As a preliminary, the thermal expansion of an adjacent piece of sterling silver was measured, using the technique of Yates and Panter<sup>(9)</sup> (1962),— i.e. the unmodified apparatus. The results for sterling silver are shown in graph 1, and the smoothed values for the thermal expansion given in table 2.

Care was taken in making the thermometer bulb to use the minimum of flux and after it was made the inside was thoroughly cleaned of flux. Figure 15 shows a section through the bulb. The gas thermometer bulb was mounted in the specimen chamber of the apparatus of Yates and Panter<sup>(9)</sup> (1962), the specimen chamber window being replaced by a copper disc during the thermometer calibrations. The thermometer bulb was supported by the  $\frac{1}{4}$  inch diameter silver tube projecting out of it,

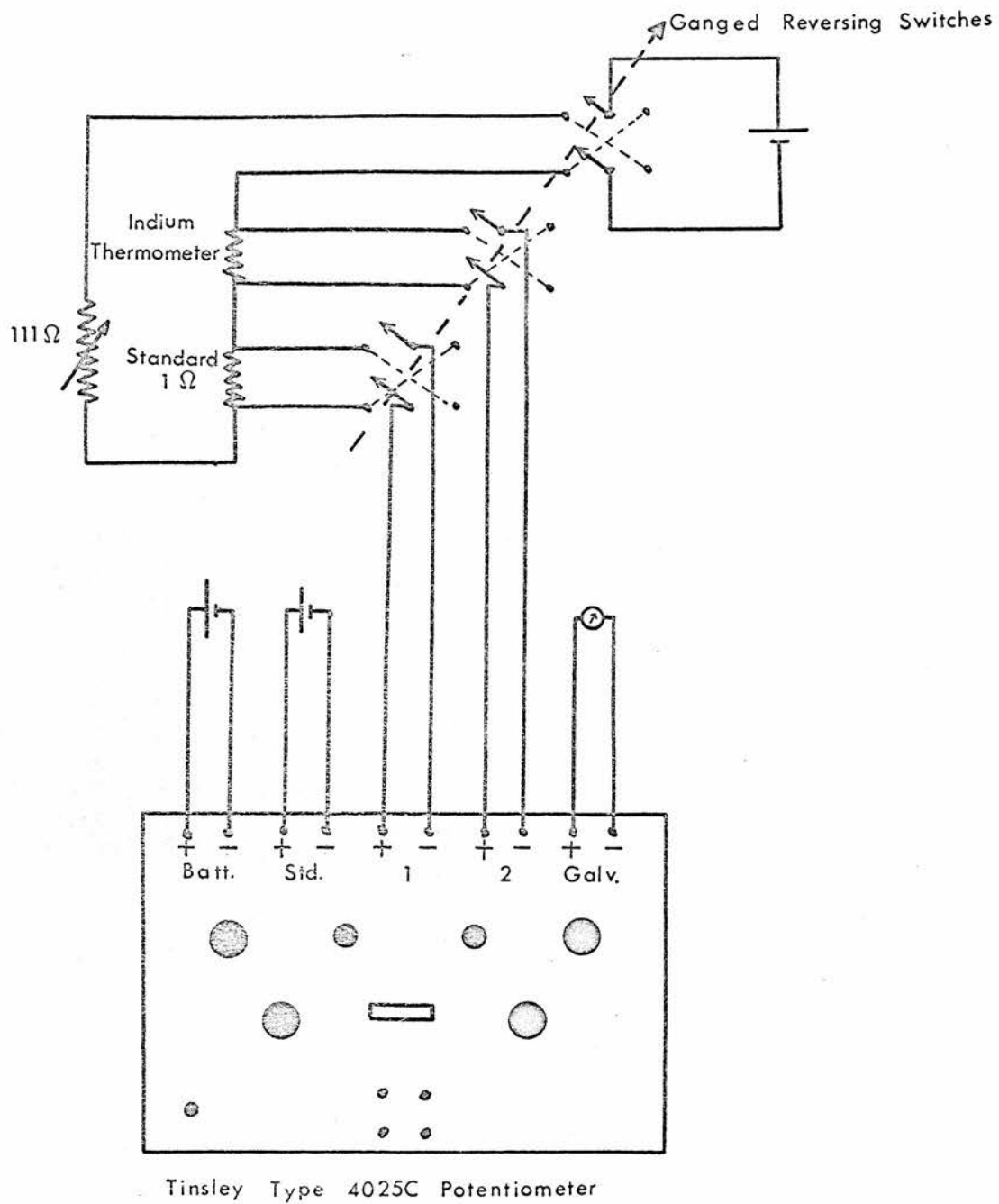


Figure 14. The Potentiometer and Resistance Thermometer Circuit.

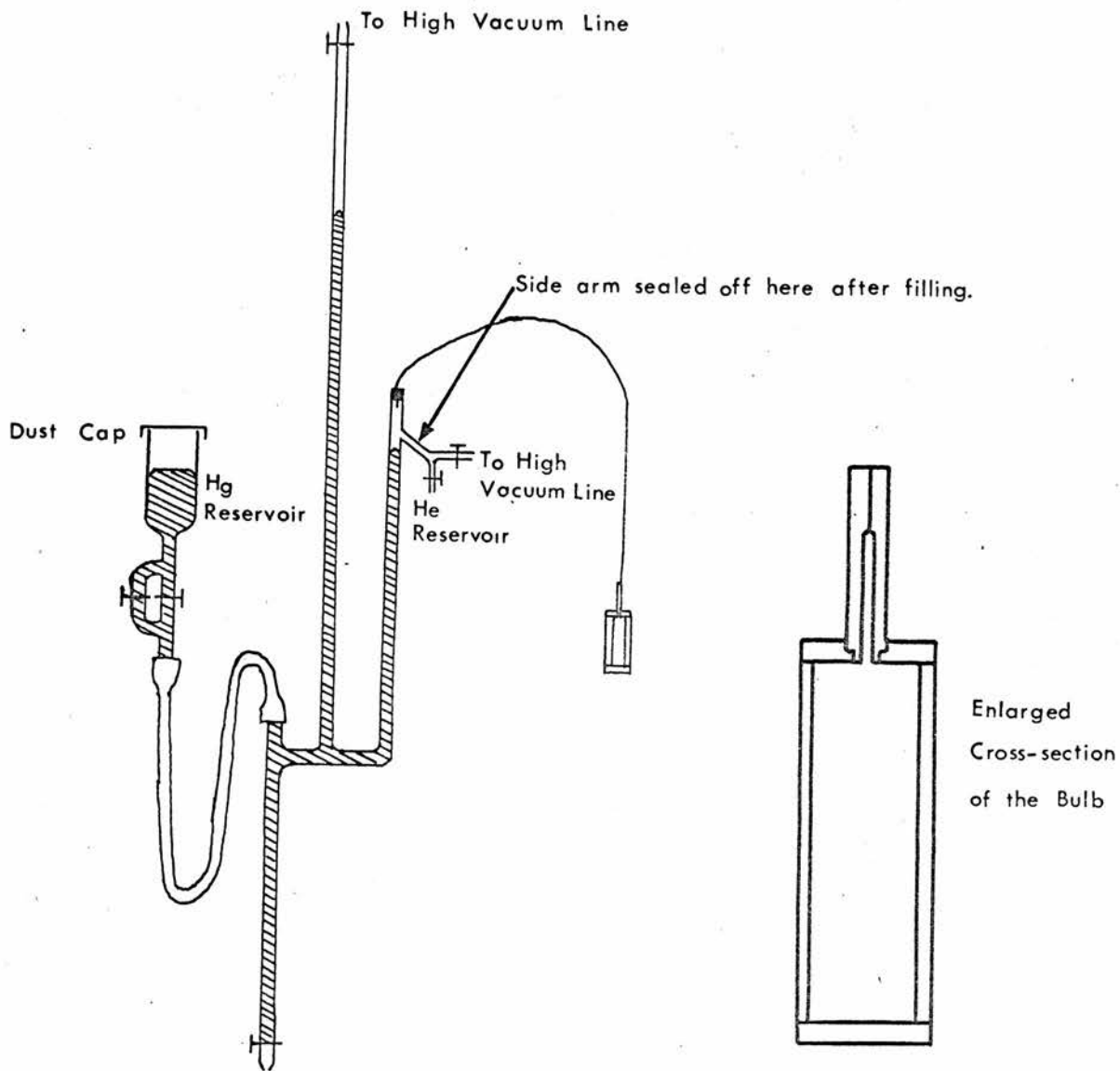


Figure 15. The Gas Thermometer and the Gas Thermometer Bulb.

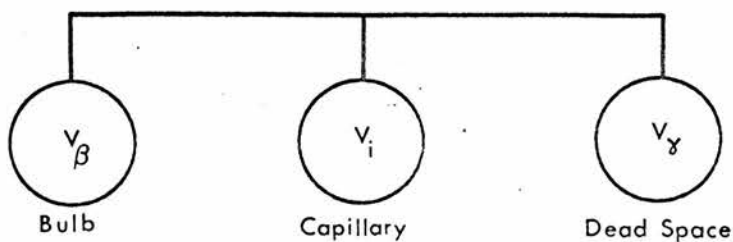
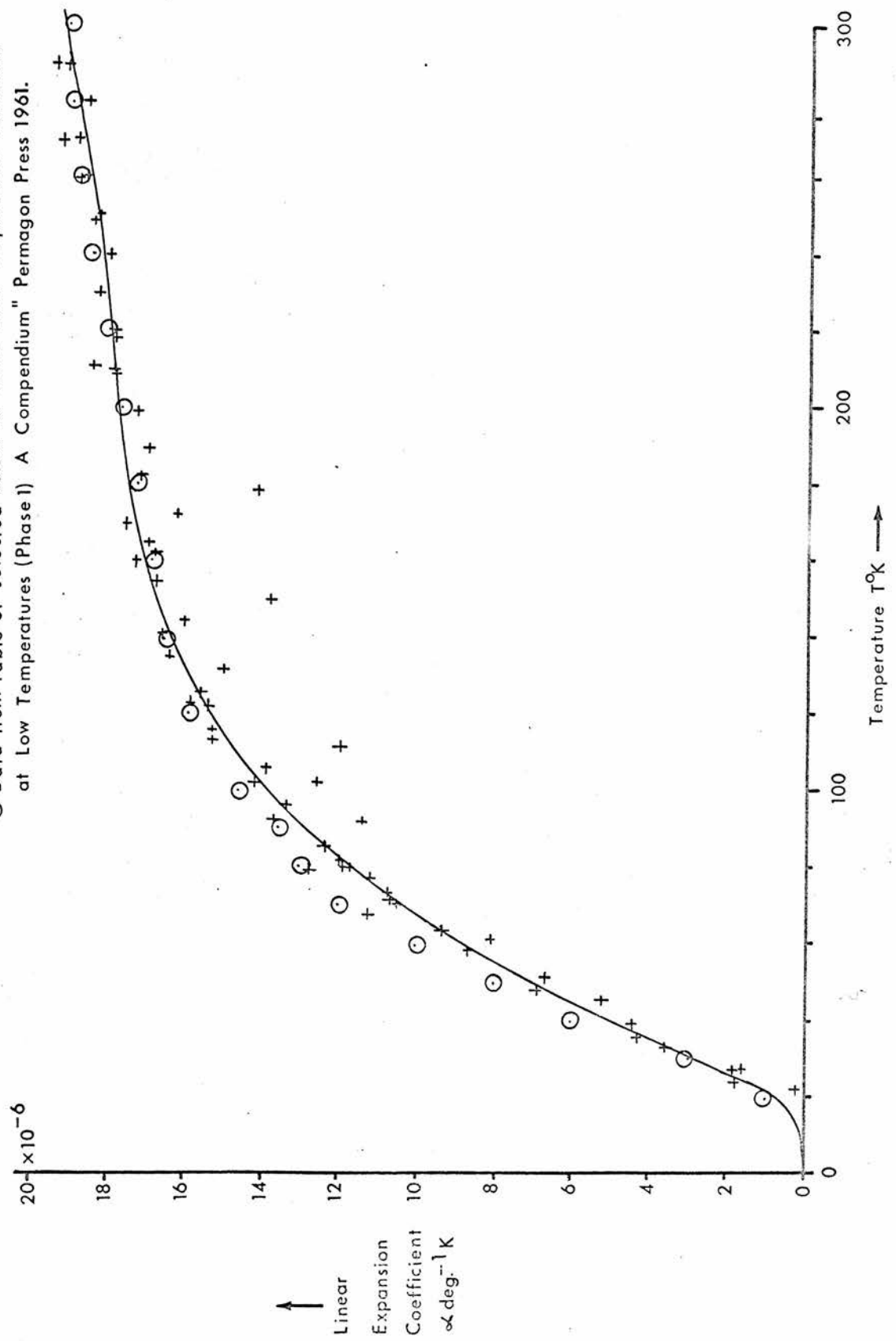


Figure 16. Diagrammatic Representation of the Gas Thermometer.

Graph 1. The Linear Thermal Expansion Coefficient of Sterling Silver.

+ Present Results

⊙ Data from table of selected values for silver from "Properties of Materials at Low Temperatures (Phase I) A Compendium" Pergamon Press 1961.



from the copper disc. The specimen chamber was filled with exchange gas during the thermometer calibration, in order to ensure good thermal equilibrium between the gas thermometer and the resistance thermometer, which was concentric with the gas thermometer. The specimen chamber was hung inside an evacuated chamber, referred to as the outer can, which was surrounded by the refrigerant, either liquid nitrogen or liquid hydrogen. The temperature of the specimen chamber could be adjusted by the thermostatic temperature controller of Yates and Panter which held temperatures steady to within  $0.01^{\circ}\text{K}$ .

The thermometer bulb was connected to the manometer by a german silver capillary tube, 0.02 cm. bore and 0.01 cm. wall thickness, (see figure 15 for a diagram of the manometer). An iron plug was araldited to the glass of the manometer with a small eccentric hole drilled for the capillary tube, and an iron spike projecting from the centre into the manometer tube so that the mercury could always be brought back to the same level. Since helium gas diffuses through pyrex glass it was necessary to use soda glass in the construction of the manometer. Pressures between 0 and 50 cm. Hg were measured with a cathetometer and pressures above 50 cm. Hg were measured with the aid of a mirror backed scale. Plates 2 and 3 show the assembled gas thermometer after it had been filled with helium.

The mercury for the manometer was freshly distilled in a vacuum distillation column. The soda glass of the manometer was cleaned with chromic acid, nitric acid, and the washed out thoroughly with distilled



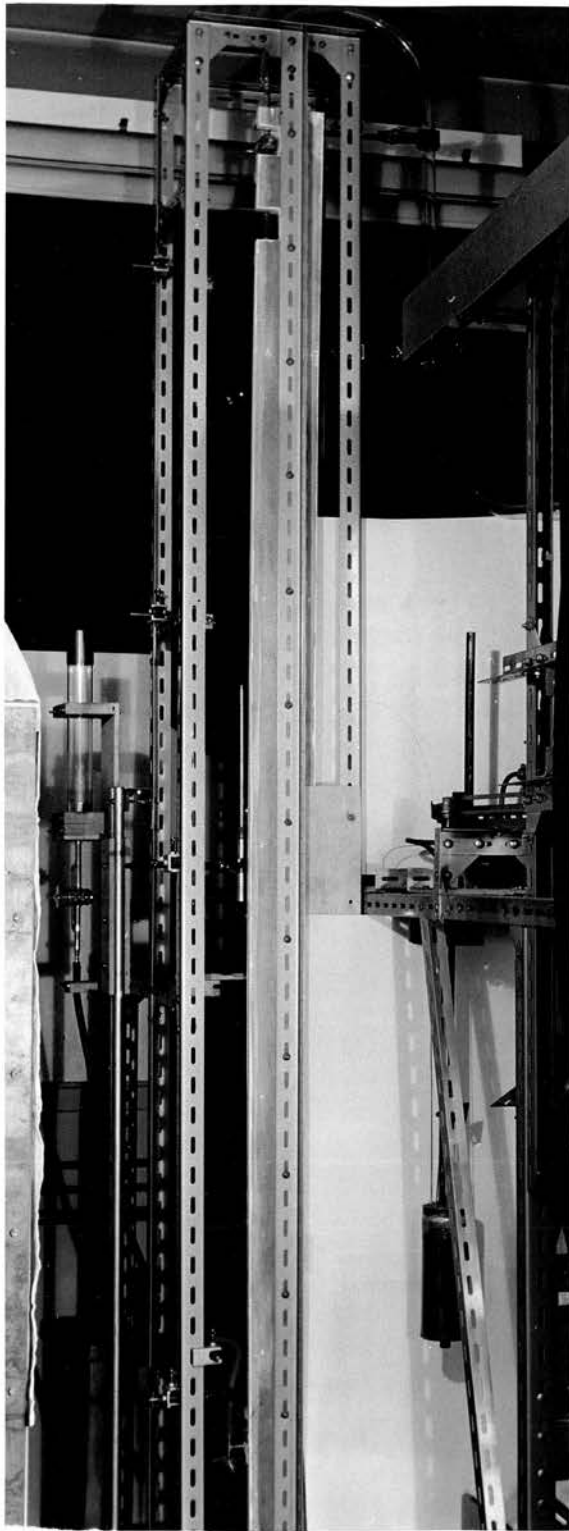


Plate 2. The Gas Thermometer - General View.

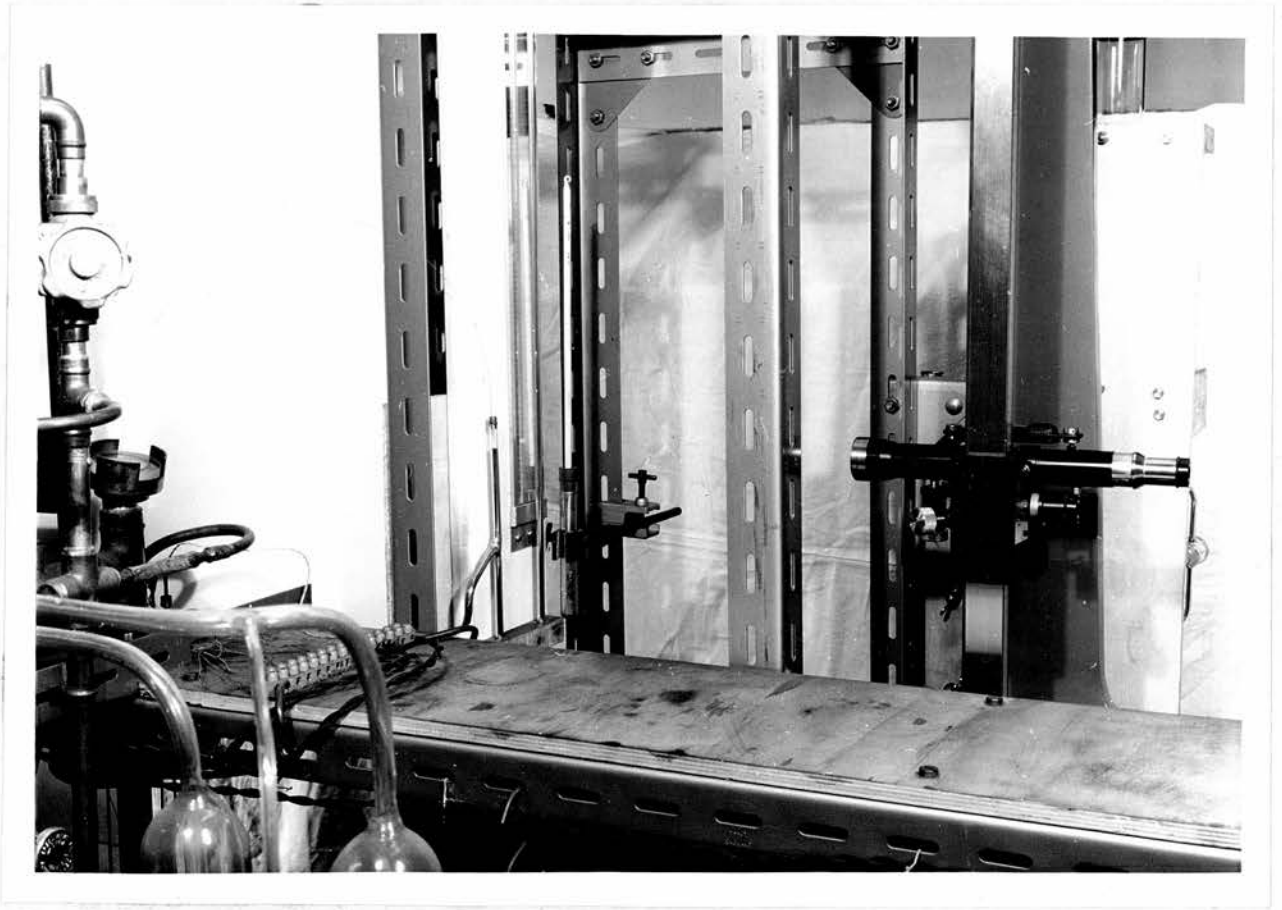


Plate 3. The Gas Thermometer - the Telescope and the Manometer.

water. After the manometer had dried out the thermometer bulb was connected up as described above. The various glass taps were then greased and put in place. The whole system was then pumped out over 48 hours. The mercury was put into the reservoir, care being taken not to trap any air. Small quantities of mercury were then admitted to the system while it was still being pumped, the reservoir being at its lowest level. The mercury level was allowed to reach half way up the metre long thermometer bulb arm of the manometer by adjusting the level of the reservoir.

Meanwhile a helium cylinder was connected up to a special purification system consisting of two copper coils, containing activated charcoal, and immersed in liquid nitrogen. These purifiers had previously been evacuated and baked for 12 hours. The helium was admitted to the gas thermometer by the side limb marked 'helium reservoir' on the diagram. The thermometer was filled with helium gas and it was then pumped out for half an hour. This procedure was repeated a second time. During the final filling the mercury level was adjusted so that, when the mercury was brought up to the index point later, the pressure in the gas thermometer was approximately one atmosphere.

After filling the gas thermometer, the glass side arm of the manometer was sealed off by melting the glass above the taps on the side arm, thus making the gas thermometer a completely sealed system. That it was completely sealed was confirmed by the constancy of the ice

point pressure of the gas thermometer, which did not vary by more than the experimental error in the four months of use. The experimental error in the ice point reading was  $\pm 0.02$  cm. The ice point values for pressure and resistance were found by surrounding the outer can with melting ice and putting helium exchange gas between the outer can and the specimen chamber. The readings were only taken when two successive readings, taken 15 minutes apart, agreed. This method gave consistently reproducible ice point pressures for the gas thermometer, and ice point resistances for the resistance thermometer.

The procedure for obtaining a calibration point was to immerse the outer can in liquid hydrogen or nitrogen, with the space between it and the specimen chamber evacuated, then to set the temperature controller for the desired temperature. Readings were taken every quarter of an hour on the resistance thermometer potentiometer until two readings were the same. The gas thermometer pressure was then determined by raising the mercury until the level in the bulb arm of the manometer reached the index point. The level in the other arm was then read and the potentiometer was also read at the same time. The mercury level was lowered and the temperature controller set to a new temperature. About two hours elapsed between calibration readings which were taken at intervals of approximately  $10^{\circ}\text{K}$ .

#### The Gas Thermometer Calculations.

For a real gas the equation of state may be written

$$PV = n(RT + BP + CP^2 + \dots)$$

where P is the pressure, V is the volume, n is the number of moles of gas, R is the molar gas constant, T is the temperature in °K, B is the second virial coefficient, and C the third virial coefficient.

Preliminary calculations (see table below) showed that the term in  $P^2$  could be neglected and thus the equation of state becomes

$$PV = n(RT + BP).$$

Table 1. The Magnitude of the Terms RT, BP, and  $CP^2$  for Various Values of T.

T°K	Approx.P atmosphere	$P^2$ (atmos.) <sup>2</sup>	B cc.mole <sup>-1</sup>	C cc.mole <sup>-1</sup> atmos.	RT cc. atmosphere mole <sup>-1</sup>	BP cc. atmosphere mole <sup>-1</sup>	$CP^2$ cc. atmosphere mole <sup>-1</sup>
300	1.099	1.208	11.99	-0.000	24,617.0	13.177	0
273	1.000	1.000	12.08	-0.000	22,401.0	12.08	0
200	0.733	0.537	12.23	-0.000	16,411.0	8.965	0
100	0.366	0.134	11.85	+0.0009	8,206.0	4.337	0.00012
20	0.073	0.0053	-2.62	+0.230	1,641.0	0.191	0.00012

Data for B and C were taken from a paper by White, Rubin, Camky, and Johnston<sup>(28)</sup> (1960).

An ideal constant volume gas thermometer would consist of a bulb, which had a zero expansion coefficient, as the temperature sensing element connected to a pressure measuring device of negligible volume by a capillary of negligible volume. However in any practical system the thermometer bulb expands, the manometer has a small dead space, and the capillary will also have a small volume. The capillary volume will not all be at the same temperature. The diameter of the capillary tube

was chosen as 0.02 cm. since thermomolecular pressure corrections for this diameter of tube would only be necessary at the lowest temperatures and even then would be very small. The corrections were based on the data of Roberts and Sydoriak<sup>(29)</sup> (1956).

Figure 16 shows the gas thermometer system diagrammatically. The contents of any volume for a gas thermometer can be described by the equation of state for a gas,

$$PV = n(RT + BP).$$

In the following calculation subscripts are used with the above symbols to denote the respective values for the different parts of the gas thermometer, and a second subscript is used to denote values taken at different times under different sets of conditions. The subscripts used are  $\beta$  for bulb variables,  $\gamma$  for manometer dead space, and  $i$  for capillary volumes. The capillary tube is treated as a number of separate sections and therefore it is usual to sum over  $i$ , i.e.  $\sum_{i=1}^{i=m} \dots$  where  $m$  is the number of capillary sections considered.

Consider a set of external conditions 1.

$$\begin{aligned} \therefore P_{\beta 1} V_{\beta 1} &= n_{\beta 1} (RT_{\beta 1} + B_{\beta 1} P_{\beta 1}) \\ P_{\gamma 1} V_{\gamma 1} &= n_{\gamma 1} (RT_{\gamma 1} + B_{\gamma 1} P_{\gamma 1}) \\ \sum_{i=1}^{i=m} P_{i1} V_{i1} &= \sum_{i=1}^{i=m} n_{i1} (RT_{i1} + B_{i1} P_{i1}) \end{aligned} \quad \left. \vphantom{\begin{aligned} \therefore P_{\beta 1} V_{\beta 1} &= n_{\beta 1} (RT_{\beta 1} + B_{\beta 1} P_{\beta 1}) \\ P_{\gamma 1} V_{\gamma 1} &= n_{\gamma 1} (RT_{\gamma 1} + B_{\gamma 1} P_{\gamma 1}) \\ \sum_{i=1}^{i=m} P_{i1} V_{i1} &= \sum_{i=1}^{i=m} n_{i1} (RT_{i1} + B_{i1} P_{i1}) \end{aligned}} \right\} \dots\dots\dots(46)$$

These might in practice be the conditions at a 'fixed point'. Now it will be required to find the bulb temperature  $T_{\beta 2}$  under a new set of conditions 2.



$$\begin{aligned} \therefore P_{\beta 2} V_{\beta 2} &= n_{\beta 2} (RT_{\beta 2} + B_{\beta 2} P_{\beta 2}) \\ P_{\gamma 2} V_{\gamma 2} &= n_{\gamma 2} (RT_{\gamma 2} + B_{\gamma 2} P_{\gamma 2}) \dots\dots\dots(47) \\ \sum_{i=1}^{i=m} P_{i2} V_{i2} &= \sum_{i=1}^{i=m} n_{i2} (RT_{i2} + B_{i2} P_{i2}) \end{aligned}$$

Now the total quantity of gas has remained constant during this change, therefore the number of moles of gas before and after are the same.

$$\therefore n_{\beta 1} + n_{\gamma 1} + \sum_{i=1}^{i=m} n_{i1} = n_{\beta 2} + n_{\gamma 2} + \sum_{i=1}^{i=m} n_{i2} \dots\dots\dots(48)$$

Rewriting equation (48) and substituting from (46) and (47), then:

$$\frac{P_{\beta 2} V_{\beta 2}}{(RT_{\beta 2} + B_{\beta 2} P_{\beta 2})} = \frac{P_{\beta 1} V_{\beta 1}}{(RT_{\beta 1} + B_{\beta 1} P_{\beta 1})} + \frac{P_{\gamma 1} V_{\gamma 1}}{(RT_{\gamma 1} + B_{\gamma 1} P_{\gamma 1})} + \frac{\sum_{i=1}^{i=m} P_{i1} V_{i1}}{\sum_{i=1}^{i=m} (RT_{i1} + B_{i1} P_{i1})} - \frac{P_{\gamma 2} V_{\gamma 2}}{(RT_{\gamma 2} + B_{\gamma 2} P_{\gamma 2})} - \frac{\sum_{i=1}^{i=m} P_{i2} V_{i2}}{\sum_{i=1}^{i=m} (RT_{i2} + B_{i2} P_{i2})}$$

therefore,

$$T_{\beta 2} = \left[ \frac{1}{\frac{P_{\beta 1} \left( \frac{V_{\beta 1}}{V_{\beta 2}} \right)}{T_{\beta 1} + \left( \frac{B_{\beta 1} P_{\beta 1}}{R} \right)} + \frac{P_{\gamma 1} \left( \frac{V_{\gamma 1}}{V_{\beta 2}} \right)}{T_{\gamma 1} + \left( \frac{B_{\gamma 1} P_{\gamma 1}}{R} \right)} - \frac{P_{\gamma 2} \left( \frac{V_{\gamma 2}}{V_{\beta 2}} \right)}{T_{\gamma 2} + \left( \frac{B_{\gamma 2} P_{\gamma 2}}{R} \right)} + \frac{1}{V_{\beta 2}} \left\{ \sum_{i=1}^{i=m} \left( \frac{P_{i1} V_{i1}}{T_{i1}} - \frac{P_{i2} V_{i2}}{T_{i2}} \right) \right\}} - \frac{B_{\beta 2}}{R} \right] P_{\beta 2} \dots\dots\dots(49)$$

The terms in the second virial coefficient for the capillary have been neglected since the capillary corrections are small and the second virial terms even smaller. A program was written for the Institute computer to calculate  $T_{\beta 2}$  from equation (49). The  $P_{i1}$  were set equal to  $P_{\gamma 1}$ , and the  $P_{i2}$  equal to  $P_{\gamma 2}$ ; the  $V_{i1}$  were assumed equal to the  $V_{i2}$ , and similarly  $V_{\gamma 1}$  was set equal to  $V_{\gamma 2}$ . Corrections were made for the

variation of  $V_{\beta 2}$  and the appropriate values of B were used.

### The Results of the Calibration.

The initial calculations of the gas thermometer results were made using the ice point as a fixed point. However it was found that when nitrogen was being used as a refrigerant the smooth curve of  $R_T/R_{273.15}$  against T, did not pass through the ice point, where  $R_T$  is the resistance at temperature T, and  $R_{273.15}$  is the ice point resistance. The curve missed the ice point by about 2°K. Transferring the fixed point from the ice point to the normal boiling point of nitrogen removed this discontinuity and the smooth curve of  $R_T/R_{273.15}$  against T then passed through the ice point when nitrogen was used as a refrigerant. The normal boiling point values of pressure and resistance were found with liquid nitrogen round the outer can and helium exchange gas between it and the specimen chamber. A vapour pressure bulb was soldered to the side of the specimen chamber, for the condensation of pure nitrogen, in order to determine the boiling point of the commercial liquid nitrogen used, and hence the specimen chamber temperature.

On two occasions during hydrogen runs it was found that the capillary from the thermometer bulb was blocked. This, together with the discontinuity which was found when the ice point was used as a fixed point, suggested that despite the care taken in purifying the gas used in the gas thermometer some impurity was present, but was frozen out when the system was used with liquid nitrogen or hydrogen.

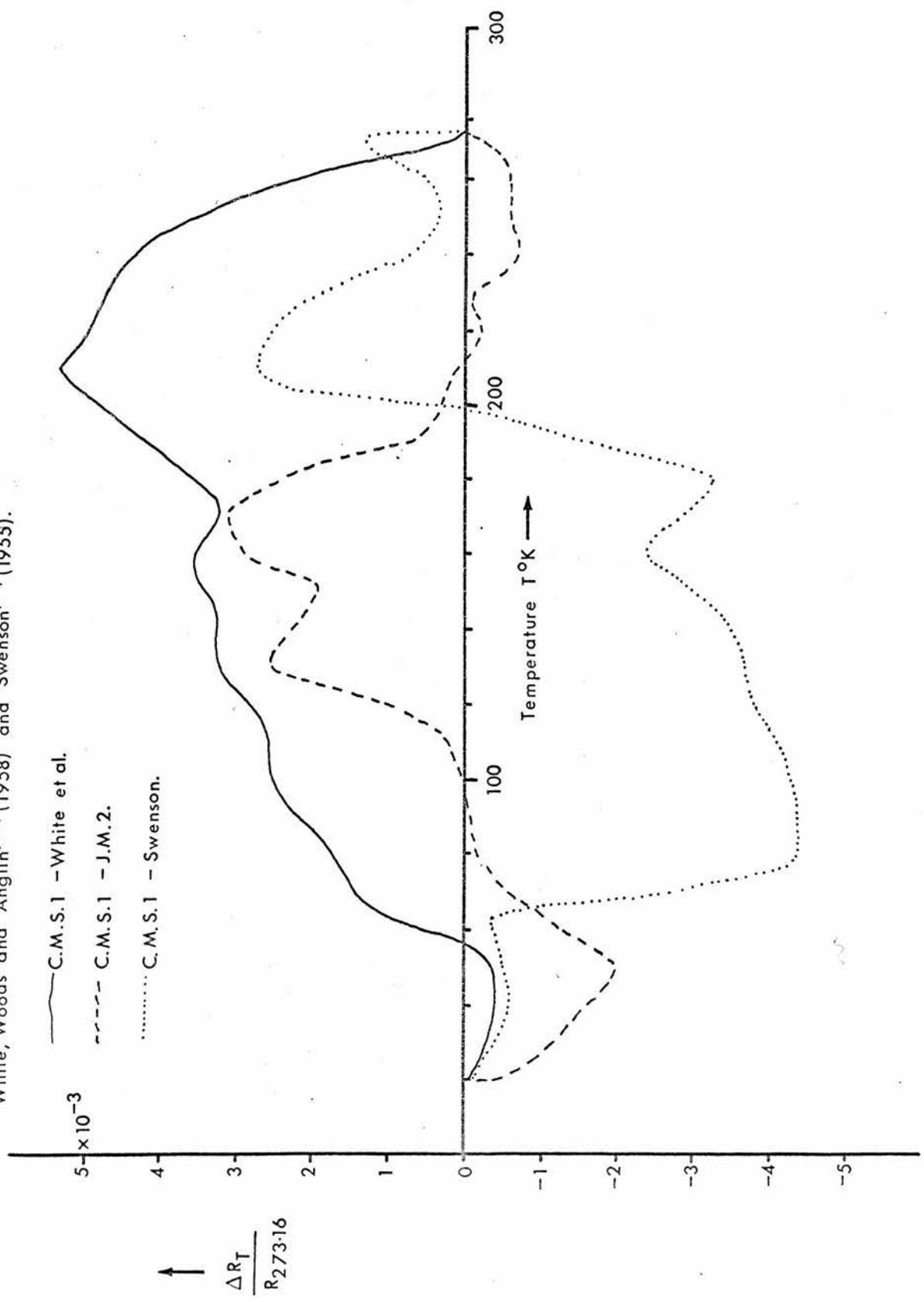
Two indium resistance thermometers were calibrated against the



gas thermometer. Because of space restrictions it was not possible to accommodate both simultaneously, but precautions were taken to reproduce conditions as far as possible during the two calibrations. The first specimen of indium wire, 0.010 inches in diameter, was obtained from Johnson, Matthey, and Co. Ltd. and contained impurities of less than 8 parts per million. This thermometer is referred to as J.M.2. The other specimen of indium wire, also 0.010 inches in diameter, was obtained from the Consolidated Mining and Smelting Co. of Canada Ltd. and it was Cominco brand 59 grade of purity 99.999%. This thermometer is referred to as C.M.S.1.

Graph 2 shows the results for  $R_T/R_{273.15}$  from this calibration compared with the values obtained by White, Woods, and Anglin<sup>(30)</sup> (1958) and Swenson<sup>(31)</sup> (1955). The results for J.M.2 and C.M.S.1 agree well with each other in the ranges 190°K to 270°K and 70°K to 110°K; the agreement is fair below 70°K, but bad between 120°K and 180°K. The results for J.M.2 in the range 120°K to 180°K were found to have rather larger scatter than in other regions and this is probably the cause of the lack of agreement in this region. The agreement of the two calibrations made during this investigation suggests that indium from different sources may be used for thermometry without the necessity of individual calibrations. The present results lie between those of White, Woods, and Anglin<sup>(30)</sup> (1958) and those of Swenson<sup>(31)</sup> (1955), for temperatures between 70°K and 200°K. The difference between the results of this calibration and those of White et al., for temperatures

Graph 2. Comparing present calibration of two indium thermometers, C.M.S.1 and J.M.2 with the results of White, Woods and Anglin<sup>(30)</sup> (1958) and Swenson<sup>(31)</sup> (1955).



above 200<sup>o</sup>K, is surprisingly large.

#### Gas Thermometer Failure.

Later, after the linear expansion coefficient of copper had been measured using the C.M.S.1 thermometer, using the calibration just described, it was found that the graph of the linear expansion coefficient against temperature, see graph 3, did not agree with other experimental results at the high temperature end. These differences in measured expansion coefficients at high temperatures could not be attributed to differences in specimens, and it was clear that the expansion measuring technique was not at fault, because good agreement was obtained at low temperatures. Therefore the fault was attributed to the thermometry, and it was found that the differences between the C.M.S.1 results and White et al.'s results were in the right direction to account for the errors in the expansion coefficients. This confirmed the earlier indication that some impurity was present in the gas thermometer. Having found that the agreement between calibrations of indium from different sources was on the whole good, it was decided, in view of the long time that would be necessary to repeat the gas thermometer calibration of the indium resistance thermometer, that using the results of White, Woods, and Anglin's<sup>(30)</sup> (1958) calibration for indium would be appropriate. Graph 4 shows the expansion coefficient of copper that was found using the C.M.S.1 indium thermometer with the results of White et al., linear interpolation of their results being used to find the temperature from a resistance value. The agreement of the expansion coefficient of copper calculated in this way with the results of other workers is good.

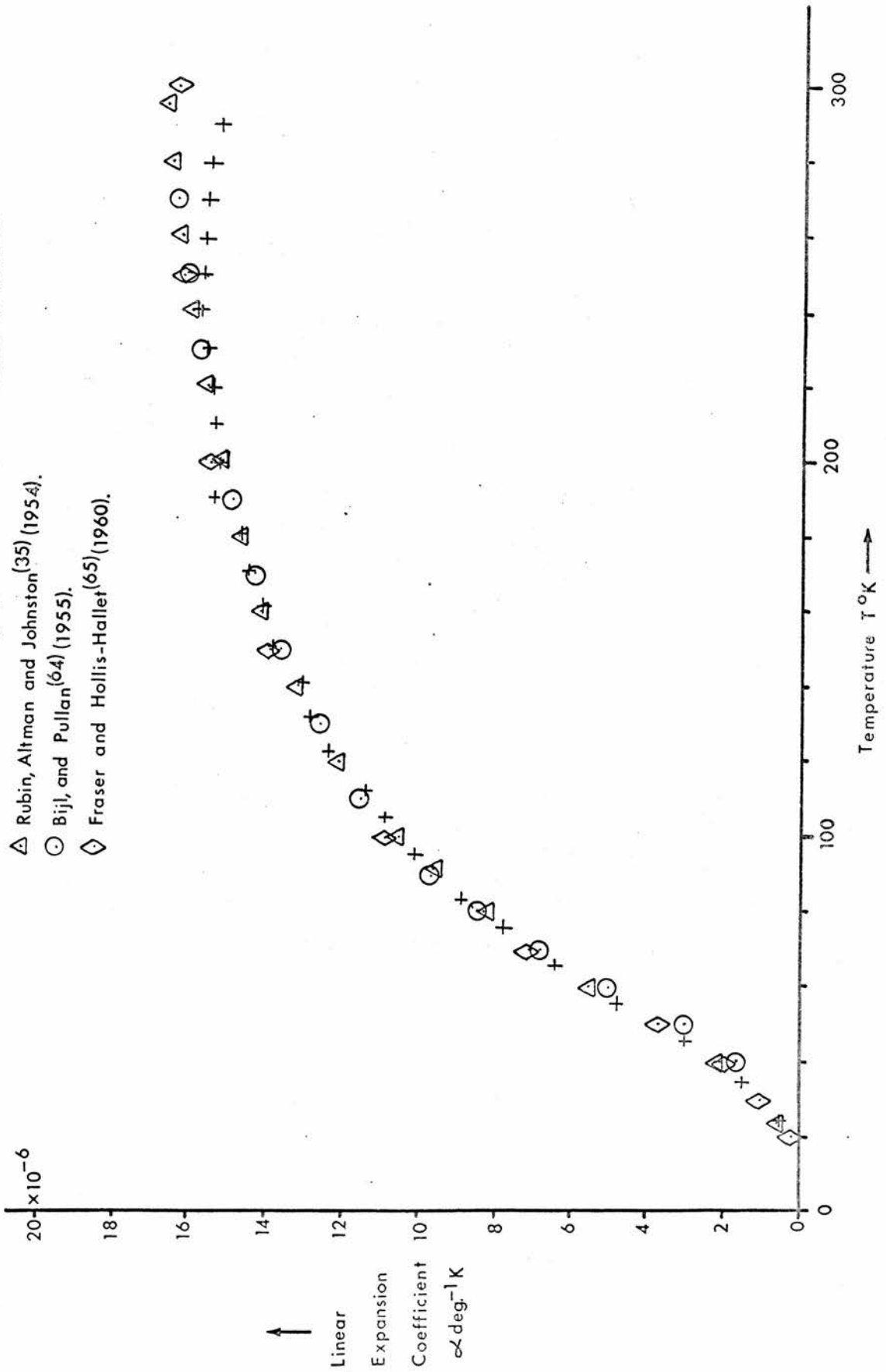
Graph 3. The Linear Thermal Expansion Coefficient of Copper.

+ Present results using gas thermometer calibration of C.M.S.I.

△ Rubin, Altman and Johnston<sup>(35)</sup> (1954).

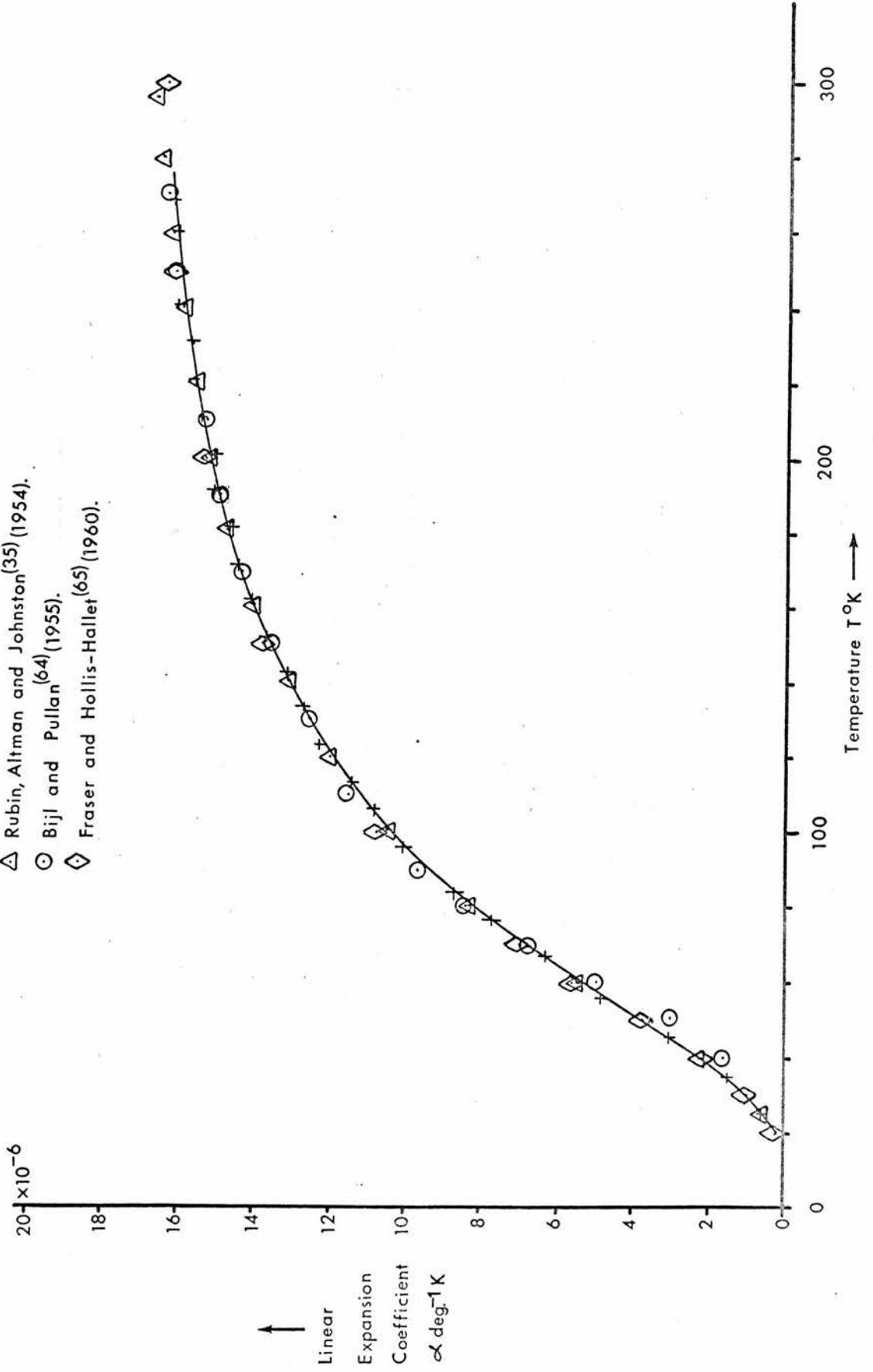
○ Bijl, and Pullan<sup>(64)</sup> (1955).

◇ Fraser and Hollis-Hallet<sup>(65)</sup> (1960).



Graph 4. The Linear Thermal Expansion Coefficient of Copper.

- + Present results using C.M.S.I with White, Woods and Anglin's<sup>(30)</sup> (1958) results.
- △ Rubin, Altman and Johnston<sup>(35)</sup> (1954).
- Bijl and Pullan<sup>(64)</sup> (1955).
- ◇ Fraser and Hollis-Hallet<sup>(65)</sup> (1960).



Chapter 5.

The Vacuum System.

Figure 17 is a diagram of the vacuum system. It really consists of two systems which operate independently, but, by means of taps, may be connected together to suit the experimenter's purpose. One of these systems is for high vacuum purposes; it pumps the outer can in order to provide thermal isolation for the specimen chamber, and it also pumps the high vacuum side of the two manometers, one for the specimen chamber and one for the vapour pressure bulb. This high vacuum system is pumped by an Edwards type 102 A diffusion pump backed by a Metrovac type DRI-K rotary pump. The other system is used to evacuate the specimen chamber and the vapour pressure bulb. Provision is also made to pump the outer bath to produce cooling of the refrigerant. This system can be pumped either by an N.G.N. type P SR 6 rotary pump or an Edwards type 2SC 20 A rotary pump. To this latter system there are also connected sources of helium gas and gas for the vapour pressure bulb. The helium gas may be admitted to the specimen chamber, after evacuation, the resulting pressure being indicated by a Bourdon gauge and accurately measured with a butyl phthalate manometer. The helium gas may also be admitted to the outer can by means of a tap connecting the outer can to the specimen chamber. The pressure of gas admitted to the vapour pressure bulb may be measured with a mercury manometer. The helium exchange gas and vapour pressure bulb gas are stored in two glass reservoirs with manometers to indicate the pressure in the

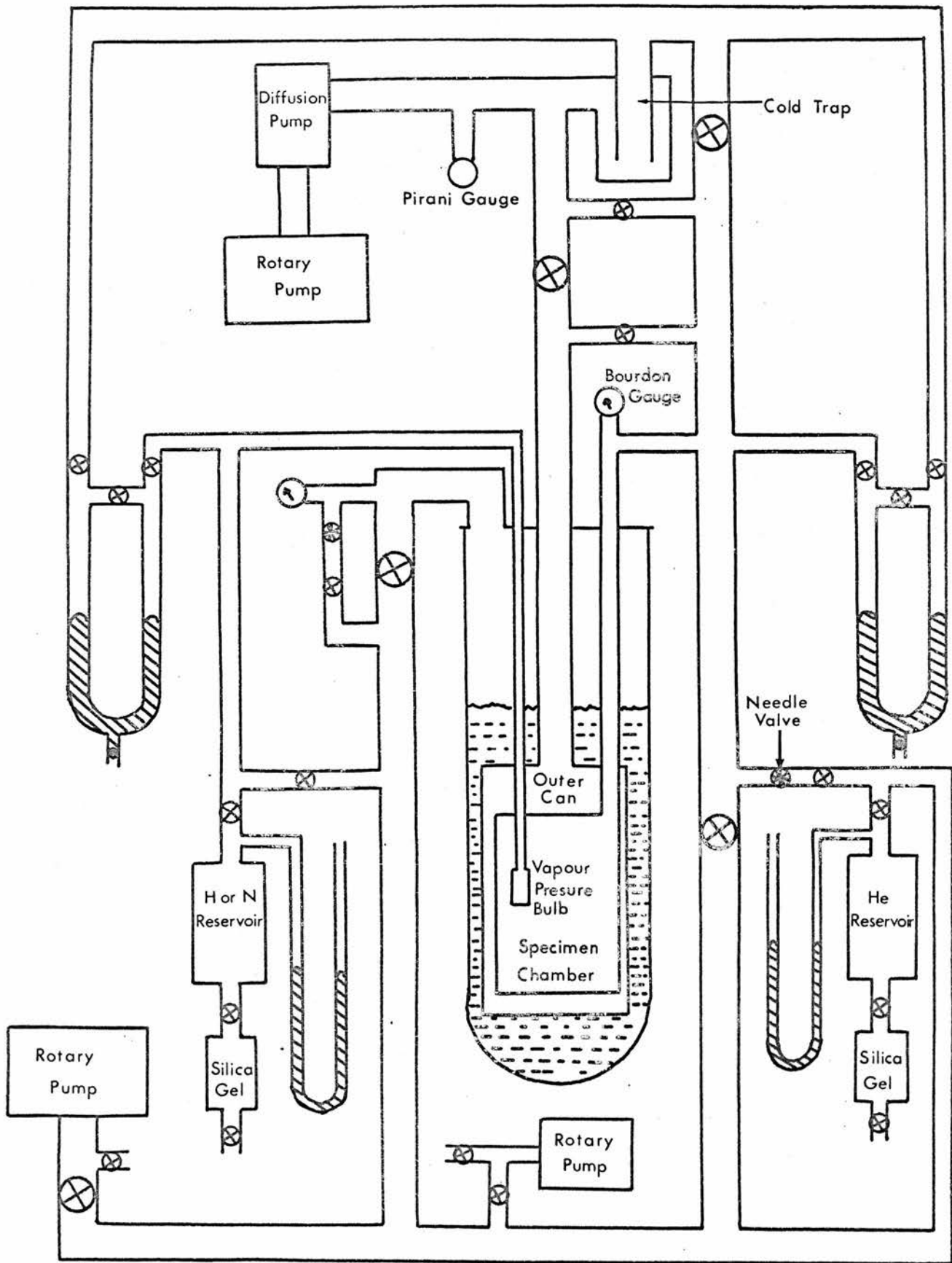


Figure 17. The Vacuum System.



reservoirs. These are filled with gas from high pressure cylinders via silica gel drying towers.

### Temperature Variation.

In low temperature work requiring a range of steady temperatures, the most convenient method of adjusting the temperatures of the specimens in question is to cool them first below the required temperature, and to apply a sufficient amount of controllable heat to obtain the required temperature. The most obvious way of cooling is to surround the specimen chamber by a refrigerant and then, after cooling, to thermally isolate the specimen chamber. Heat may then be applied by means of a heater attached to the specimen chamber. When heating is carried out it may be done either so that the temperature rises continuously, or so that the temperature is changed from some initial steady temperature to some new steady temperature, at which the specimens may be held until there is thermal equilibrium. The continuous heating method, resulting in a uniform rise of temperature throughout the experiment, has the disadvantage that it may be difficult to determine whether the temperature of the thermometer is the same as that of the specimens, though with manually controlled heating it may be the easier method. When observations are made at a steady temperature, the thermometer will be in thermal equilibrium with the specimens, and a reliable reading will be obtained. For the present experiment involving the photography of the fringe pattern, an exposure of about five minutes was required, and therefore a steady temperature was

was needed for each reading taken. A thermostatic heater controller built by C.H.Panter based on a design by Parkinson and Quarrington<sup>(45)</sup> (1954) was used throughout these measurements.

#### Procedure for Measuring Thermal Expansion.

When the apparatus was set up with a specimen in the interferometer in the specimen chamber, and when the specimen chamber and the outer can were airtight, and the various vacuum lines and electrical leads had been connected, the apparatus was ready to begin a series of measurements. (Plate 4 shows the specimen chamber.) Whenever the apparatus was taken apart to make some change in the specimen chamber there was the risk that some mechanical shock might alter the ice point resistance, even with the improved support for the indium wire; therefore an ice point was taken at the beginning of each run as a check. The procedure for an ice point determination has been described in the previous chapter. The ice point was also checked each time the apparatus was brought back to room temperature after any period at nitrogen or hydrogen temperatures. Over the eighteen months of use, involving considerable handling, the resistance changed by 20 parts in 30,000. During any one run however no change greater than experimental error was detectable, i.e. 1 part in 30,000.

After the ice point resistance had been determined, a thin walled Dewar was placed round the outer can and held in position by means of a ring below the Dewar. This ring, in turn, was supported by  $\frac{1}{4}$ " iron rods fixed to the framework of the apparatus. Plate 5 shows a general



Plate 4. The Specimen Chamber.

view of the apparatus. The specimen chamber, outer can and vapour pressure bulb were then evacuated. Liquid nitrogen was poured into the outer bath (or Dewar) until the outer can was completely immersed. With the vacuum inside the cryostat, the rate of cooling was slow, thus avoiding undue stresses on the specimen chamber window. It usually took about twelve hours for the specimen chamber to cool to about the temperature of the liquid nitrogen. This cooling was arranged to take place overnight. If measurements were to be taken below nitrogen temperatures, hydrogen was used as the refrigerant. In this case the apparatus was cooled as above to about the temperature of liquid nitrogen and when sufficient hydrogen had been obtained from an adjacent hydrogen liquifier, Yates and Hoare<sup>(46)</sup> (1961), the liquid nitrogen was emptied from the Dewar, and the hydrogen was syphoned into the Dewar. A trace of helium exchange gas was admitted to the outer can and the specimen chamber reached the refrigerant temperature within one hour. There was usually sufficient liquid hydrogen for the time taken to make measurements of the thermal expansion over the range  $20^{\circ}\text{K}$  to  $80^{\circ}\text{K}$ .

The procedure for taking measurements was to start from the temperature of the liquified gas being used. Equilibrium and stability of the specimen chamber at the refrigerant temperature were obtained by putting helium exchange gas in the outer can. Successive readings of the resistance of the thermometer were taken at intervals of a quarter of an hour. When two successive readings agreed to within the limits

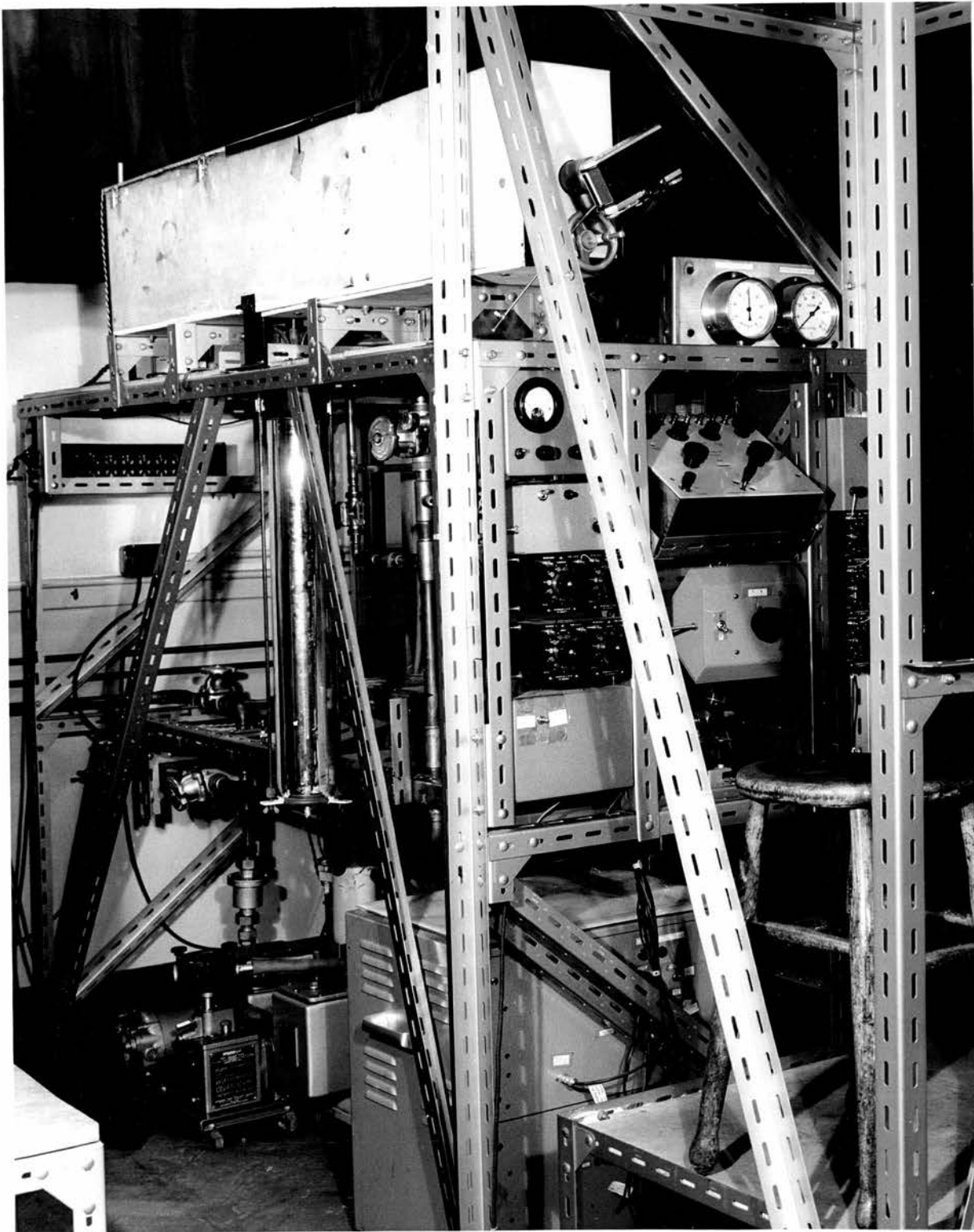


Plate 5. General View of the Apparatus.



of experimental error, the reading was noted, a photograph of the fringe pattern was taken, the specimen chamber pressure was measured, and the fringe position was noted. The outer can was evacuated after the observations had been made. The thermostatic temperature controller was switched on and set for a temperature about  $10^{\circ}\text{K}$  above the first reading. As the specimen chamber warmed up a count was taken of the whole number of fringes crossing the index mark. After between one and two hours, when two successive readings of the resistance thermometer again agreed, indicating that equilibrium had been attained, the value was noted, a new photograph of the fringe pattern taken, the specimen chamber pressure measured, and the fringe position noted. The specimen chamber was warmed up in intervals of approximately  $10^{\circ}\text{K}$ . The above procedure was repeated for each set of observations. If hydrogen was the refrigerant, a temperature of about  $80^{\circ}\text{K}$  would be reached before all the hydrogen was used. If nitrogen was the refrigerant the whole range from  $77^{\circ}\text{K}$  to  $270^{\circ}\text{K}$  could not be covered in one day, and the outer can was kept immersed in nitrogen for several days. Each day measurements would commence where measurements on the previous day finished. The warming up for the first reading of a day usually took about four hours, since the thermostatic temperature controller was not left on overnight. On some occasions measurements were taken with the temperature of the specimen chamber falling, in which case the temperature controller was set for a temperature  $10^{\circ}\text{K}$  less than the previous setting, otherwise the procedure was the same. Measurements

from room temperature downwards were often taken when it was not convenient to cool the apparatus over the previous night. The whole temperature range  $20^{\circ}\text{K}$  to  $270^{\circ}\text{K}$  was covered twice for each of the alkali halides, the readings taken being arranged so that the values for the thermal expansion coefficient would fall alternately from each series of measurements when plotted on a graph.

### Photography.

As described earlier this technique of accurate measurement of thermal expansion depends upon taking photographs of the fringe pattern and later analysing the photographs on a microphotometer. The camera used was a 35mm. single lens reflex camera. This was chosen so that the fringe pattern could be viewed when a photograph was not being taken. Initial photographs using panchromatic film required an exposure of about ten minutes. Kodak Limited suggested that their special green sensitive film 'Flurodak' would help to reduce this exposure time, the illumination being the Cd  $5085.822^{\circ}\text{Å}$  green line. Photographs using the 'Flurodak' film required exposures of about six minutes. These exposures were taken with a Wratten combination filter (No. 45 + No. 48), but later the exposure required was halved by using an interference filter with a No. 3 Wratten filter. The photographs were developed in Kodak D19b developer and fixed in Unifix. All the processing was carried out at  $20^{\circ}\text{C}$  and all the rinsing water used was brought to this temperature. All solutions were filtered before use and the films were dried carefully away from dust.



The Use of the Microphotometer for Fractional Fringe Shifts.

At the end of each set of measurements on a specimen, when the temperature range  $20^{\circ}\text{K}$  to  $270^{\circ}\text{K}$  had been covered twice, all the photographs were analysed on a Hilger Recording Microphotometer type H.670. The microphotometer was adjusted to give a trace across the full width of the chart on the Honeywell Brown chart recorder attached to it. The speed of the microphotometer was selected to give about ten feet of chart for one photograph; this was most convenient for easy analysis. This method usually gave the intensity variation across two or three fringes, and then across the index mark and two additional fringes. The variation of intensity across the fringes was a sinusoidal shape, and across the index mark the intensity variation was an inverted U shape. These maxima of intensity were symmetrical but the tops were rather flat. In order to find the centres of the maxima, the mid-points of several chords parallel to the x-axis were used. The distances between the fringe maxima, and from the fringe maxima to the centre of the index mark, were noted. From these distances the fractional fringe position relative to the index mark was found accurately. When the fractional fringe positions for all the readings were known, the fractional fringe shift between two readings could be determined and hence the thermal expansion coefficient could be accurately calculated.

Chapter 6.

The Results, and the Specimen Purities.

1. Copper. The modified apparatus was first used to measure the linear expansion coefficient  $\alpha = \frac{1}{L_{295}} \frac{dL}{dT}$  of copper. This measurement was done as an overall check on the apparatus. The discrepancy which this check revealed in the thermometry, and how this discrepancy was overcome, have been discussed in chapter 4. The graph 4 in chapter 4 shows the present results compared with those of other workers. The smoothed results are given in table 2. The copper specimen was made from a cylinder of spectrographically standardised copper obtained from Johnson, Matthey, and Co. Ltd. The following is an extract from a test report by Johnson, Matthey, and Co. Ltd.

Impurity Content.	Fe	2 p.p.m.
	Si	1 p.p.m.
	Ag	1 p.p.m.
	Mg	1 p.p.m.

Not detected: Al, As, Au, Ba, Bi, Ca, Cd, Co, Cr, Cs, Ga, Ge, Hf, Hg, In, Ir, K, Li, Mn, Mo, Na, Nb, Ni, Os, P, Pb, Pd, Pt, Re, Ru, Sb, Se, Sn, Sr, Ta, Te, Ti, Tl, V, W, Zn, Zr.

For the thermal expansion measurements on the alkali halides, the crystals chosen were NaF, RbBr, and CsI. These are the crystals in which the constituent ions of the molecules are of approximately equal mass. KCl was omitted as its thermal expansion coefficient had already been measured by White<sup>(61)</sup> (1961), Rubin, Johnston and Altman<sup>(62)</sup> (1962) and Yates and Panter<sup>(9)</sup> (1962).

2. Caesium Iodide. Like all the alkali halides this crystallizes into a cubic crystal, but not one like NaCl but like CsCl i.e. a 'body centred cubic structure'. The experimental results of  $\alpha = \frac{1}{L_{295}} \frac{dL}{dT}$  are given in table 3 and plotted in graph 5. The results of other workers shown on the graph around 300°K agree fairly well with the present results except for the isolated value found by Johnson, Argon and Bredig<sup>(54)</sup> (1955). The results of Pathak and Pandya<sup>(55)</sup> (1960), who used an X-ray method, fall systematically below the extrapolation of the present results. Whether this is a real difference between bulk measurements and X-ray measurements could only be clarified by measurements on the same specimen. The CsI specimen was obtained from Hilger and Watts Ltd. The following is an extract from their test report:

Impurities	SO <sub>4</sub>	0.005%	K	0.002%
	Pb	0.0003%	Al	0.001%
	Cu	0.0003%	Mg	0.0005%
	Zn	0.0003%	Li	0.00004%
	Fe	0.0003%	Na	0.008%

3. Rubidium Bromide. This alkali halide crystallizes into a cubic crystal with an NaCl structure, i.e. a 'face centred cubic structure'. The experimental results of  $\alpha = \frac{1}{L_{295}} \frac{dL}{dT}$  are given in table 4 and plotted in graph 6. The results of other workers, shown around 300°K, agree fairly well with the present results. The RbBr specimen was obtained from L.Light and Co. Ltd. The following is an extract from their test report.

Impurities	Cs	30 p.p.m.	Na	20 p.p.m
------------	----	-----------	----	----------

No other detectable impurities.

4. Sodium Fluoride. This alkali halide crystallizes into a cubic crystal with an NaCl structure, i.e., a 'face centred cubic structure'. The experimental results of  $\alpha = \frac{1}{L_{295}} \frac{dL}{dT}$  are given in table 5 and plotted in graph 7. The results of other workers agree fairly well around 300°K, but the results of Rianõ and Amoros<sup>(48)</sup> (1960), who used an X-ray method, are in poor agreement with the present results below 200°K. The NaF specimen was obtained from Harshaw Chemicals Ltd. The following is an extract from their test report:

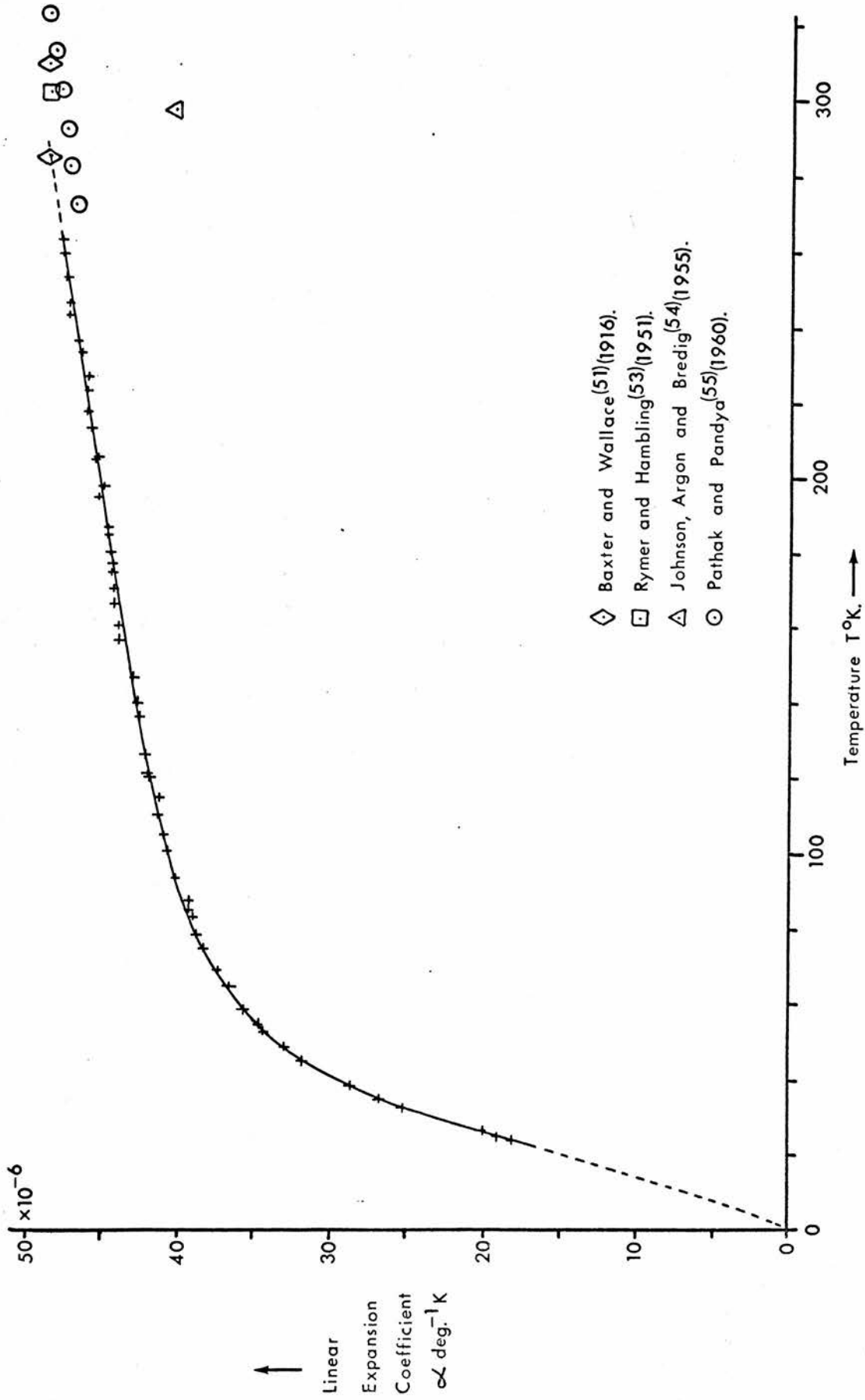
Impurities	Fe	}	between 0.001% and 0.01% each
	Ca		
	Al	}	less than 0.001% each.
	Cu		
	Mg		
	Mn		
	Ni		
	Si		
	Ag		

Sought but not found: As, Au, B, Ba, Be, Bi, Cd, Co, Cr, Ga, Ge, In, La, Li, Hg, Mo, P, Pb, Pt, Sb, Sn, Sr, Tl. Graph 8 shows the thermal expansion on an enlarged scale at low temperatures for NaF. Table 2 gives smoothed values for the linear thermal expansion coefficient  $\alpha = \frac{1}{L_{295}} \frac{dL}{dT}$  at 10°K intervals for all the materials examined.

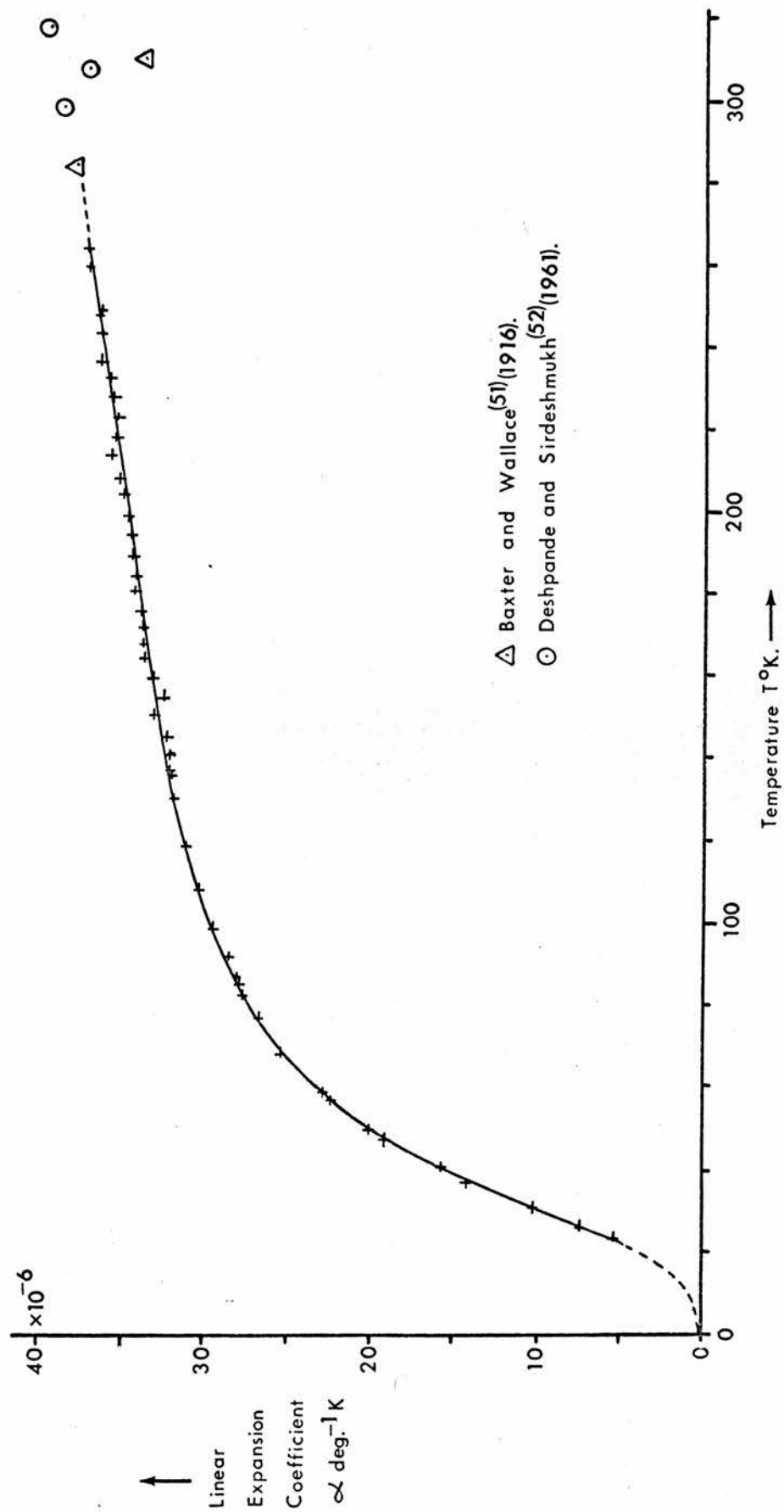
Analysis of the Results.

As pointed out in the introduction, it has only been possible to make a reliable analysis of the results in the case of RbBr, since this is the only material for which enough of the necessary associated

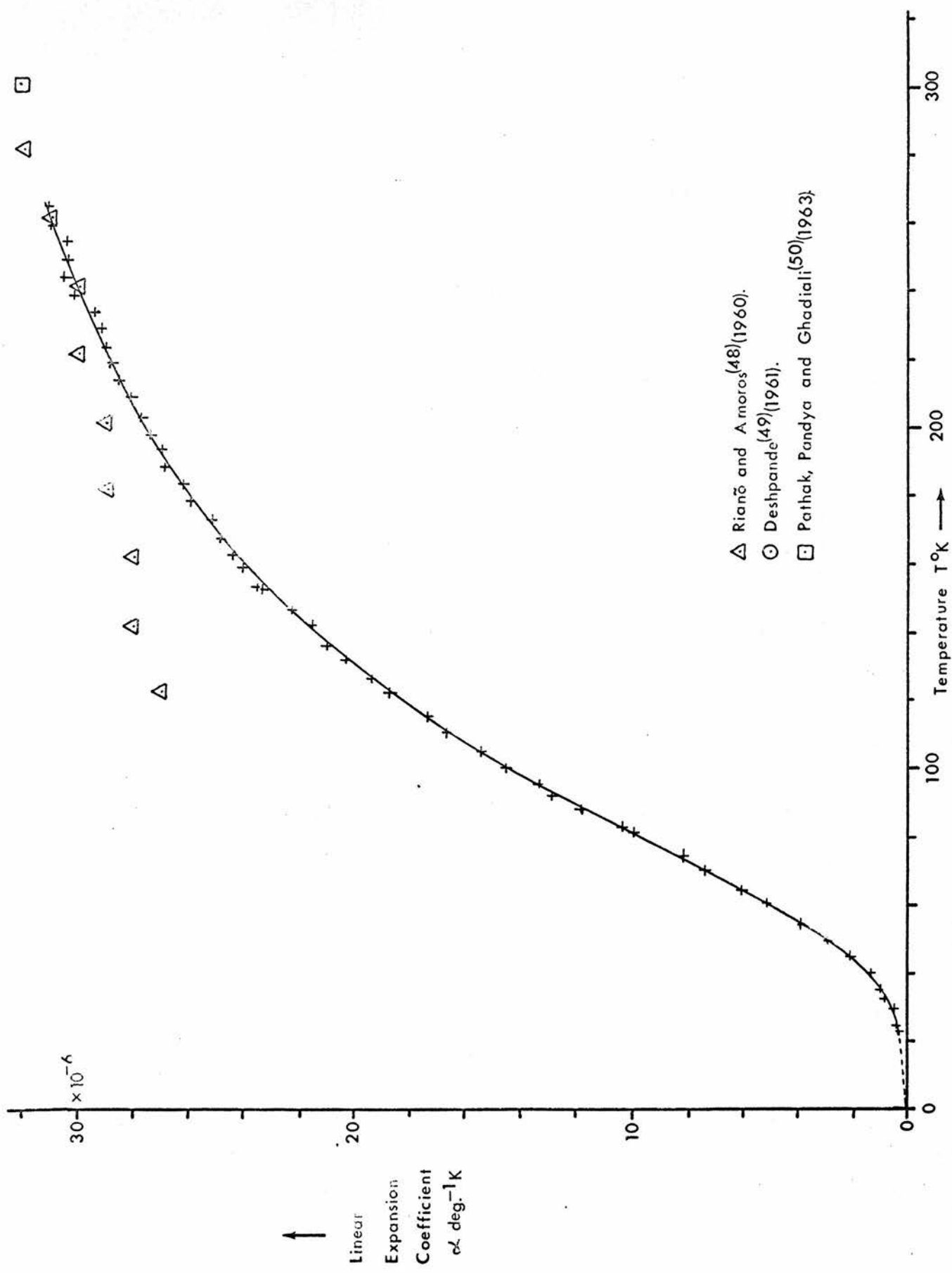
Graph 5. Linear Expansion Coefficient of CsI against Temperature.



Graph 6. Linear Thermal Expansion Coefficient of RbBr against Temperature.

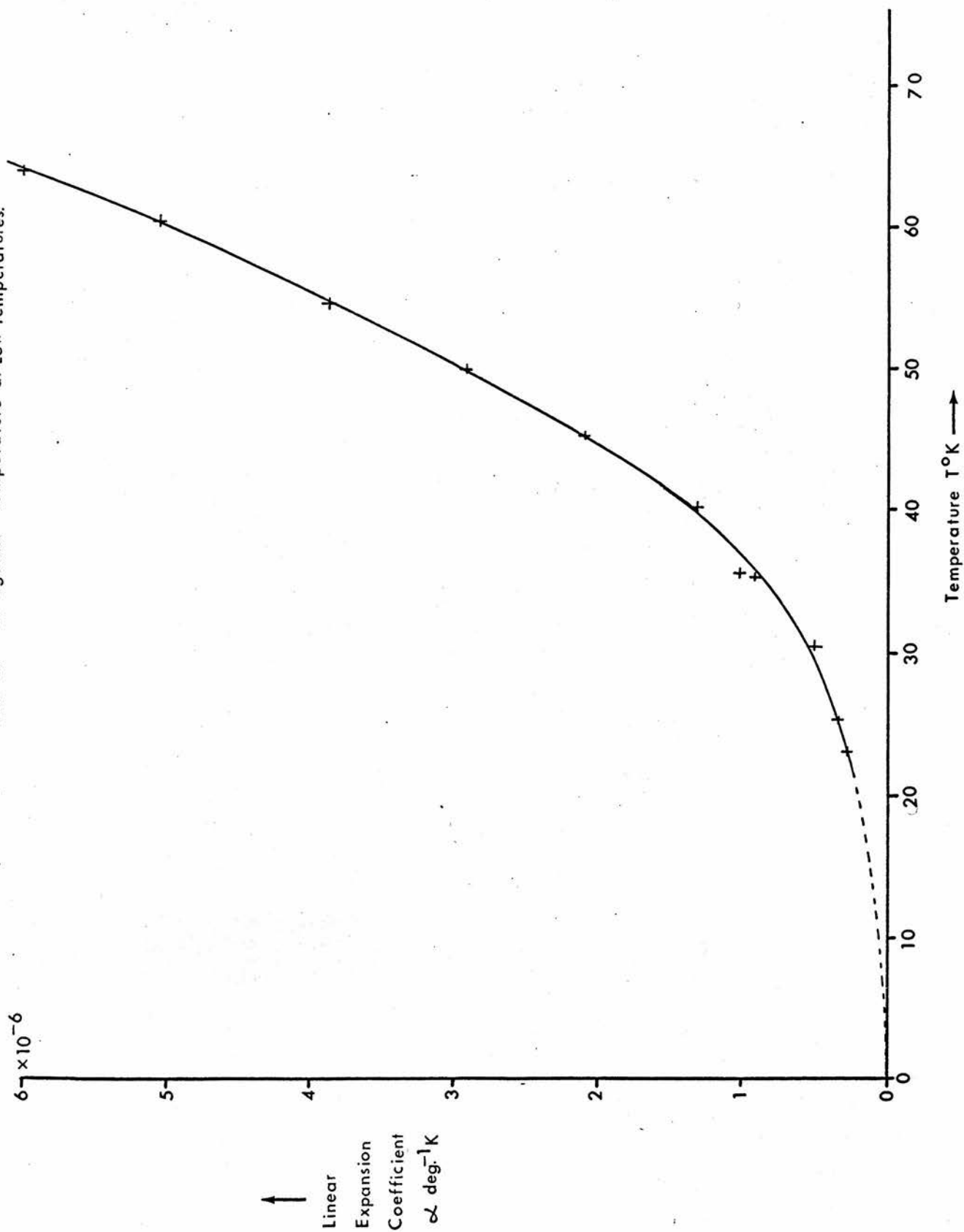


Graph 7. Linear Thermal Expansion Coefficient of NaF against Temperature.





Graph 8. Linear Thermal Expansion Coefficient of NaF against Temperature at Low Temperatures.



data are available. Even for RbBr there are no experimental elasticity data below room temperature, and no specific heat data below 10°K.

Smoothed values of the specific heat at constant pressure,  $C_p$ , were obtained from a graph of  $C_p$  against temperature  $T$  drawn from the results of Clusius, Goldmann, and Perlick<sup>(56)</sup> (1949). These smoothed values are given in table 6. The adiabatic compressibility  $\chi_s$  of RbBr at 295°K was found from the experimental results of Reinitz<sup>(57)</sup> (1961). The theoretical predictions of Krishnan and Roy<sup>(58)</sup> (1952) were used to find  $\chi_s$  at 0°K. Values of  $\chi_s$  at temperatures between 0°K and 295°K were obtained by linear interpolation<sup>of  $\chi_s$</sup>  and are given in table 6. The density at 295°K was taken as 3.35<sub>3</sub> gm. cm.<sup>-3</sup> and the molecular weight was taken as 165.40 gm.

The Grüneisen Parameter and the Debye Characteristic Temperature.

In chapter 1, equation (27) relates the Grüneisen parameter at temperature  $T$ ,  $\gamma_T$ , to the specific heat at constant volume  $C_v$ , the linear expansion coefficient at temperature  $T$ ,  $\alpha_T$ , the molar volume at temperature  $T$ ,  $V_T$ , and the isothermal compressibility  $\chi_T$  thus:

$$\gamma_T = \frac{3\alpha_T V_T}{\chi_T C_v}$$

Now the experimentally measured quantities are  $\chi_s$  and  $C_p$ , and the thermodynamic relation  $\chi_s C_p = \chi_T C_v$  enables the equation for  $\gamma_T$  to be rewritten as

$$\gamma_T = \frac{3\alpha_T V_T}{\chi_s C_p} \dots\dots\dots(50)$$

In this equation the linear expansion coefficient is defined as

$\alpha_T = \frac{1}{L_T} \frac{dL}{dT}$  where  $L_T$  is the length at the temperature  $T$ , and  $V_T$  is the molar volume at temperature  $T$ . Now  $3\alpha_T = \beta_T = \frac{1}{V_T} \frac{dV}{dT}$  where  $\beta_T$  is the volume expansion coefficient at temperature  $T$ . The measured linear expansion coefficient is in terms of the length at  $295^\circ\text{K}$ ,

i.e.,  $\alpha = \frac{1}{L_{295}} \frac{dL}{dT}$  and similarly  $\beta = 3\alpha = \frac{1}{V_{295}} \frac{dV}{dT}$ .

$$\begin{aligned} \therefore \beta_T &= \beta \frac{V_{295}}{V_T} \\ \therefore 3\alpha_T &= 3\alpha \frac{V_{295}}{V_T} \\ \therefore \gamma_T &= \frac{3\alpha \frac{V_{295}}{V_T} V_T}{C_p \chi_s} \end{aligned}$$

and finally  $\gamma_T = \frac{3\alpha V_{295}}{C_p \chi_s} \dots\dots\dots(51)$

Thus the values of  $\gamma_T$ , the Grüneisen parameter at temperature  $T$ , may be evaluated in terms of the measured quantities. The values of  $\gamma_T$  calculated using equation (51) are given in table 6 and plotted in graph 9.

As pointed out in chapter 1 the specific heat at constant volume  $C_v$  may be found from experimentally measured quantities by using the thermodynamic relation

$$C_p - C_v = \frac{C_p}{\left(1 + \frac{\chi_s C_p}{V \beta^2 T}\right)} \dots\dots\dots(52)$$

where  $\beta = 3\alpha$ . Equation (52) has been used to calculate the values of  $C_v$  given in table 6.

$C_v$  has been used in conjunction with a table of values of  $C_v$  for various values of  $\Theta_D/T$ , Roberts and Miller<sup>(15)</sup> (1951), to obtain  $\Theta_D$ , the Debye characteristic temperature. The values of  $\Theta_D$  are given in table 6 and plotted on graph 10. The theoretical high temperature value of the Debye characteristic temperature,  $\Theta_\infty$ , was obtained by plotting a graph of  $\Theta_D^2$  against  $1/T^2$  in the region where  $\Theta_D$  was increasing with temperature, and extrapolating to  $1/T^2 = 0$ , as shown in graph 11. This follows the procedure which Barron, Berg, and Morrison<sup>(16)</sup> (1957) found gave the least ambiguity in determining  $\Theta_\infty$ .

As de Launay<sup>(59)</sup> (1959) has pointed out the Debye characteristic temperature at  $0^\circ\text{K}$ ,  $\Theta_0$ , may be obtained from the elastic constants  $c_{11}$ ,  $c_{12}$ , and  $c_{44}$  at  $0^\circ\text{K}$  by computation of the following equation

$$\Theta_0^3 = \frac{9N}{4\pi V} \left(\frac{h}{K}\right)^3 \left(\frac{c_{44}}{\rho}\right)^{3/2} \left[\frac{9}{18 + \sqrt{3}}\right] f(S,t) \dots\dots\dots(53)$$

where  $\rho$  is the density,  $V$  the molar volume,

$$S = (c_{11} - c_{44}) / (c_{12} + c_{44})$$

$$t = (c_{12} - c_{44}) / c_{44}$$

and the function  $f(S,t)$  is an anisotropy factor. The theoretical predictions for the elastic constants at  $0^\circ\text{K}$  of Krishnan and Roy<sup>(58)</sup> (1952) have been used to evaluate  $S$  and  $t$ . The anisotropy factor  $f(S,t)$  has been found by using the interpolation formula given by de Launay<sup>(59)</sup> (1959) for use with his tables of  $S$  and  $t$ . The thermal expansion coefficients found in this investigation have been used together with the factor  $f(S,t)$  and  $c_{44}$  to calculate  $\Theta_0 = 147^\circ\text{K}$  from equation (53).

Following the procedure described by Barron, Leadbetter, and

Morrison<sup>(22)</sup> (to be published) a parameter  $T_R = 0.2\theta_\infty$  was chosen in plotting  $\gamma_T$  against  $t = [1 + (T/T_R)^2]^{-1}$  and extrapolating to  $t = 0$  to give  $\gamma_\infty$ . Although the variations of  $C_V$  and  $\alpha$  with temperature displayed no obvious peculiarities, the graph of  $\gamma_T$  against  $T$  turned upwards at the higher temperature end. This behaviour may not be unique, since the less precise results for KI, Yates and Panter<sup>(9)</sup> (1962) suggest a similar trend. Analysis of graph 12 between the values of  $t$  corresponding to  $30^\circ\text{K}$  and  $180^\circ\text{K}$  gives a value of  $\gamma_\infty = 1.40$ , whilst for  $t$  corresponding to temperatures between  $230^\circ\text{K}$  and  $270^\circ\text{K}$  a value of  $\gamma_\infty = 1.55$  is given. Extrapolation of graph 9 of  $\gamma_T$  against  $T$  to  $T = 0$  yields a value of  $\gamma_0 = 0.569$  but smooth curves could be drawn to give  $\gamma_0$  between 0.56 and 0.60.

The value for  $\gamma_\infty$  lies within the range 1.50 to 1.76 predicted by Blackman<sup>(8)</sup> (1957) on the basis of the point charge ion model, in which equality of the masses of the ions was assumed. The value of  $\gamma_0$  is well below the values predicted by the point charge ion model, namely  $\gamma_0 = 1.15$  to 1.46. Following a suggestion of Blackman<sup>(63)</sup> (1958), Meincke and Graham<sup>(36)</sup> (1963), have shown that by using a value of  $n > 8$  in the repulsive force term  $a/r^n$ , the weighting factor in the expression for  $\gamma_0$  may be altered in such a way that the predicted value of  $\gamma_0$  is reduced. The anisotropic continuum model of Sheard<sup>(24)</sup> (1958) has given values of  $\gamma_0$  in decidedly better agreement with the experimental results for KCl. In the absence of experimental data on the pressure variation of the elastic moduli of RbBr, predictions of  $\gamma_0$  using the

anisotropic continuum model cannot be made. The maximum variation of  $\gamma_T$  is in the region  $T/\theta_D \doteq 0.2$ , which is the region which Barron<sup>(7)</sup> (1955) predicted, whereas Blackman<sup>(8)</sup> (1959) predicted that the maximum change in  $\gamma_T$  would be in the region  $T/\theta_D \doteq 0.14$ .

Moments of the Frequency Distribution.

The nth moment of the frequency distribution function  $g(\nu)$  is defined by  $\overline{\nu^n} = \frac{\int_0^{\nu_D} \nu^n g(\nu) d\nu}{\int_0^{\nu_D} g(\nu) d\nu}$ .

In chapter 1 equation (30), the Thirring expansion is used to relate the positive even moments of the frequency spectrum to the Debye characteristic temperature. Using this relation (i.e. equation (30), chapter 1) the positive even moments of the real frequency distribution function could be found. The values of A and B in equation (30), viz.,

$$\theta_D^2 = \theta_\infty^2 \left[ 1 - A(\theta_\infty/T)^2 + B(\theta_\infty/T)^4 - \dots \right] \dots\dots\dots(54)$$

where

$$\theta_\infty = \frac{h}{K} \left( \frac{5}{3} \overline{\nu^2} \right)^{\frac{1}{2}} \dots\dots\dots(55)$$

$$A = \frac{3}{100} \left[ \frac{\overline{\nu^4}}{(\overline{\nu^2})^2} - \frac{25}{21} \right] \dots\dots\dots(56)$$

$$B = \frac{1}{1400} \left[ \left( \frac{\overline{\nu^6}}{(\overline{\nu^2})^3} - \frac{125}{81} \right) - 100A \right] \dots\dots\dots(57)$$

have been found from the intercept and slope of a graph of  $\left[ 1 - (\theta_D/\theta_\infty)^2 \right] (T/\theta_\infty)^2$  against  $(\theta_\infty/T)^2$ , the range  $2.5 < \theta_\infty/T < 6$  being chosen when drawing the tangent, the region in which Barron, Berg, and Morrison<sup>(16)</sup> (1957) conclude that the anharmonicity of the vibrations is still small. The plot of  $\left[ 1 - (\theta_D/\theta_\infty)^2 \right] (T/\theta_\infty)^2$  against  $(\theta_\infty/T)^2$  is shown in graph 13; the values of A and B are given on this



graph. The even moments calculated from equations (54), (55), and (56) are given in table 7.

Equation (31), chapter 1, has been used to find the moments  $\overline{\nu^{-1}}$  and  $\overline{\nu^{-2}}$  of the frequency spectrum. The evaluation of the integral  $\int_0^\infty (C_V/T^n) dT$  ( $1 < n < 4$ ) between  $0^\circ\text{K}$  and  $10.5^\circ\text{K}$  involved some estimation of  $C_V$ , in the absence of experimental specific heat data in this region. After observing that the temperatures of the maxima in graphs of  $C_V/T^3$  against  $T$  for KI, NaI, KBr, and KCl, Berg and Morrison<sup>(60)</sup> (1957), were closely similar to the temperatures of the minima,  $T_m$ , in the corresponding graphs of  $\Theta_D$  against  $T$ , the temperature of this maximum in the case of RbBr was obtained by interpolation on graph 14 of  $T_m$  against  $\Theta_0$  for these salts. The corresponding value of  $\Theta_D$  was then estimated by interpolation on graph 15 of  $\Theta_D$  (at  $T_m$ ), against  $\Theta_0$  for these salts, from which  $C_V/T_m^3$  was calculated. The experimental evidence suggested a somewhat higher value, and a compromise was made in the drawing of the curve in the region of the maximum in the plot of  $C_V/T^3$  against  $T$  for the integration.  $C_V/T^3$  at  $T = 0^\circ\text{K}$  was taken as  $929/\Theta_0^3$  cal.mole<sup>-1</sup>deg.<sup>-4</sup> The values of  $\overline{\nu^{-1}}$  and  $\overline{\nu^{-2}}$  are given in table 7.

Equation (28) chapter 1 has been used to get the corresponding maximum frequencies of Debye spectra with the same  $n$ th moment  $\nu_D(n)$ , corresponding to  $\overline{\nu^n}$ , as the actual crystal. The values of  $\nu_D(n)$  are given in table 7.  $\nu_D(-3)$  was calculated from equation (34) chapter 1.  $\nu_D(0)$  was obtained from the geometric mean frequency  $\nu_g$  of the



spectrum using the relation  $\nu_D(0) = e^{\frac{1}{2}} \nu_g$ . (Equation (32) chapter 1.)

The geometric mean frequency  $\nu_g$  of the frequency distribution function

$g(\nu)$  is defined by 
$$\nu_g = \left[ \prod_{i=1}^{3N-3} \nu_i g(\nu_i) \right]^{1/\sum_{i=1}^{3N-3} g(\nu_i)}$$

As mentioned in chapter 1, Salter<sup>(20)</sup> (1955) has pointed out that the

slope of a graph of  $\exp\left(\frac{S}{3NK} - 1\right)$  against  $T$  at high temperatures is

equal to  $h \nu_g / K$ . Values of  $S$  have been calculated from  $S = \int_0^T (C_p/T') dT'$

where  $T'$  represents the temperature on a graph of  $C_p/T'$  against  $T'$ , which

is integrated numerically. Graph 16 shows a plot of  $\exp\left(\frac{S}{3NK} - 1\right)$

against  $T$ . The slope in the region  $T = \Theta_\infty$  has been used to calculate  $\nu_g$ .

The value of  $\nu_D(1)$  has been found by interpolation and is given in

table 7. Now the zero point energy is given by

$$E_z = \frac{3}{2} (N h \overline{\nu^1})$$

from equation (35) chapter 1. Hence the zero point energy has been

calculated,  $E_z = 587 \pm 6 \text{ cal.mole}^{-1}$ , which is some 6% lower than the

value calculated from the approximation  $E_z = 9NK\Theta_\infty/8$  of Domb and

Salter<sup>(18)</sup> (1952).

Debye-Waller Factor.

As pointed out in chapter 1 the Debye-Waller factor may be calculated

from thermodynamic data. Equation (37) has been used to calculate

$\Theta_0^M = 128.8^\circ\text{K}$ , and equation (39) to calculate  $\Theta_\infty^M = 132.3^\circ\text{K}$ . Equation (36)

has been used to find the initial curvature on a graph of  $\Theta_T^M$  against  $T$ .

The variation of  $\Theta_T^M$  above about  $0.3\Theta_D$  has been corrected for thermal

expansion by using equation (40), i.e.

$$\frac{\Theta^M(T, V_T)}{\Theta^M(T, V_0)} = \left( \frac{V_0}{V_T} \right)^\gamma$$

where  $\gamma = \gamma(-2)$  which was obtained from evaluation of equation (41),

$$\text{i.e. } \gamma(n) = \frac{\int_0^{\infty} \gamma_r C_v T^{(n-1)} dT}{\int_0^{\infty} C_v T^{(n-1)} dT} \quad \text{when } n = -2.$$

The variation of  $\epsilon_T^M$ , given in table 6, is plotted against T on graph 18.

The value of  $\gamma(-1)$  was also calculated using equation (41).

Graph 19 shows a plot of  $\gamma(n)$  against n, where  $\gamma(-3) = \gamma_0$  and  $\gamma(0) = \gamma_{\infty}$ .

The values of  $\gamma(n)$  are given in table 7.

#### Errors in Thermal Expansion Measurements.

1). Temperature Errors. White, Woods, and Anglin<sup>(30)</sup> (1958) have stated that their resistance values were reproducible to within the limits of their experimental error which corresponded to about  $\pm 0.01^\circ\text{K}$  at most temperatures. This will introduce an error of  $\pm 0.2\%$  in a measurement of a temperature interval of  $10^\circ\text{K}$ . The use of the present potentiometer will introduce a further error into the measurement of  $10^\circ\text{K}$  intervals, this error amounting to  $\pm 0.25\%$  at  $25^\circ\text{K}$  and  $\pm 0.2\%$  at  $270^\circ\text{K}$ .

2). Fringe Shift Errors. The measurement of the fringe shifts over a  $10^\circ\text{K}$  interval will be subject to a certain error, which depends on the accuracy with which the fractional fringe position at each temperature may be determined. The fringe widths were noticed to vary as the fringe pattern moved across the interferometer. The difference between the maximum and the minimum fringe widths was  $1/50$  of a fringe width.

Therefore the probable error on a single fractional fringe position is estimated to be  $1/100$  of a fringe width. For an expansion measurement two fractional fringe positions are used, and it is therefore estimated

that the fringe shifts may be measured to within  $\pm 1/50$  of a fringe width. This will give rise to various percentage errors depending on the magnitude of the thermal expansion being measured and the temperature intervals used.

The total error in an expansion measurement is the sum of the temperature error and the fringe shift error. Table 8 gives the estimated errors in the temperature measurements and in the fringe shift measurements over a  $10^{\circ}\text{K}$  interval, and also the total error in an expansion coefficient measurement over this temperature interval.

Table 8. Errors of Measurement Expressed as Percentages.

$T^{\circ}\text{K}$	Temperature errors.		Fringe shift error for $10^{\circ}\text{K}$ interval.				Total error in $\alpha$ for $10^{\circ}\text{K}$ interval.			
	(a)	(b)	Cu	CsI	RbBr	NaF	Cu	CsI	RbBr	NaF
25	0.2	0.25	10	0.5	0.7	15	10	1.0	1.5	15
35	0.2	0.23	3.5	0.2	0.4	6	4	0.63	0.83	6.5
45	0.2	0.22	2	0.2	0.3	3	2.5	0.62	0.72	3.5
55	0.2	0.21	1	0.17	0.2	1	1.5	0.58	0.61	1.5
150	0.2	0.2	0.5	0.12	0.17	0.25	0.9	0.52	0.57	0.65
270	0.2	0.2	0.4	0.1	0.15	0.2	0.8	0.5	0.55	0.6

(a) Errors arising from White et al.'s calibration.

(b) Errors arising from the present potentiometer measurements.

The plotted results of  $\alpha$  against  $T$ , however, indicate a greater deviation from the smooth variation, and it is found that the maximum

deviation is nowhere less than about  $\pm 2\%$ . This larger deviation may be due to a lack of thermal equilibrium when the readings were taken, or to inaccuracies in the results used for the thermometry. The third differences of  $R_T/R_{273}$  from White, Woods, and Anglin's<sup>(30)</sup> (1958) results, where  $R_T$  is the resistance at temperature T, showed large random variations, some of which could account for an error of  $\pm 2\%$ . Also it was noted that the values of the expansion coefficients of the various materials deviated from a smooth curve in the same direction in the same temperature ranges, indicating that the thermometer calibration was likely to be the cause of the larger deviations.

#### Estimated Errors in Associated Data.

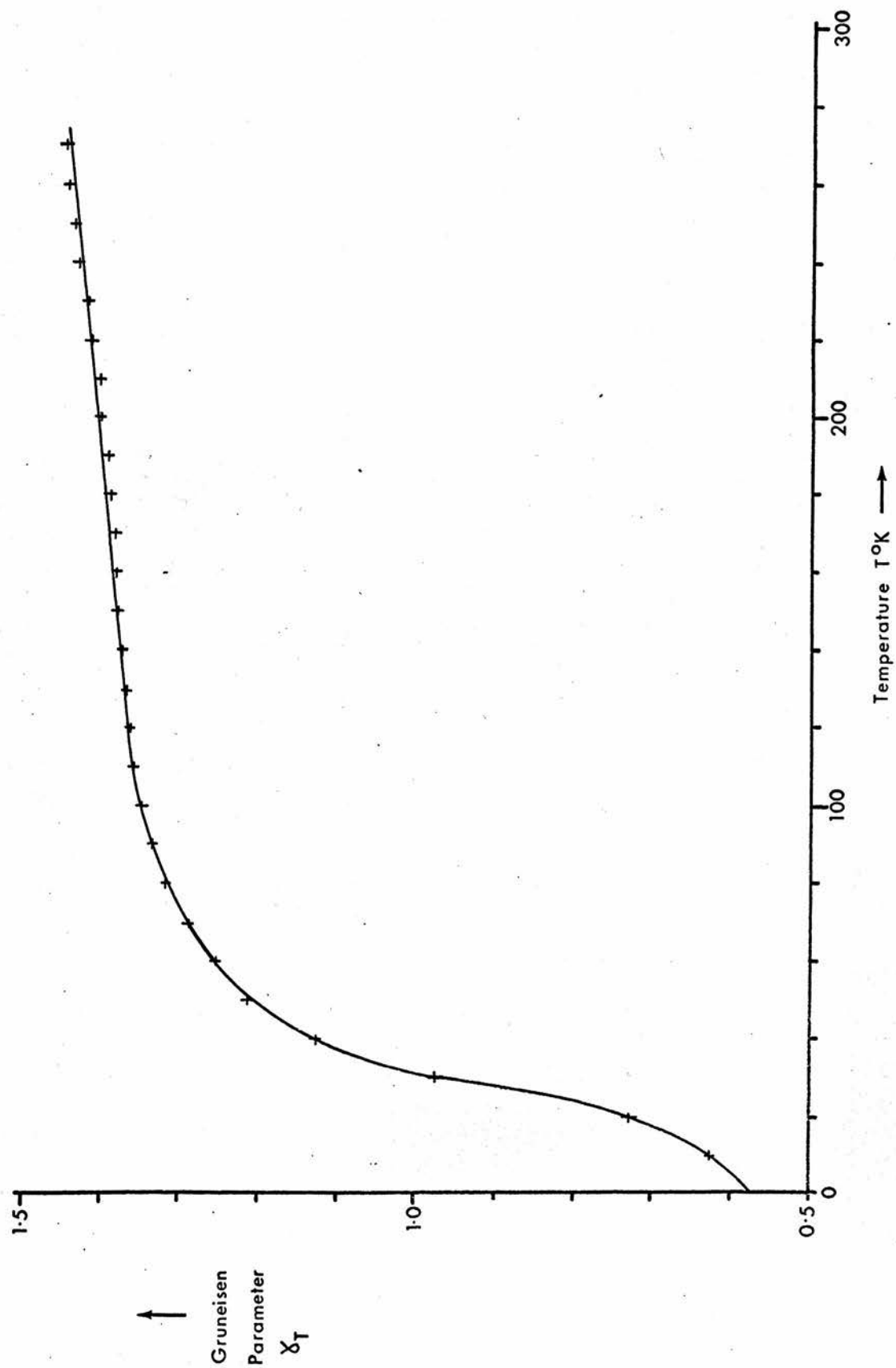
The errors discussed above are those present in the present experimental investigation. In analysing the results it is necessary to use the results of other workers and to allow for their experimental errors so that errors in the results of the analysis may be quoted. The experimental results for  $C_p$  were plotted on a graph so that smoothed values at  $10^\circ\text{K}$  intervals could be used in the analysis. From this graph the errors in  $C_p$  are estimated to be  $\pm 1\%$  over the range  $10^\circ\text{K}$  to  $270^\circ\text{K}$ . The error in  $\chi_s$  at  $295^\circ\text{K}$  is  $\pm 0.7\%$  according to the author of the elasticity measurements.  $\chi_s$  at  $0^\circ\text{K}$  was taken from a theoretical prediction, the error being estimated to be  $\pm 6\%$ .

#### Errors in the Results of the Analysis.

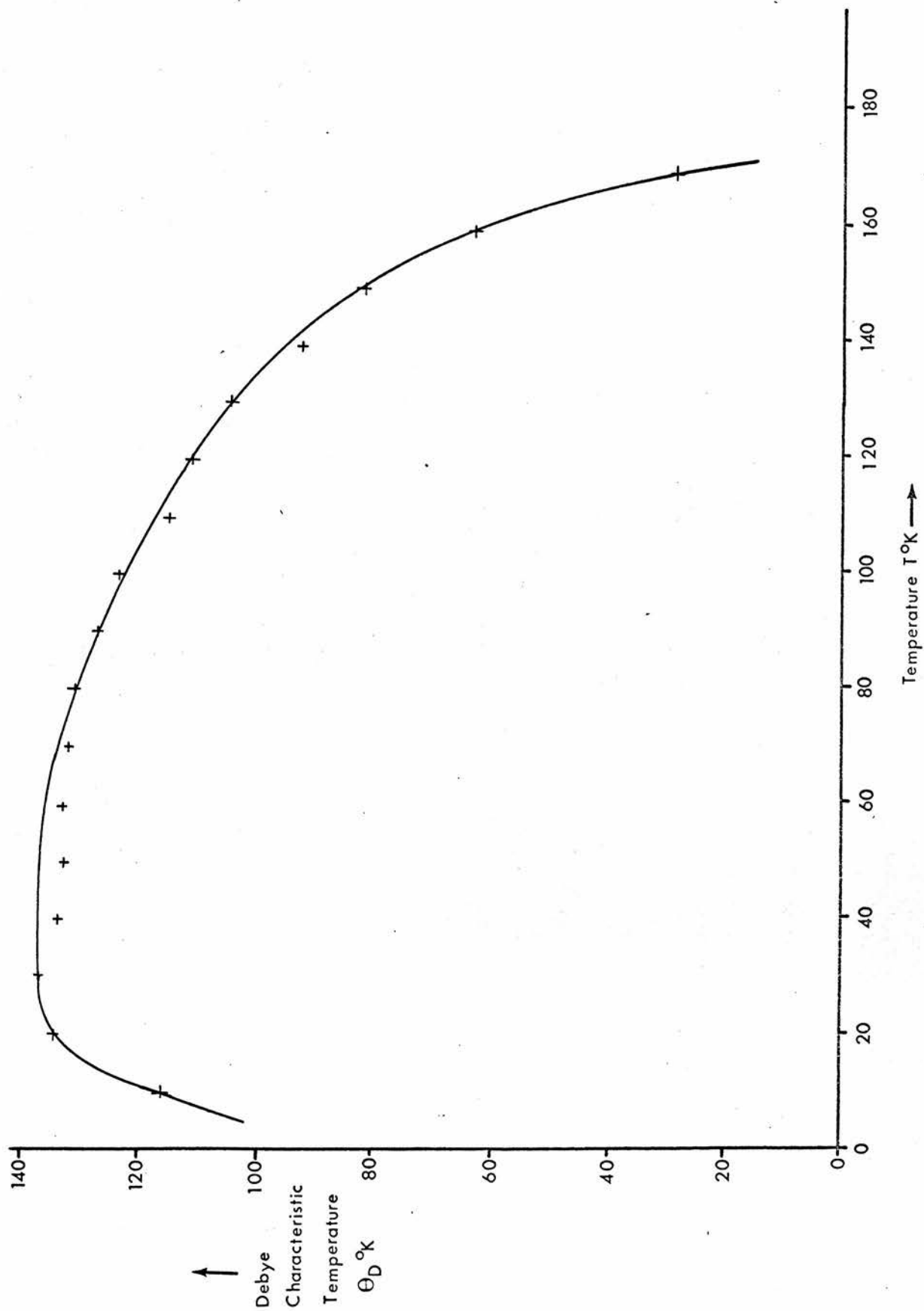
The error in the Grüneisen parameter  $\gamma_T$ , defined by  $\gamma_T = \beta V / (C_p \chi_s)$  is estimated to be  $\pm 9\%$  at  $20^\circ\text{K}$ , and  $\pm 4\%$  at  $270^\circ\text{K}$ . The error in  $\theta_\infty$  is

estimated to be  $\pm 1\%$  and the error in  $\Theta_0$ , calculated from theoretical predictions of the elastic constants, is estimated to be  $\pm 5\%$ . The estimated errors of  $\nu_p(n)$  and  $\delta(n)$  are given in table 7. The error in the zero point energy, obtained from  $\overline{\nu^1}$ , which was found by interpolation for  $\nu_p(1)$  on the graph of  $\nu_p(n)$  against  $n$ , is estimated to be  $\pm 1\%$ . The error in  $\Theta_T^M$  is estimated to vary between  $\pm 1\%$  at  $0^\circ\text{K}$  and  $\pm 2\%$  at  $270^\circ\text{K}$ .

Graph 9. Grüneisen Parameter against Temperature for RbBr.

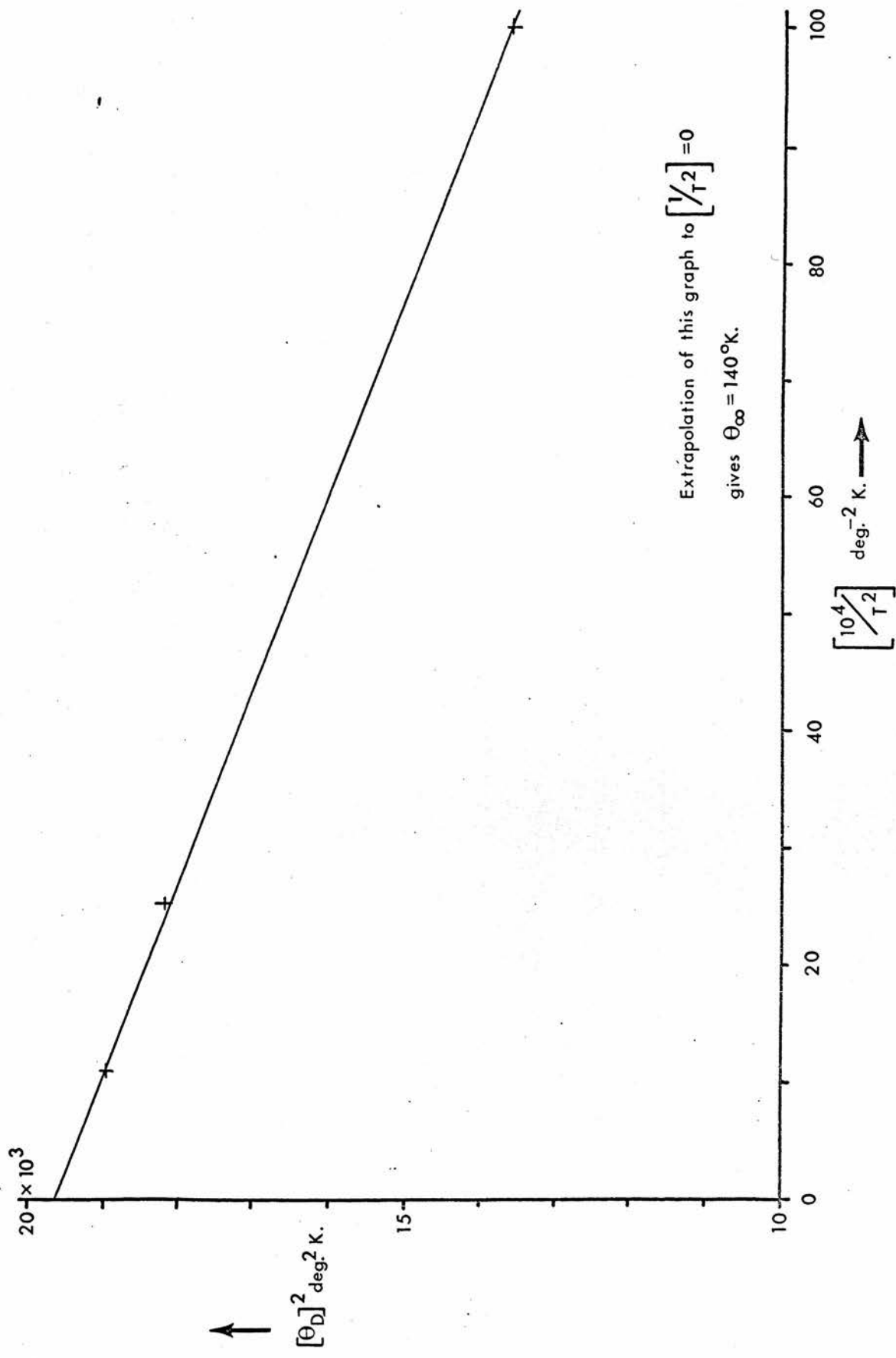


Graph 10. Debye Characteristic Temperature against Temperature for RbBr.

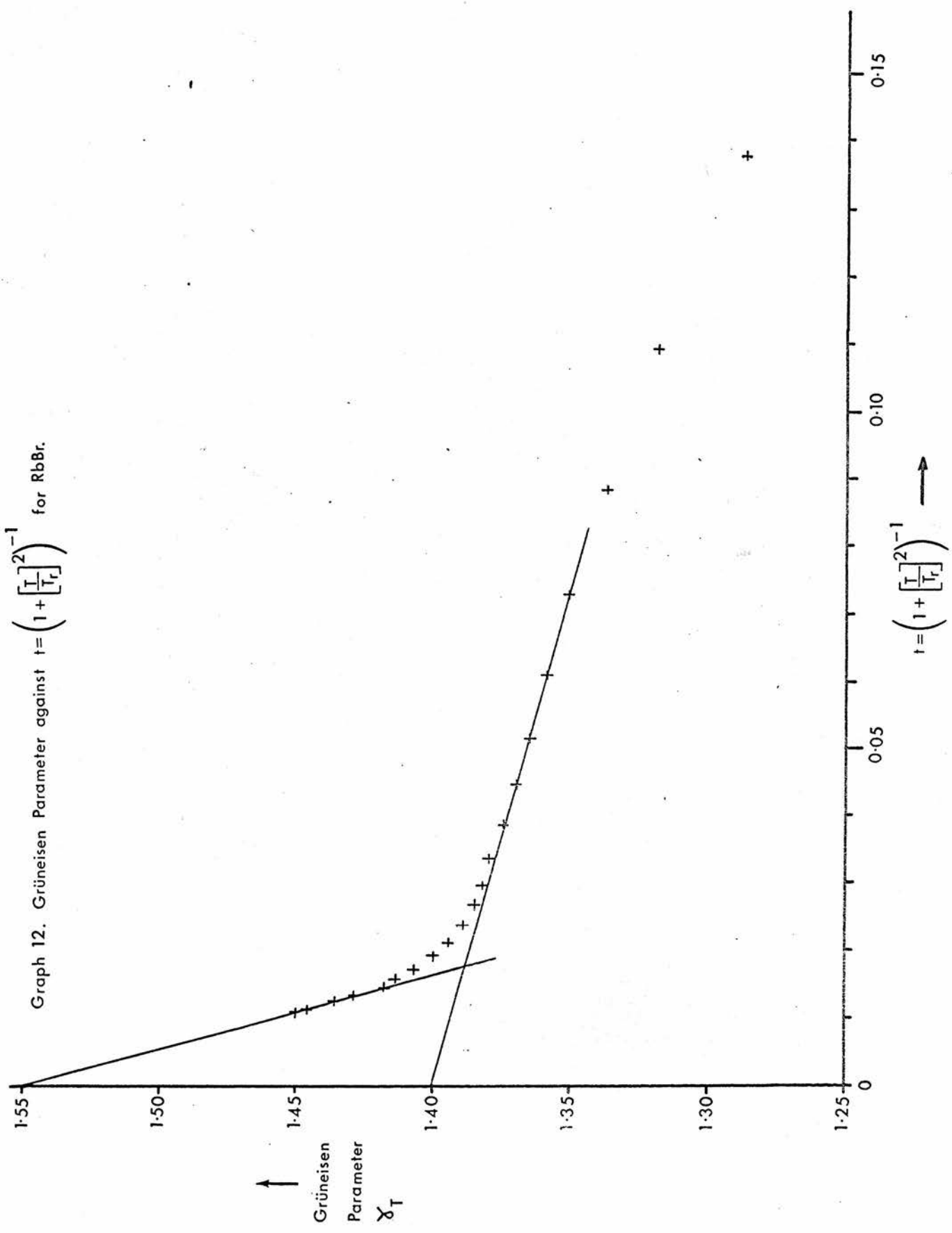




Graph 11.  $[\theta_D]^2$  against  $[\frac{1}{T^2}]$  for RbBr.



Graph 12. Grüneisen Parameter against  $t = \left(1 + \left[\frac{T}{T_r}\right]^2\right)^{-1}$  for RbBr.



Graph 13.  $\left[1 - \left(\frac{\theta_D}{\theta_{\infty}}\right)^2\right] \left(\frac{T}{\theta_{\infty}}\right)^2$  against  $\left(\frac{\theta_{\infty}}{T}\right)^2$

$30 \times 10^{-3}$

25

20

15

10

5

0

↑

$\left[1 - \left(\frac{\theta_D}{\theta_{\infty}}\right)^2\right] \left(\frac{T}{\theta_{\infty}}\right)^2$

Intercept,  $A = 15.8 \times 10^{-3}$   
 Slope,  $B = 0.760 \times 10^{-3}$

The dashed lines indicate the possible tangents considered in the estimation of errors.

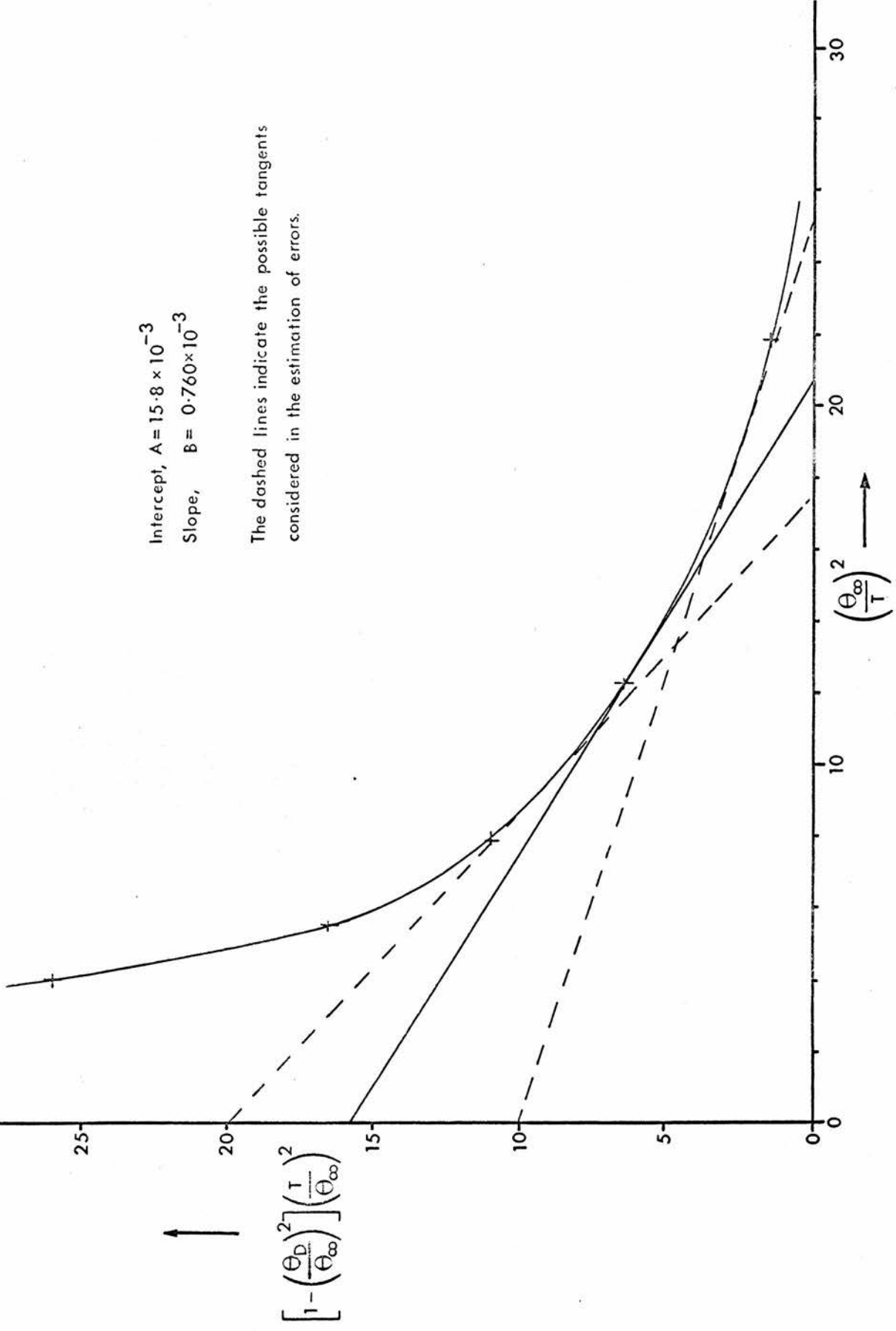
$\left(\frac{\theta_{\infty}}{T}\right)^2$

→

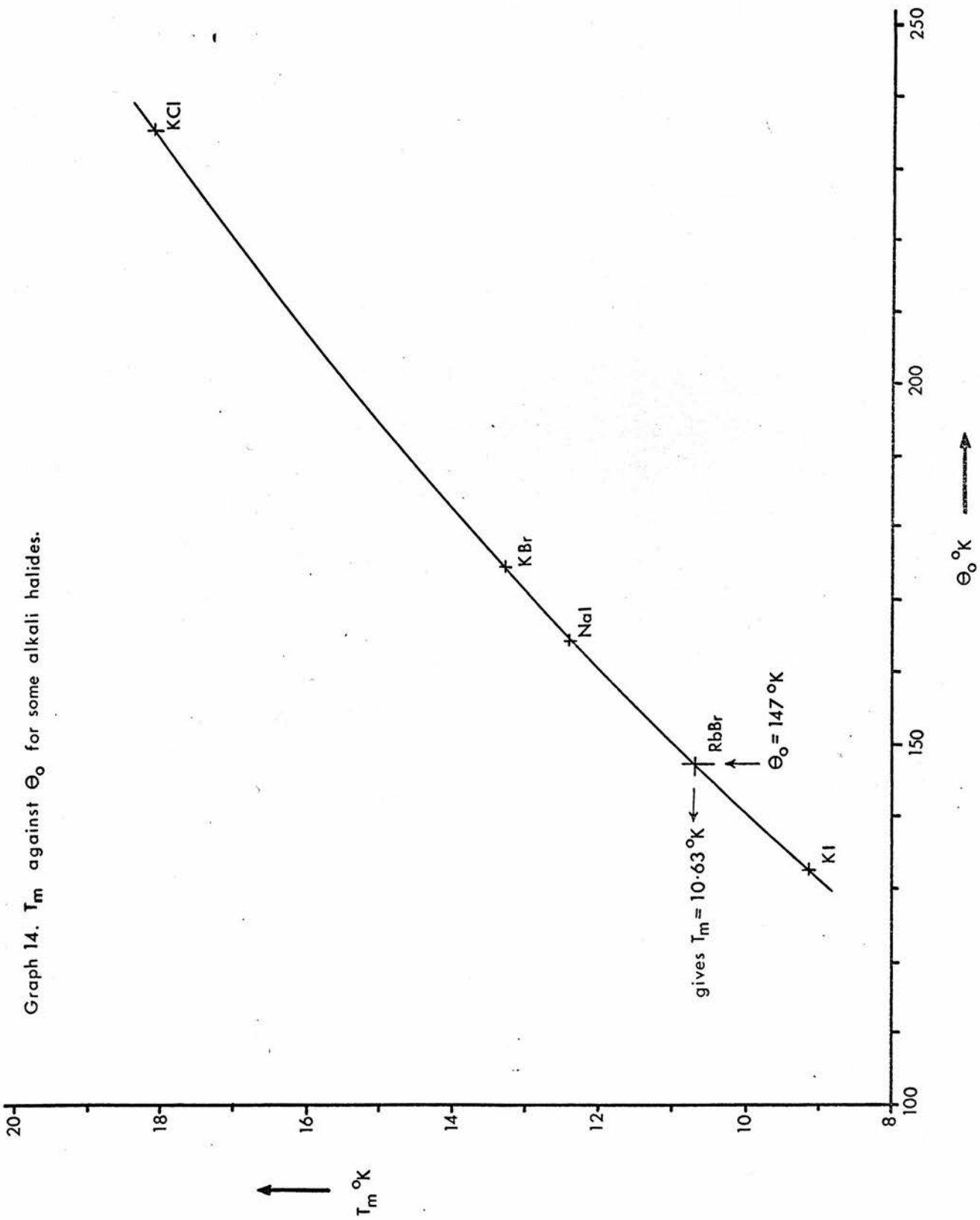
10

20

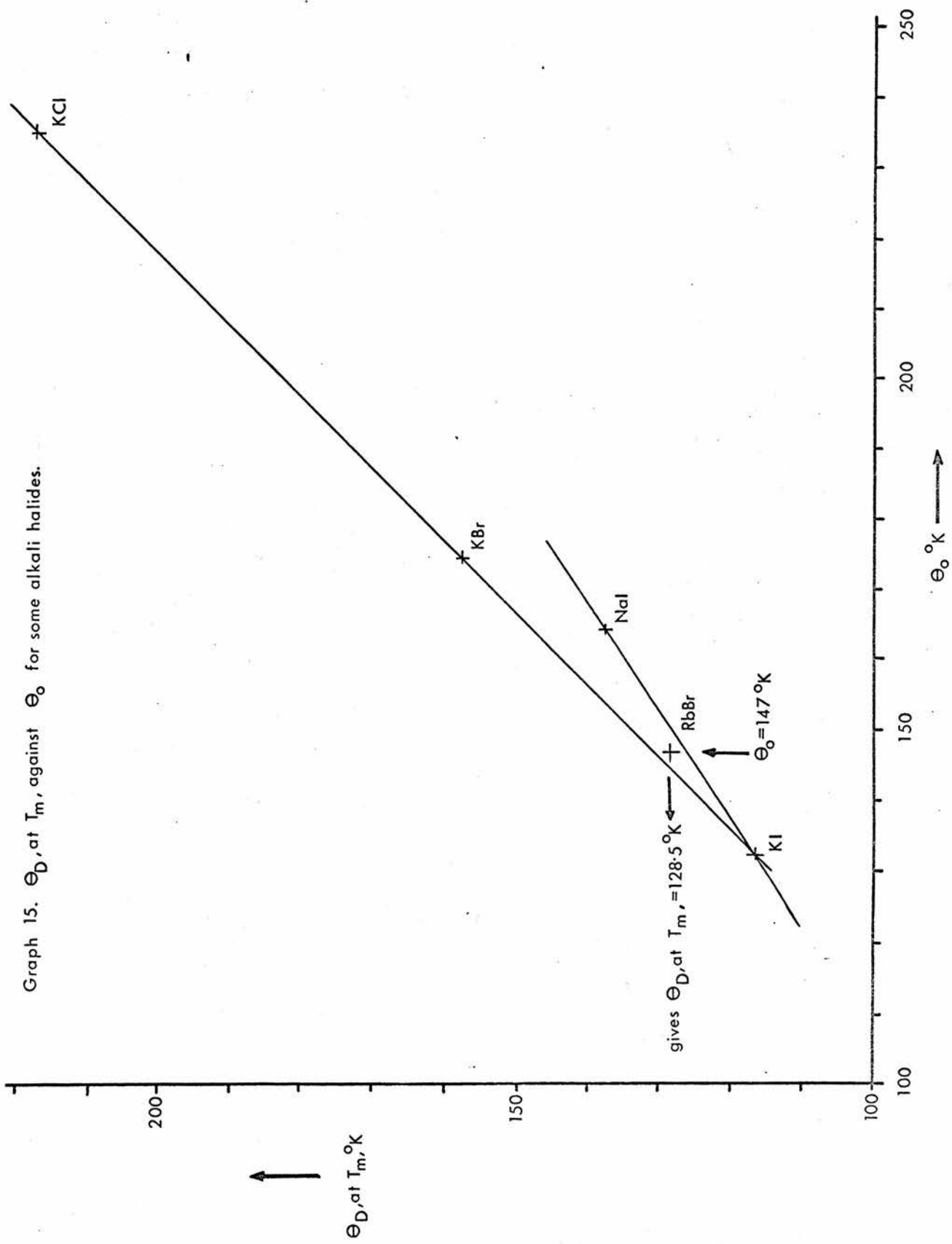
30



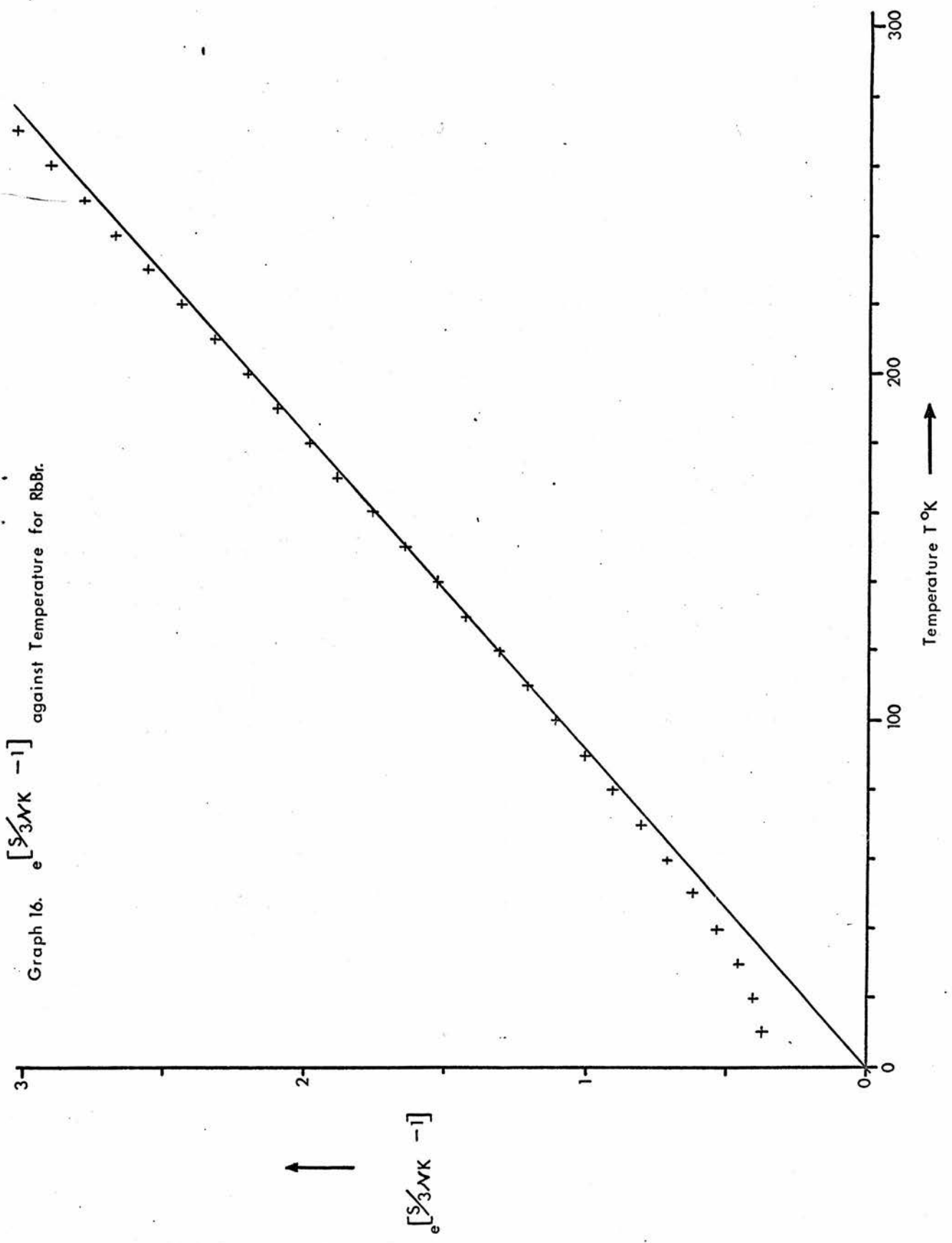
Graph 14.  $T_m$  against  $\Theta_0$  for some alkali halides.



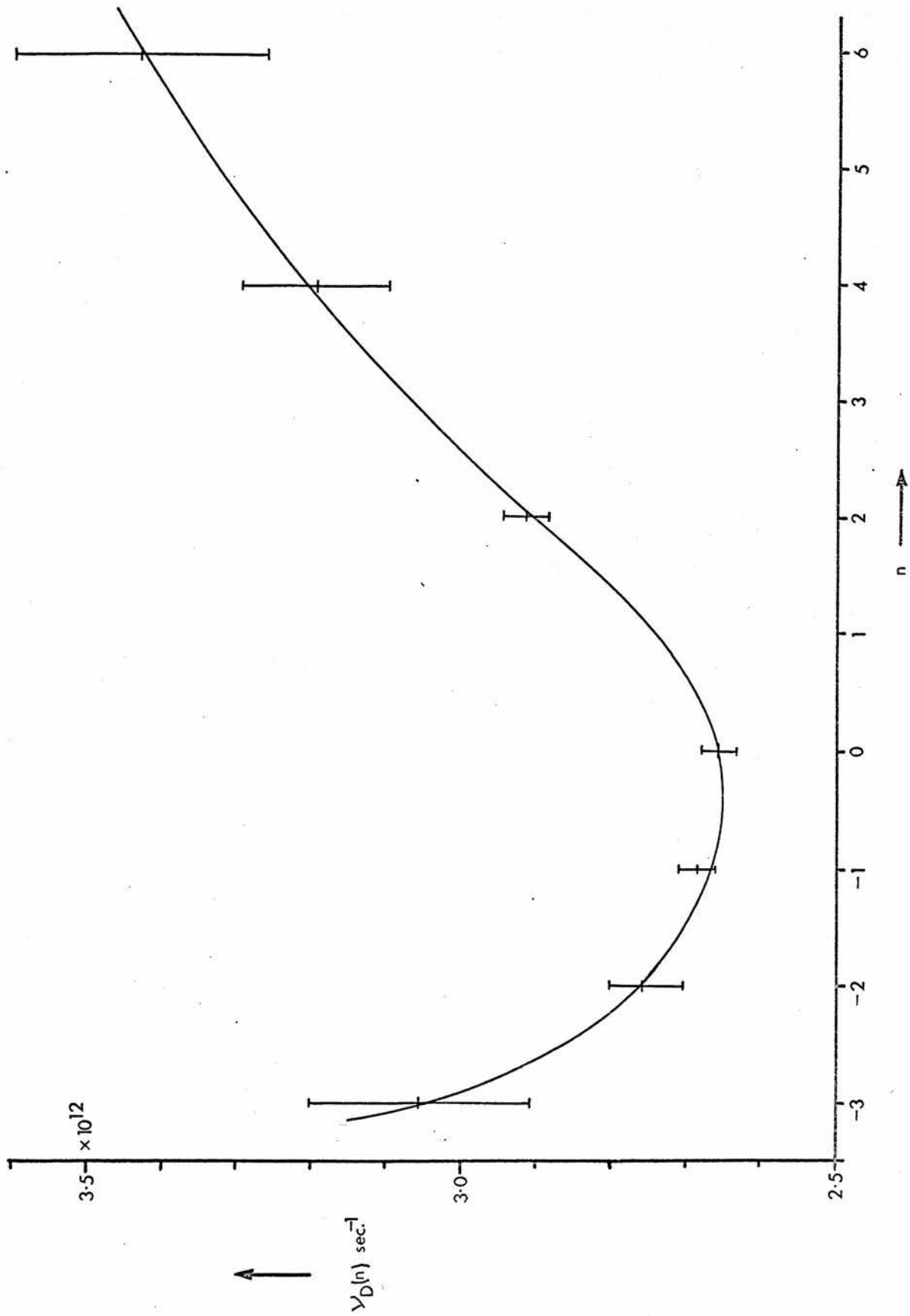
Graph 15.  $\Theta_D$  at  $T_m$ , against  $\Theta_0$  for some alkali halides.



Graph 16.  $e^{-\frac{S}{3MK} - 1}$  against Temperature for RbBr.

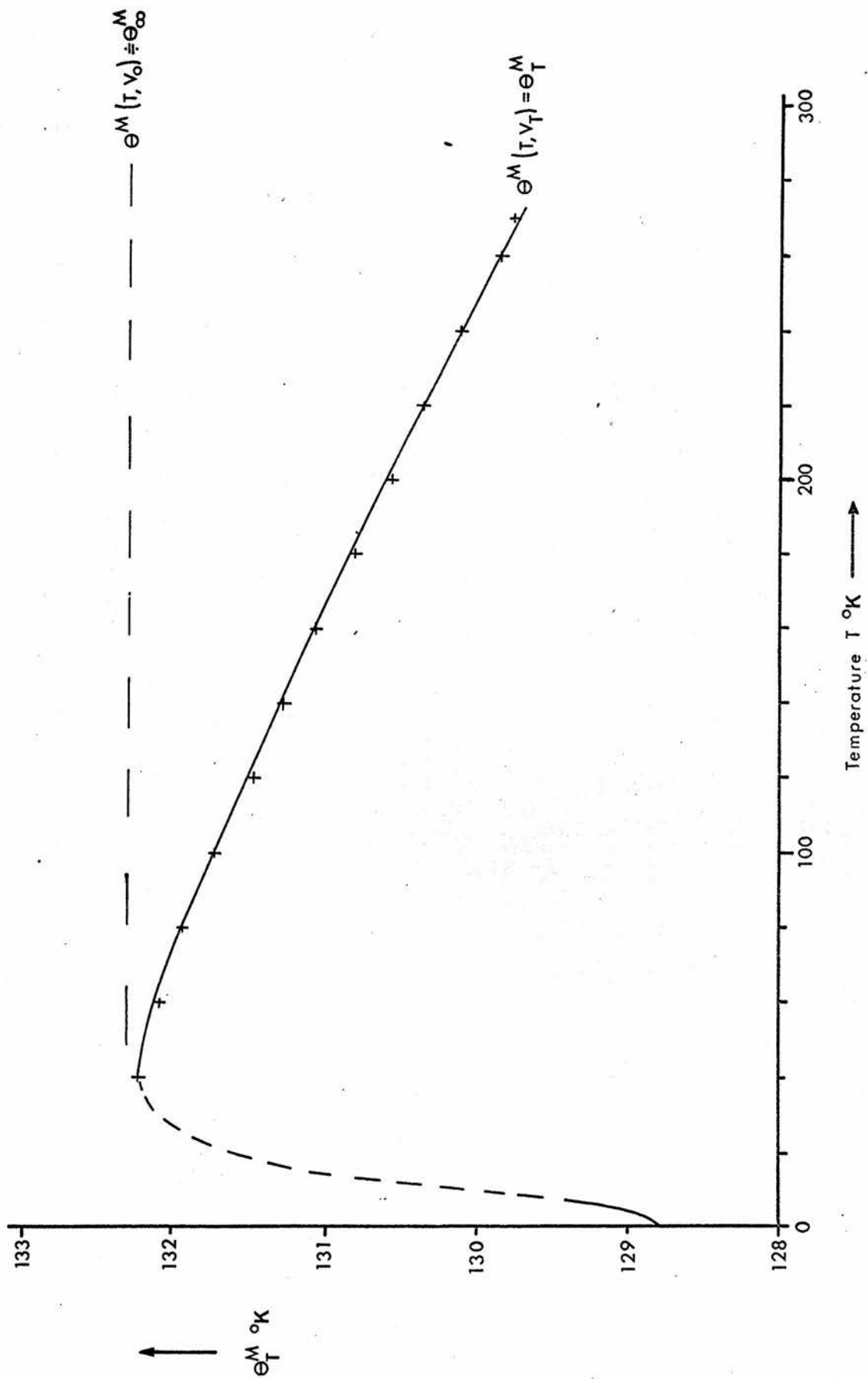


Graph 17.  $\gamma_D(n)$  against  $n$  for RbBr.





Graph 18  $e_T^M$  against Temperature for RbBr.



Graph 19.  $\chi(n)$  against  $n$  for RbBr.

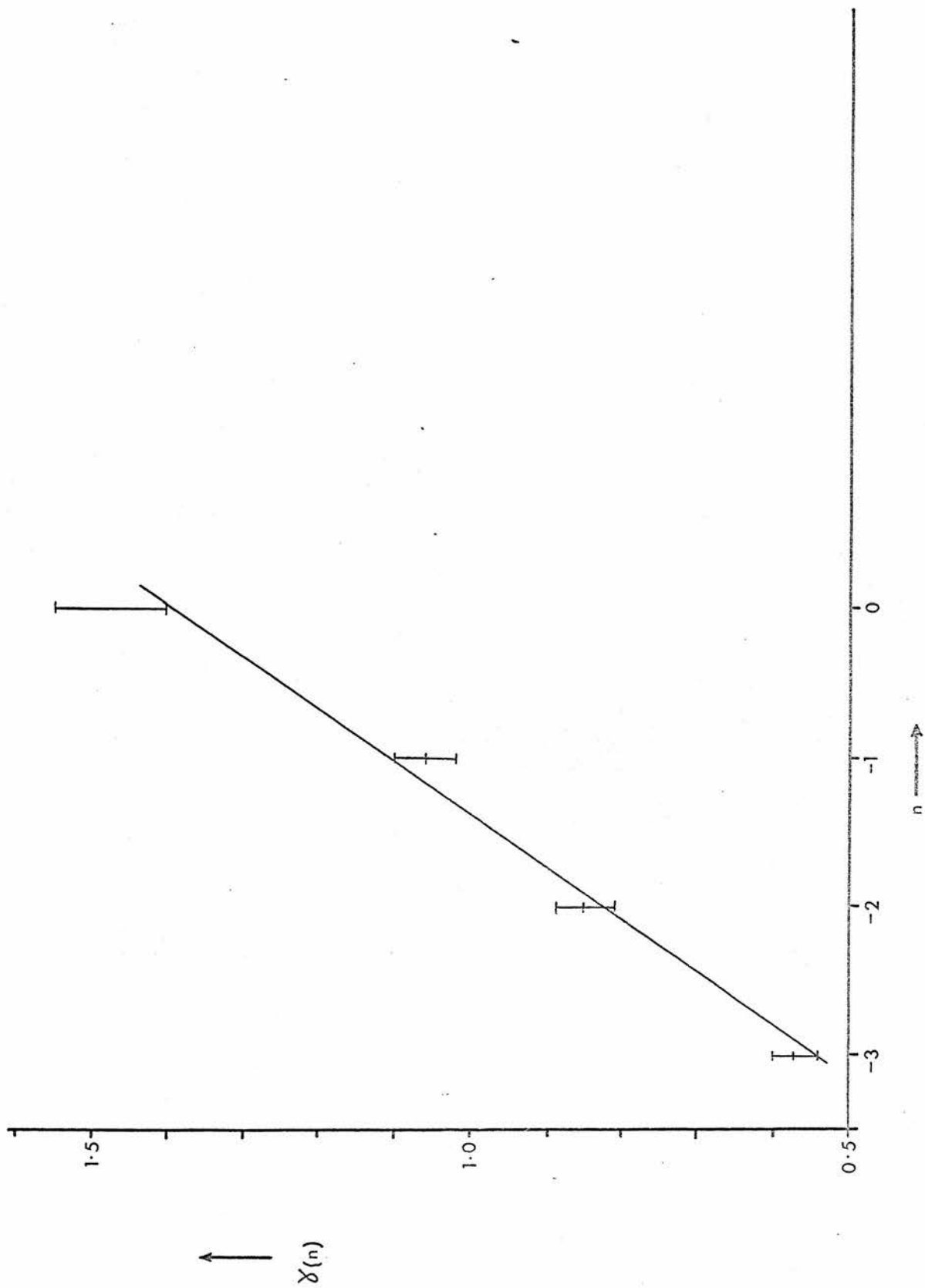


Table 2. Smoothed Values of the Linear Expansion Coefficient.

T°K	Thermal Expansion Coefficient $\alpha \times 10^6$ degrees <sup>-1</sup> K.				
	Sterling Silver.	Copper	NaF	RbBr	CsI
0	0			0	
10	(0.1)			(0.7)	
20	(0.73)	(0.23)	(0.25)	(3.48)	(15.1)
30	2.88	1.00	0.51	9.48	22.92
40	5.13	2.15	1.33	15.72	29.80
50	7.16	3.71	2.90	20.23	33.65
60	8.92	5.30	4.92	23.15	36.00
70	10.48	6.83	7.20	25.41	37.65
80	11.77	8.30	9.65	27.20	38.85
90	12.90	9.40	12.05	28.59	39.83
100	13.86	10.40	14.32	29.67	40.70
110	14.65	11.20	16.24	30.53	41.40
120	15.33	11.92	18.08	31.23	42.01
130	15.94	12.60	19.81	31.82	42.55
140	16.45	13.15	21.30	32.33	43.02
150	16.81	13.60	22.60	32.81	43.45
160	17.12	14.05	23.75	33.23	43.85
170	17.35	14.35	24.84	33.61	44.23
180	17.50	14.70	25.80	33.99	44.62
190	17.62	15.00	26.68	34.36	45.01
200	17.78	15.20	27.44	34.72	45.40
210	17.91	15.40	28.12	35.08	45.79
220	18.05	15.55	28.72	35.42	46.18
230	18.20	15.70	29.25	35.68	46.55
240	18.31	15.80	29.78	36.10	46.95
250	18.49	15.95	30.30	36.41	47.33
260	18.64	16.10	30.81	36.70	47.72
270	18.79	16.21	31.35	36.98	48.09
280	18.91			(37.32)	
290	19.09			(37.60)	
300	(19.22)				

Key to Column Headings for Tables 3, 4, and 5.

Column 1. Reading number.

2. Reduced resistance,  $R_T/R_{273.15}$ .
3. Specimen chamber temperature,  $T^{\circ}\text{K}$ .
4. Mean temperature for the thermal expansion coefficient,  $T_m^{\circ}\text{K}$ .
5. Approximate fringe shift,  $\Delta F$ .
6. Fractional fringe position,  $\Delta f$ .
7. Specimen chamber pressure,  $P$ , cm. of butyl phthalate.
8. Room temperature,  $t^{\circ}\text{C}$ .
9. Accurate fringe shift.
10. Linear thermal expansion coefficient  $\alpha \times 10^6$  degree<sup>-1</sup>K.

Table 3. Linear Thermal Expansion of CsI. Specimen Length =  $0.9850 \pm 0.0010$  cm.  
at  $22^\circ\text{C}$ .

1	2	3	4	5	6	7	8	9	10
	$R_T/R_{273}$	$T^\circ\text{K}$	$T_m^\circ\text{K}$	$\Delta F$	$\Delta f$	P cm.	$t^\circ\text{C}$	Fringe shift	$\alpha \times 10^6$ deg. $^{-1}$ K.
69	97.768	268.357			1.530	77.03	21.30		
70	93.173	258.482	263.419	18.3	1.867	76.77	21.45	18.340	47.95
71	88.554	248.381	253.431	18.4	1.420	76.70	21.70	18.557	47.43
72	21.350	77.891			2.303	77.59	20.80		
73	25.285	89.122	83.506	16.7	2.383	77.52	21.15	16.967	39.00
74	28.609	98.519	93.820	14.8	1.783	76.77	21.10	14.614	40.15
75	29.043	99.739			1.944	76.50	21.70		
76	32.325	108.938	104.338	14.7	1.343	76.14	21.47	14.617	41.02
77	36.144	119.530	114.234	16.9	1.379	76.94	21.35	16.984	41.40
78	36.595	120.765			1.426	77.51	21.35		
79	40.462	131.286	126.025	17.1	2.177	77.13	21.30	17.270	42.38
80	44.198	141.297	136.291	16.6	1.673	77.45	21.07	16.519	42.60
81	44.342	141.682			2.032	77.40	20.85		
82	48.085	151.588	146.635	16.4	1.508	77.00	21.00	16.538	43.10
83	51.706	160.906	156.247	15.9	1.637	76.47	21.30	15.884	44.01
84	52.082	161.865			2.069	76.91	22.65		
85	55.436	170.369	166.117	14.9	1.469	76.29	22.67	14.610	44.35
86	59.285	180.039	175.204	16.4	1.827	76.77	22.72	16.650	44.45
87	63.197	189.677	184.858	16.7	2.123	76.58	22.72	16.710	44.76
88	63.333	190.012			1.585	76.97	22.65		
89	67.306	199.613	194.812	16.8	1.727	76.46	22.15	16.867	45.35
90	71.532	209.658	204.635	17.7	2.020	76.17	21.70	17.714	45.53
91	2.137	20.498			1.806	76.40	20.87		
92	5.761	32.711	26.604	9.1	1.767	74.47	20.34	9.582	20.25
93	9.333	43.339	38.025	11.5	2.130	75.92	20.00	11.835	28.75
94	12.735	53.175	48.257	12.5	1.650	75.61	20.60	12.604	33.08
95	16.092	62.823	57.999	13.3	1.403	75.07	21.10	13.342	35.70
96	16.140	62.961			1.228	75.37	21.40		
97	19.942	73.868	68.414	16.0	1.521	75.09	20.77	15.775	37.34
98	23.060	82.777	78.322	13.1	2.152	75.18	21.10	13.409	38.86
99	2.140	20.524			1.863	77.44	19.80		
100	4.267	28.016	24.270	4.8	1.997	75.95	21.00	5.269	18.16
101	7.439	37.798	32.907	10.4	1.566	75.17	21.30	9.715	25.38
102	10.858	47.757	42.777	10.9	1.706	74.58	21.50	11.004	28.52
103	14.215	57.428	52.592	12.5	1.944	74.72	21.30	12.859	34.33
104	70.875	208.108			1.798	75.86	25.00		
105	75.257	218.351	213.229	18.1	1.579	76.64	25.00	18.224	45.93
106	79.421	227.950	223.150	17.2	1.444	75.22	25.00	17.143	46.11
107	83.838	237.969	232.959	18.0	1.408	76.02	25.55	18.040	46.48
108	88.401	248.045	243.007	18.5	1.956	76.36	25.36	18.456	47.29
109	91.300	254.404			1.274	76.84	25.05		
110	95.775	264.103	259.253	17.9	1.361	75.54	24.98	17.919	47.70
113	21.382	77.983			1.410	77.65	23.30		
114	27.337	94.944	86.463	25.5	1.635	75.03	23.00	25.852	39.35

Table 3 continued. Linear Thermal Expansion of CsI.

1	2	3	4	5	6	7	8	9	10
	$R_T/R_{273}$	$T^{\circ}K$	$T_m^{\circ}K$	$\Delta F$	$\Delta f$	P cm.	$t^{\circ}C$	Fringe shift	$\alpha \times 10^6$ deg. <sup>-1</sup> K
115	27.655	95.838			2.234	76.44	22.70		
116	30.787	104.638	100.238	14.0	1.361	77.40	22.80	13.894	40.76
117	34.400	114.634	109.636	15.8	2.325	73.18	22.80	16.075	41.52
118	34.653	115.434			2.230	77.82	22.00		
119	38.458	125.853	120.631	17.0	2.277	77.11	22.10	16.975	42.13
120	42.091	135.663	130.749	16.0	2.193	75.70	21.00	16.104	42.30
121	45.708	145.331	140.497	16.1	1.176	76.56	20.80	16.029	42.80
122	46.156	146.517			2.170	78.47	21.90		
123	49.882	156.231	151.374	16.3	1.803	75.52	22.08	16.386	43.55
124	53.509	165.500	160.865	15.9	1.999	77.02	22.50	15.811	44.04
125	57.529	175.648	170.574	17.3	1.578	77.49	22.25	17.430	44.34
126	2.150	20.563			1.846	78.51	20.45		
127	4.919	30.085	25.324	6.6	1.276	75.94	20.45	7.059	19.14
128	8.197	40.046	35.065	10.0	2.126	77.53	20.40	10.367	26.87
129	11.496	49.612	44.829	11.7	1.441	76.88	20.58	11.831	31.93
130	14.911	59.428	54.502	13.2	1.288	75.24	20.73	13.260	34.87
131	14.945	59.526			2.141	75.86	20.90		
132	18.347	69.305	64.415	14.0	1.285	77.81	20.27	13.912	36.73
133	21.875	79.391	74.348	14.9	1.362	75.26	19.50	14.989	38.37
134	25.320	89.237	84.314	14.7	1.425	74.87	19.95	14.977	39.27
135	56.386	172.768			2.099	77.01	25.27		
136	60.204	182.303	177.535	16.4	2.692	75.80	25.15	16.418	44.45
137	60.269	182.463			2.437	76.85	25.30		
138	64.379	192.551	187.507	17.3	1.970	76.64	24.72	17.475	44.72
139	68.477	202.416	197.483	17.3	2.760	76.57	24.20	17.217	45.06
140	72.655	212.286	207.351	17.4	2.377	77.12	24.00	17.389	45.48
141	72.522	211.975			2.023	76.11	24.20		
142	76.894	222.139	217.057	18.0	1.895	76.99	24.80	18.133	46.06
143	81.160	231.921	227.030	17.5	2.437	76.34	25.00	17.465	46.09
144	85.553	241.783	236.852	17.9	2.585	76.47	24.80	17.857	46.75
145	90.151	251.884	246.833	18.4	2.114	75.06	24.83	18.478	47.23

Table 4. Linear Thermal Expansion of RbBr. Specimen Length =  $1.0160 \pm 0.0010$  cm. at  $22^\circ\text{C}$ .

1	2	3	4	5	6	7	8	9	10
	$R_T/R_{273}$	$T^\circ\text{K}$	$T_m^\circ\text{K}$	$\Delta F$	$\Delta f$	P cm.	$t^\circ\text{C}$	Fringe shift	$\alpha \times 10^6$ deg. <sup>-1</sup> K
152	98.205	269.240			2.070	76.37	22.60		
153	93.557	259.317	264.278	14.7	1.739	77.82	22.73	14.675	37.01
154	93.557	259.317			1.652	76.53	22.35		
155	88.833	248.993	254.439	15.1	1.732	75.81	22.40	15.083	36.57
156	84.375	239.173	244.083	14.2	1.946	76.36	22.47	14.220	36.24
157	21.388	78.000			2.020	76.36	21.50		
158	26.727	93.220	85.610	16.9	2.053	77.21	22.25	17.025	28.00
159	26.953	93.859			1.315	76.20	22.80		
160	30.367	103.458	98.398	11.3	2.040	76.07	22.40	11.304	29.47
161	34.042	113.735	108.596	12.3	1.674	75.35	23.08	12.395	30.19
162	37.894	124.317	119.026	13.2	1.537	75.80	22.90	13.157	31.12
163	38.192	125.130			1.552	76.43	22.80		
164	42.116	135.730	130.430	13.5	2.077	75.98	22.15	13.494	31.86
165	45.873	145.768	140.749	13.1	1.258	76.40	22.12	12.834	32.00
166	45.883	145.794			2.195	76.42	23.45		
167	49.602	155.513	150.653	12.9	1.342	76.63	22.86	12.865	33.13
168	53.037	164.301	159.907	11.7	1.772	75.44	22.22	11.583	32.99
169	56.018	171.838	168.069	10.0	1.610	75.87	22.62	10.169	33.77
170	55.984	171.753			1.736	76.42	23.05		
171	59.498	180.564	176.158	11.9	1.822	76.54	22.50	11.922	33.87
172	63.193	189.667	185.115	12.4	1.402	76.05	22.24	12.429	34.17
173	67.168	199.281	194.474	13.3	2.150	76.19	22.10	13.259	34.52
174	71.335	209.193	204.237	13.7	1.358	76.17	21.98	13.800	34.85
175	71.263	209.024			1.620	76.00	22.84		
176	75.440	218.777	213.900	13.8	1.775	76.21	23.10	13.850	35.54
177	79.535	228.211	223.494	13.3	1.570	76.43	23.08	13.210	35.05
178	83.955	238.231	233.221	13.3	1.293	76.38	23.00	14.283	35.68
179	21.384	77.989			2.111	75.97	23.65		
180	24.734	87.561	82.775	10.4	1.568	75.84	23.95	10.565	27.63
181	24.868	87.945			2.136	76.28	23.18		
182	27.848	96.380	92.162	9.7	1.513	74.97	21.40	9.657	28.65
183	30.487	103.795	100.087	8.8	1.732	75.89	23.10	8.800	29.70
184	33.834	113.154	108.474	11.2	1.467	75.67	23.45	11.290	30.19
185	37.657	123.669	118.411	13.0	1.398	76.14	23.60	13.089	31.16
187	2.136	20.508			1.674	76.18	19.50		
188	5.702	32.530	26.519	3.0	1.641	75.90	19.37	3.570	7.43
189	9.034	42.472	37.501	5.5	1.209	75.05	19.08	5.651	14.23
190	12.394	52.195	47.333	7.2	1.900	74.95	20.10	7.437	19.14
191	15.703	61.705	56.950	8.6	1.453	74.82	21.10	8.535	22.46
192	19.190	71.718	66.711	9.8	1.602	74.35	21.25	9.919	24.79
193	22.905	82.334	77.026	11.3	1.295	75.33	21.60	11.355	26.77
194	26.423	92.362	87.348	11.2	2.050	76.88	21.90	11.276	28.14
196	96.127	264.862			1.744	75.93	21.56		
197	91.359	254.533	259.976	15.1	1.820	76.29	21.90	15.081	36.90
198	86.864	244.672	249.463	14.4	2.095	75.78	22.07	14.279	36.24



Table 4 continued. Linear Thermal Expansion of RbBr.

1	2 $R_T/R_{273}$	3 $T^{\circ}K$	4 $T_m^{\circ}K$	5 $\Delta F$	6 $\Delta f$	7 P cm.	8 $t^{\circ}C$	9 Fringe shift	10 $\alpha \times 10^6$ deg. <sup>-1</sup> K
199	37.317	122.739			1.757	76.49	21.58		
200	40.936	132.561	127.650	12.5	2.198	75.97	21.90	12.578	32.05
201	43.630	139.778	136.169	9.2	2.004	76.22	22.38	9.205	31.92
202	47.715	150.630	145.204	13.9	2.060	75.00	22.60	13.962	32.20
203	50.966	159.012	154.821	11.1	1.890	75.94	22.57	11.178	33.38
204	51.697	160.883			1.389	76.56	22.62		
205	54.856	168.903	164.893	10.7	1.618	76.05	23.00	10.781	33.64
206	58.007	176.843	172.873	10.6	1.950	75.52	23.10	10.687	33.69
207	61.579	185.690	181.266	12.1	1.880	75.86	23.18	12.077	34.17
208	61.203	184.764			1.186	76.26	24.10		
209	64.984	194.019	189.391	12.7	1.504	76.05	21.50	12.690	34.32
210	68.901	203.431	198.725	13.0	1.450	75.70	23.40	13.062	34.73
211	73.266	213.714	208.572	14.4	2.063	75.48	23.42	14.394	35.04
212	73.396	214.018			1.673	76.07	23.15		
213	77.505	223.509	218.763	13.5	1.228	76.80	22.85	13.450	35.47
214	81.801	233.379	228.444	13.8	1.308	76.26	22.52	13.927	35.32
215	81.767	233.302			1.445	76.28	21.81		
216	86.149	243.096	238.199	14.1	1.289	76.35	21.40	14.161	36.19
217	90.750	253.197	248.146	14.7	1.644	75.00	21.50	14.652	36.30
218	2.119	20.441			1.598	75.42	19.95		
219	3.839	26.598	23.519	1.0	1.625	74.64	18.70	1.322	5.37
220	3.835	26.585			1.633	74.18	18.80		
221	6.676	35.499	31.042	3.4	1.245	76.34	20.00	3.630	10.19
222	9.937	45.090	40.294	5.8	1.398	76.62	20.50	6.022	15.72
223	13.235	54.612	49.851	7.5	1.904	76.00	21.00	7.613	20.01
224	16.343	63.545	59.178	8.1	1.783	75.25	21.22	8.202	22.98
225	19.603	72.899	68.222	9.4	1.358	75.55	21.55	9.482	25.37



Table 5. Linear Thermal Expansion of NaF. Specimen Length =  $0.9874 \pm 0.0010$ cm. at  $22^{\circ}\text{C}$ .

1	2	3	4	5	6	7	8	9	10
	$R_T/R_{273}$	$T^{\circ}\text{K}$	$T_m^{\circ}\text{K}$	$\Delta F$	$\Delta f$	Pccm.	$t^{\circ}\text{C}$	Fringe shift	$\alpha \times 10^6$ deg. $^{-1}\text{K}$
1	99.258	271.549				77.75	21.40		
2	94.419	261.181	266.365	12.5	1.552	77.13	21.40	12.543	31.16
3	89.685	250.816	255.998	12.2	1.092	77.30	21.50	12.269	30.48
4	84.934	240.419	245.595	12.4	1.356	77.31	21.50	12.333	30.55
5	84.968	240.494			1.602	77.33	21.60		
6	80.347	230.032	235.263	11.9	1.549	77.41	21.80	11.953	29.42
7	21.375	77.963			1.047	78.16	21.30		
8	24.968	88.230	83.096	4.1	1.993	78.80	21.90	4.099	10.28
9	25.039	88.433			1.907	76.53	21.41		
10	27.852	96.391	92.412	4.0	0.980	76.32	21.80	3.955	12.80
11	31.232	105.883	101.187	5.4	1.660	76.60	22.03	5.349	14.50
12	35.095	116.648	111.265	6.9	1.706	76.47	22.22	6.980	16.70
13	35.156	116.816			1.592	76.83	22.18		
14	39.128	127.674	122.245	7.9	1.726	76.91	22.25	7.888	18.71
15	42.665	137.198	132.436	7.5	1.243	76.65	21.87	7.499	20.28
16	46.531	147.509	142.353	8.6	1.635	76.27	21.60	8.624	21.54
18	47.102	149.021			1.395	77.19	20.70		
19	50.584	158.032	153.526	8.2	1.249	76.39	21.37	8.159	23.32
20	54.802	168.767	163.399	10.2	1.100	76.23	21.91	10.161	24.38
21	59.040	179.427	174.097	10.3	1.690	75.95	21.60	10.421	25.18
22	59.126	179.642			1.484	76.53	21.68		
23	63.108	189.458	184.600	9.9	1.495	76.50	21.97	9.998	26.23
24	67.127	199.182	194.320	10.3	1.317	76.49	22.40	10.185	26.98
25	67.048	198.992			1.579	76.70	21.93		
26	71.283	209.071	204.031	10.9	1.726	75.90	22.00	10.716	27.75
27	75.737	219.467	214.269	11.5	1.219	76.46	22.80	11.513	28.52
28	80.026	229.337	224.402	12.0	1.106	76.38	23.00	12.119	29.02
30	96.678	266.037			1.116	77.29	19.70		
31	91.900	255.713	260.875	12.5	1.560	77.88	20.08	12.450	31.06
32	87.160	245.323	250.518	12.5	1.831	77.30	20.10	12.274	30.42
33	82.556	235.094	240.208	11.8	1.821	80.37	20.40	12.000	30.21
34	82.552	235.085			1.834	78.82	19.85		
35	78.068	224.846	229.965	11.6	1.457	76.72	20.32	11.625	29.24
37	5.017	30.392			1.000	77.53	19.00		
38	8.503	40.933	35.662	0.2	1.834	77.58	18.42	0.412	1.01
39	13.633	55.756			1.371	74.50	19.00		
40	17.055	65.592	60.674	1.9	1.490	78.25	19.10	1.936	5.07
41	20.653	75.900	70.746	2.8	1.607	77.75	18.80	2.947	7.36
42	24.351	86.467	81.183	4.0	1.579	77.29	18.32	4.077	9.94
43	21.318	77.800			1.053	77.23	20.17		
44	23.728	84.686	81.243	2.7	1.467	76.98	20.10	2.618	9.79

Table 5 continued. Linear Thermal Expansion of NaF.

1	2	3	4	5	6	7	8	9	10
	$R_T/R_{273}$	$T^{\circ}K$	$T_m^{\circ}K$	$\Delta F$	$\Delta f$	$P$ cm.	$t^{\circ}C$	Fringe shift	$\alpha \times 10^6$ deg. <sup>-1</sup> K.
45	23.803	84.900			1.380	76.50	20.40		
46	26.346	92.144	88.522	3.2	1.105	76.54	19.80	3.303	11.79
47	29.428	100.820	96.482	4.5	1.586	77.01	20.20	4.543	13.45
48	33.047	110.955	105.887	6.1	1.529	77.35	20.20	6.082	15.45
49	36.902	121.605	116.280	7.2	1.381	77.40	20.30	7.171	17.34
50	36.937	121.700			1.335	76.80	20.15		
51	40.627	131.729	126.714	6.4	1.791	77.07	20.15	6.561	19.42
52	44.414	141.874	136.741	8.3	1.534	76.64	20.10	8.274	21.00
53	48.173	151.816	146.845	8.5	1.946	76.38	20.08	8.602	22.28
54	48.266	152.057			1.874	76.68	21.90		
55	49.670	155.688	153.872	3.4	1.550	75.60	22.00	3.330	23.62
56	49.687	155.731			1.511	76.47	21.90		
57	52.845	163.811	159.771	7.6	0.954	76.48	22.25	7.565	24.11
58	56.826	173.879	168.835	9.8	1.265	75.72	22.08	9.701	24.81
59	57.114	174.606			1.656	76.73	22.90		
60	60.945	184.128	179.367	9.5	1.060	76.42	23.00	9.606	25.98
61	65.046	194.170	189.099	11.4	1.707	75.62	22.90	11.362	26.84
62	69.249	204.263	199.216	10.7	0.977	77.19	23.07	10.735	27.39
63	73.699	214.727	209.595	11.5	1.567	76.45	22.18	11.418	28.10
64	73.753	214.853			1.458	77.02	22.00		
65	78.066	224.841	219.852	11.2	1.273	76.95	22.10	11.191	28.86
66	82.458	234.873	229.857	11.2	1.903	76.19	22.10	11.376	29.20
68	2.153	20.575			1.695	77.22	18.10		
69	3.554	25.640	23.114	-0.1	0.941	76.34	17.85	0.055	0.28
70	3.558	25.654			1.054	75.76	17.80		
71	6.654	35.432	30.543	-0.1	1.054	76.04	17.82	0.191	0.50
72	9.989	45.240	40.336	0.4	1.733	75.90	17.25	0.498	1.31
73	13.383	55.037	50.138	1.0	1.728	76.23	17.40	1.115	2.93
74	2.146	20.547			1.732	77.20	17.50		
75	4.959	30.210	25.378	-0.4	1.076	76.07	18.37	0.124	0.33
76	8.390	40.606	35.408	0.05	0.950	76.16	18.78	0.368	0.91
77	11.702	50.207	45.406	0.75	1.305	75.92	19.00	0.782	2.10
78	14.938	59.506	54.856	1.2	0.992	76.12	19.00	1.401	3.88
79	18.270	69.083	64.294	2.1	1.815	77.90	19.15	2.234	6.01
80	21.770	79.091	74.087	3.2	1.730	76.07	19.20	3.147	8.10

Table 6. Rubidium Bromide Analysis.

$T^{\circ}\text{K}$	$\alpha \times 10^6$ deg. <sup>-1</sup> K	$C_p$ cal. mole <sup>-1</sup> deg.	$\chi_s \times 10^{12}$ cm. <sup>2</sup> dyne <sup>-1</sup>	$\gamma_T$	$C_v$ cal. mole <sup>-1</sup> deg.	$\Theta_D^{\circ}\text{K}$	$t = \left[1 + \left(\frac{\Theta_D}{T}\right)^2\right]^{-1} e_M^T$ °K	
0	0	0	6.817	(0.569)	0			
10	(0.7)	0.578	6.831	0.627	0.578	116.8	0.8869	
20	(3.48)	2.476	6.845	0.727	2.476	134.9	0.6622	
30	9.48	5.016	6.859	0.975	5.012	137.7	0.4656	
40	15.72	7.176	6.873	1.128	7.162	134.32	0.3289	132.22
50	20.23	8.580	6.887	1.211	8.550	133.75	0.2387	132.13
60	23.15	9.480	6.901	1.253	9.428	135.56	0.1788	132.08
70	25.41	10.100	6.916	1.287	10.032	132.51	0.1379	131.98
80	27.20	10.552	6.930	1.319	10.446	131.68	0.1091	131.92
90	28.59	10.900	6.944	1.337	10.792	127.80	0.0883	131.77
100	29.67	11.172	6.959	1.351	11.042	124.10	0.0727	131.71
110	30.53	11.400	6.974	1.359	11.248	115.61	0.0609	131.59
120	31.23	11.548	6.988	1.365	11.412	111.36	0.0516	131.47
130	31.82	11.740	7.003	1.370	11.548	105.04	0.0443	131.36
140	32.33	11.864	7.018	1.374	11.650	92.75	0.0385	131.28
150	32.81	11.968	7.032	1.380	11.732	82.01	0.0337	131.14
160	33.23	12.078	7.047	1.382	11.822	63.20	0.0297	131.05
170	33.61	12.164	7.062	1.385	11.886	28.9	0.0264	130.97
180	33.99	12.240	7.077	1.389	11.940		0.0236	130.81
190	34.36	12.300	7.092	1.394	11.976		0.0213	130.72
200	33.72	12.344	7.107	1.400	11.998		0.0192	130.57
210	35.08	12.388	7.123	1.407	12.018		0.0175	130.44
220	35.42	12.432	7.138	1.413	12.038		0.0159	130.36
230	35.68	12.448	7.153	1.418	12.032		0.0146	130.20
240	36.10	12.472	7.168	1.429	12.028		0.0134	130.11
250	36.41	12.484	7.184	1.437	12.016		0.0124	129.96
260	36.70	12.504	7.199	1.443	12.010		0.0115	129.84
270	36.98	12.516	7.215	1.449	11.996		0.0106	129.76
280	(37.32)		7.231					
290	(37.60)		7.246					
295	(37.74)		7.257					

Table 6 continued. Rubidium Bromide Analysis.

$T^{\circ}\text{K}$	$(\theta_D)^2$ deg. <sup>2</sup> K	$\frac{10^4}{T^2}$ deg. <sup>-2</sup> K	$\frac{\theta_{\infty}^2}{T^2}$	$\left[1 - \left(\frac{\theta_D}{\theta_{\infty}}\right)^2\right] \left(\frac{T}{\theta_{\infty}}\right)^2$
0				
10	13,642.2	100	196.00	0.00155
20	18,198.0	25	49.00	0.00145
30	18,961.3	11.1	21.78	0.00149
40			12.25	0.00649
50			7.84	0.01113
60			5.44	0.01651
70			4.00	0.02603

Table 7. Moments of the Frequency Spectrum for RbBr.

n	$\overline{\nu^n}$	$\nu_D(n)\text{sec.}^{-1}$	$\gamma(n)$	% errors in $\nu_D(n)$ $\gamma(n)$	
-3		$3.06 \times 10^{12}$	0.569	5	
-2	$3.45 \times 10^{-27} \text{sec.}^2$	$2.76 \times 10^{12}$	0.849	2	4
-1	$5.59 \times 10^{-13} \text{sec.}$	$2.68 \times 10^{12}$	1.060	1	4
0		$2.66 \times 10^{12}$	1.400	1	
1		$(2.74 \times 10^{12})$		1	
2	$5.11 \times 10^{24} \text{sec.}^{-2}$	$2.92 \times 10^{12}$		1	
3					
4	$4.48 \times 10^{49} \text{sec.}^{-4}$	$3.20 \times 10^{12}$		3	
5					
6	$5.47 \times 10^{74} \text{sec.}^{-6}$	$3.43 \times 10^{12}$		5	

## Chapter 7.

### Conclusions.

This investigation has provided useful data for the thermal expansion coefficients of NaF, RbBr, and CsI. The results have been used in the case of RbBr, together with other data for this crystal, to find the variation of the Grüneisen parameter with temperature, to calculate the moments of the frequency spectrum, and to calculate the Debye-Waller factor. The absence of other experimental data for NaF and CsI has precluded any reliable analysis of these results.

It has not been considered profitable to follow the procedure used by Barron and Morrison<sup>(21)</sup> (1960) to determine frequency spectra for some alkali halides, since the moments found for the real frequency spectrum of RbBr are not sufficiently accurate for this analysis. The analysis that has been carried out provides useful information about RbBr. It is however very desirable that both more extensive data and more accurate data for  $C_p$  and  $\chi_s$  for RbBr, NaF, and CsI should be obtained experimentally, so that a more complete theory of lattice vibrations of the alkali halides may be formulated.

Measurements of the thermal expansion coefficients could usefully be extended to lower temperatures, using the present method in the case of RbBr and CsI, whenever liquid helium becomes readily available at Bradford Institute of Technology. Because the difficulties encountered, i.e., the rotations and the changes in width of the fringes, took so long to solve, it was not possible to investigate fully the possibilities of further improving the sensitivity to small fringe movements. The



technique described has been adequate for the present investigation, but for measurements to lower temperatures for NaF an increased sensitivity would be required. The Rayleigh criterion for the resolving power of an optical system is of no use in estimating the maximum sensitivity of which the method is capable, since the measurements do not depend on the resolution of two peaks close together, but on the accuracy with which the centre of a single fringe may be found.

The sensitivity that can be obtained with the microphotometer is limited by the silver grains of the photographic emulsion that have been exposed to the fringes and developed. These grains may not be uniformly distributed and will therefore lead to inaccuracies in locating the centre of the fringe. If the number of grains per unit area is larger, i.e. if the grain of the film is finer, then the precision with which the fringe centre may be located will be greater. There is however a drawback here in that fine grain films require longer exposures. Another way of increasing the accuracy with which fringe centres may be located is to have a larger image, but again a longer exposure would be necessary. It might be possible to increase the sensitivity by an order of magnitude by accepting much longer exposures. If the sensitivity were increased further, optical flats of greater flatness would be required.

The thermometry would need to be extended to  $4.2^{\circ}\text{K}$  if measurements at lower temperatures were to be made. If greater accuracy is required at the higher temperatures covered in this investigation it would seem desirable to obtain an N.P.L. calibrated platinum resistance thermometer, or to build a more reliable constant volume gas thermometer in order to calibrate an indium thermometer with a larger ice point resistance.

References.

- 1). Grüneisen, E., 1912, Ann. Phys., Lpz., 39, 257.
- 2). Grüneisen, E., 1926, Hand. der Phys., 10, 1.
- 3). Debye, P., 1912, Ann. Phys., Lpz., 39, 789.
- 4). Debye, P., 1913, Phys. Z., 14, 259.
- 5). Born, M., 1923, Atomtheorie des festen Zustandes, (Leipzig; Teubner).
- 6). Dayal, B., 1944, Proc. Ind. Acad. Sci., A 20, 145.
- 7). Barron, T.H.K., 1955, Phil. Mag., 46, 720.
- 8). Blackman, M., 1957, Proc. Phys. Soc., B, 70, 827.
- 9). Yates, B., and Panter, C.H., 1962, Proc. Phys. Soc., 80, 373.
- 10). Barron, T.H.K., Leadbetter, A.J., Morrison, J.A., and Salter, L.S.,  
1963, Inelastic Scattering of Neutrons in Solids and Liquids, 1, 49.
- 11). Nernst, W., 1906, Preuss. Akad. Wiss., Berlin, Sitz. ber., 52, 933.
- 12). Einstein, A., 1907, Ann. Physik, 22, 180.
- 13). Zemansky, M.W., 1957, Heat and Thermodynamics, McGraw-Hill Book Co.,  
New York, Toronto, London.
- 14). Born, M., and von Kármán, T., 1912, Phys. Z., 13, 297.  
Born, M., and von Kármán, T., 1913, Phys. Z., 14, 15.
- 15). Roberts, J.K., and Miller, A.R., 1951, The Student's Physics, Vol.IV,  
Heat and Thermodynamics, Blackie & Son Ltd., London and Glasgow.
- 16). Barron, T.H.K., Berg, W.T., and Morrison, J.A., 1957, Proc. Roy. Soc.,  
A, 242, 478.
- 17). Thirring, H., 1913, Phys. Z., 14, 867.
- 18). Domb, C., and Salter, L., 1952, Phil. Mag., 43, 1083.



- 19). Hwang, J-L., 1954, J.Chem. Phys., 22, 154.
- 20). Salter, L., 1955, Proc. Roy. Soc., London, A 233, 418.
- 21). Barron, T.H.K., and Morrison, J.A., 1960, Proc. Roy. Soc., London, A 256, 427.
- 22). Barron, T.H.K., Leadbetter, A.J., and Morrison, J.A., (to be published)
- 23). Blackman, M., 1937, Proc. Roy. Soc., London, A 159, 416.
- 24). Sheard, F.W., 1958, Phil. Mag., 3, 1381.
- 25). White, G.K., and Woods, S.B., 1957, Rev. Sci. Instrum., 28, 638.
- 26). Yates, B., and Panter, C.H., 1961, J. Sci. Instrum., 38, 196.
- 27). James, B.W., and Yates, B., 1963, J. Sci. Instrum., 40, 193.
- 28). White, D., Rubin, T., Camky, P., and Johnston, H.L., 1960, J. Phys. Chem., 64, 1607.
- 29). Roberts, T.R., and Sydoriak, S.G., 1956, Phys. Rev., 102, 304.
- 30). White, G.K., Woods, S.B., and Anglin, F., 1958, Rev. Sci. Instrum., 29, 181.
- 31). Swenson, C.A., 1955, Phys. Rev., 100, 1607.
- 32). Huzan, E., Abbiss, C.P., and Jones, G.O., 1961, Phil. Mag., 6, 277.
- 33). Jones, R.V., 1960, J. Sci. Instrum., 38, 37.
- 34). Andres, K., 1961, Cryogenics, 2, 93.
- 35). Rubin, T., Altman, H.W., and Johnston, H.L., 1954, J. Am. Chem. Soc., 76, 5289.
- 36). Meincke, P.P.M., and Graham, G.M., 1962, 8<sup>th</sup> Int. Conf. on Low Temp. Phys
- 37). Figgins, B.F., Jones, G.O., and Riley, D.P., 1956, Phil. Mag., 1, 747.
- 38). White, G.K., 1961, Cryogenics, 1, 151.

- 39). Born, M., and Wolf, E., Principles of Optics, Pergamon Press.
- 40). Fizeau, H., 1862, Ann. Chem. Phys., (3) 66, 429.
- 41). Roberts, V., 1954, J. Sci. Instrum., 31, 251.
- 42). Timoshenko, S.P., and Woinowsky-Krieger, S., 1959, Theory of Plates and Shells, p.425, Engineering Society Monographs, McGraw-Hill Book Co., London, New York, and Toronto.
- 43). Longhurst, R.S., 1957, Geometrical and Physical Optics, p.423, Longmans, Green, & Co., London, New York, and Toronto.
- 44). Kaye, G.W.C., and Laby, T.H., 1947, Tables of Physical and Chemical Constants, p.88, Longmans, Green, & Co., London, New York, Toronto.
- 45). Parkinson, D.H., and Quarrington, J.E., 1954, Proc. Phys. Soc., A 67, 569.
- 46). Yates, B., and Hoare, F.E., 1961, Cryogenics, 2, 84.
- 47). Pathak, P.D., and Pandya, N.V., 1960, Indian J. Phys., 34, 416.
- 48). Rianõ, E., and Amoras, J.L., 1960, Bol. R. Soc. Esp. Hist. Nat., 58, 181.
- 49). Deshpande, V.T., 1961, Acta Cryst., 14, 794.
- 50). Pathak, P.D., Pandya, N.V., and Ghadiali, M.P., 1963, Indian J. Phys., 37, 293.
- 51). Baxter, G.P., and Wallace, C.C., 1916, J. Am. Chem. Soc., 38, 259.
- 52). Deshpande, V.T., and Sirdeshmukh, D.B., 1961, Acta Cryst., 14, 353.
- 53). Rymer, T.B., and Hambling, P.G., 1951, Acta Cryst., 4, 565.
- 54). Johnson, J.W., Argon, P.A., and Bredig, M.A., 1955, J. Am. Chem. Soc., 77, 2734.
- 55). Pathak, P.D., and Pandya, N.V., 1960, Current Sci., 29, 14.
- 56). Clusius, V.K., Goldmann, J., and Perlick, A., 1949, Z. Naturforsch., 4a, 424.

- 57). Reinitz, K., 1961, Phys. Rev., 123, 1615.
- 58). Krishnan, K.S., and Roy, S.K., 1952, Proc. Roy. Soc., London, A 210, 481.
- 59). de Launay, J., 1959, J. Chem. Phys., 30, 91.
- 60). Berg, W.T., and Morrison, J.A., 1957, Proc. Roy. Soc., London, A 242, 467.
- 61). White, G.K., 1961, Phil. Mag., 6, 1425.
- 62). Rubin, T., Johnston, H.L., and Altman, H.W., 1962, J. Phys. Chem., 66, 948.
- 63). Blackman, M., 1958, Phil. Mag., 3, 831.
- 64). Bijl, D., and Pullan, H., 1955, Physica, 21, 285.
- 65). Fraser, P.B., and Hollis-Hallet, A.C., 1960, Proc. 7<sup>th</sup> Int. Conf. Low Temp. Phys., Toronto, p.689.

Acknowledgements.

The author wishes to acknowledge the various forms of assistance given by Dr. B.Yates, of Bradford Institute of Technology, who suggested the investigation and was always available for discussions. The author also wishes to acknowledge the interest of Professor J.F.Allen, of St.Andrews University, for helpful discussions about the work, and the interest of Dr. D.L.Smare of Bradford Institute of Technology.

The author wishes to thank Mr. C.H.Panter who built the original apparatus, Dr. R.K.Angus for valuable discussions, and Drs. T.H.K.Barron, A.J.Leadbetter, and J.A.Morrison for access to their unpublished work.